

ORIGINAL: ENGLISH

GARTEUR/TP-088-22

April 4, 1997

GARTEUR Open

RCAM Design Challenge Presentation Document: an Eigenstructure Assignment  
Approach

by

J.M. de la Cruz

P. Ruipérez

J. Aranda

GARTEUR aims at stimulating and co-ordinating  
co-operation between Research Establishments and Industry  
in the areas of Aerodynamics, Flight Mechanics, Helicopters,  
Structures & Materials and Propulsion Technology

ORIGINAL: ENGLISH

GARTEUR/TP-088-22

April 4, 1997

GARTEUR Open

RCAM Design Challenge Presentation Document: an Eigenstructure Assignment  
Approach

by

J.M. de la Cruz

P. Ruipérez

J. Aranda

(Funded by the spanish project CICYT TAP94-0832-C02-01)

This report has been prepared under auspices of  
the Responsables for Flight Mechanics, Systems  
and Integration of the Group for Aeronautical  
Research and Technology in EUROpe (GARTEUR)

Group of Resp. : FM-GoR  
Report Resp. : J.M. de la Cruz/  
Project Man. : J.C. Terlouw/  
Monitoring Resp. : J.T.M. van Doorn/

Action Group : FM(AG08)  
Version : 3  
Completed : April 4, 1997

© GARTEUR 1997

**List of authors**

Jesús M. de la Cruz<sup>1</sup>, Pablo Ruipérez<sup>2</sup> and Joaquín Aranda<sup>2</sup>

**Acknowledgements**

We wish to thank Ignacio Delgado and Alberto Martínez from INTA for introducing us in this project and for their good advises.

<sup>1</sup> Dpt. Informática y Automática. Facultad de Ciencias Físicas. Universidad Complutense. 28040-Madrid. Spain.

<sup>2</sup> Dpt. Informática y Automática. Facultad de Ciencias. U.N.E.D. 28040-Madrid. Spain

## Summary

In this document the Eigenstructure Assignment Method is applied to the Research Civil Aircraft Model (RCAM) benchmark problem. This problem was formulated under the auspices of the Group for Aeronautical Research and Technology in EUROpe (GARTEUR), Action Group FM(AG08).

The design is done by making use of the classical approach of splitting up the controller into two parts, a longitudinal and a lateral controller, and in using the standard inner-outer loop control structure. This method allows to directly satisfy specifications in terms of transient response and modes decoupling. However, it does not cope directly with system uncertainties. In order to cope with robustness, measurements of multiloop gain and phase margins are used in the choice of a robust eigenstructure.

Both channels make use of a constant gain matrix in the inner loop and a scalar gain in the outer loop. In spite of the controller simplicity, good performance and robustness results are obtained. However robustness may be increased by means of gain scheduling with respect to airspeed.

**Distribution list****FM(AG08) Principal Persons**

Ahmed S (UK)	CCL	1 copy
Ambrosino G (IT)	UNAP	1 copy
Bernussou J (FR)	LAAS	1 copy
Cruz J de la (ES)	UCM	1 copy
Delgado I (ES)	INTA	1 copy
Dormido S (ES)	UNED	1 copy
Duda H (DE)	DLR	1 copy
Escande B (FR)	ONERA	1 copy
Faleiro L (UK)	LUT	1 copy
Fielding C (UK)	BAe-MA	1 copy
Game G (UK)	BAeDD	1 copy
Gautrey J (UK)	CUN	1 copy
Helmersson A (SE)	LiTH	1 copy
Joos H (DE)	DLR	1 copy
Laidlaw D (UK)	AVRO	1 copy
Luckner R (DE)	DASA	1 copy
Maciejowski J (UK)	UCAM	1 copy
Magni J (FR)	ONERA	1 copy
Muir E (UK)	DRA	1 copy
Postlethwaite I (UK)	ULES	1 copy
Schram G (NL)	DUT-EE	1 copy
Ståhl-Gunnarsson K (SE)	SMA	1 copy
Terlouw J (NL)	NLR	1 copy
Tonon A (IT)	ALN	1 copy
Vaart J van der (NL)	DUT-AE	1 copy
Verde L (IT)	CIRA	1 copy

**Members of the Flight Mechanics, Systems and Integration Group of  
Responsables**

Brännström B (SE)	FMV	1 copy
Doorn J van (NL)	NLR	1 copy
England P (UK)	DRA	1 copy
Muñoz F (IT)	INTA	1 copy
Rodloff R (DE)	DLR	1 copy
Verbrugge R (FR)	ONERA	1 copy

---

**Members of the Executive Committee**

Chéret J (FR)	ONERA	1 copy
Coleman G (UK)	DRA	1 copy
Gustafsson A (SE)	FFA	1 copy
Haupt R (DE)	DLR/PD-L	1 copy
Moreno Labata G (ES)	INTA	1 copy
Slooff J (NL)	NLR	1 copy

**Secretary GARTEUR**

Jonasson K (SE)	FFA	1 copy
-----------------	-----	--------

## Contents

<b>List of figures</b>	<b>ix</b>
<b>List of tables</b>	<b>xii</b>
<b>List of symbols and abbreviations</b>	<b>xiv</b>
<b>1 Introduction</b>	<b>1</b>
<b>2 Eigenstructure Assignment Method</b>	<b>2</b>
2.1 Theoretical Aspects . . . . .	2
2.1.1 Global Goal . . . . .	2
2.1.2 System Model . . . . .	2
2.1.3 Brief account of the transient time response . . . . .	3
2.1.4 Controller Structure . . . . .	4
2.1.5 Design Specification . . . . .	4
2.1.6 Analysis Information . . . . .	4
2.1.7 Controller Synthesis . . . . .	5
2.1.8 Practical Aspects of Implementation . . . . .	7
2.1.9 Measure of Robustness . . . . .	8
2.2 Applications . . . . .	9
2.3 A Simple Design Example . . . . .	10
2.3.1 Model . . . . .	10
2.3.2 Analysis . . . . .	11
2.3.3 Controller design . . . . .	12
<b>3 Controller architecture</b>	<b>14</b>
3.1 Introduction . . . . .	14
3.2 Longitudinal Controller . . . . .	14
3.2.1 Measurement Signals . . . . .	15
3.2.2 Actuator Signals . . . . .	15
3.2.3 Reference Signals . . . . .	15
3.2.4 Controller Structure . . . . .	15
3.3 Lateral Controller . . . . .	17
3.3.1 Measurement Signals . . . . .	17
3.3.2 Actuator Signals . . . . .	17
3.3.3 Reference Signals . . . . .	17
3.3.4 Controller Structure . . . . .	17

<b>4</b>	<b>The Translation of RCAM design criteria into method dependent objectives</b>	<b>19</b>
4.1	Introduction . . . . .	19
4.2	Performance Criteria . . . . .	19
4.2.1	Longitudinal Specifications . . . . .	19
4.2.1.1	Airspeed . . . . .	19
4.2.1.2	Flight path angle . . . . .	20
4.2.1.3	Altitude . . . . .	20
4.2.1.4	Cross coupling between airspeed $V_A$ and altitude $h$ . . . . .	20
4.2.2	Lateral Specifications . . . . .	21
4.2.2.1	Heading angle response . . . . .	21
4.2.2.2	Lateral deviations . . . . .	21
4.2.2.3	Engine failure . . . . .	21
4.3	Robustness Criteria . . . . .	22
<b>5</b>	<b>The description of the design cycle</b>	<b>23</b>
5.1	Longitudinal controller . . . . .	24
5.1.1	Analysis of the linear longitudinal model of the plant . . . . .	24
5.1.1.1	Longitudinal model . . . . .	24
5.1.1.2	Coupling of the modes with the states . . . . .	25
5.1.1.3	Coupling of the modes with the outputs and the inputs . . . . .	26
5.1.1.4	Outputs selection . . . . .	27
5.1.1.5	Integrators selection . . . . .	27
5.1.2	Inner loop controller design . . . . .	27
5.1.3	Analysis of the closed inner loop . . . . .	29
5.1.3.1	Step in flight path angle . . . . .	30
5.1.3.2	Step in airspeed . . . . .	30
5.1.3.3	Loop stability margins . . . . .	33
5.1.4	Outer loop controller . . . . .	35
5.1.4.1	Altitude step response . . . . .	36
5.1.4.2	Step in airspeed . . . . .	37
5.2	Lateral controller . . . . .	38
5.2.1	Analysis of the linear lateral model of the plant . . . . .	38
5.2.1.1	Lateral model . . . . .	38
5.2.1.2	Inner loop controller design . . . . .	39
5.2.2	Analysis of the closed inner loop . . . . .	42
5.2.2.1	Step in heading angle . . . . .	42
5.2.2.2	Loop stability margins . . . . .	43
5.2.3	Outer loop design . . . . .	44
5.2.3.1	Lateral step response . . . . .	47
5.3	Controller with proportional action on the output error . . . . .	48



5.3.1	Longitudinal model . . . . .	49
5.3.1.1	Inner loop stability margins . . . . .	49
5.3.1.2	Step in flight path angle . . . . .	50
5.3.2	Longitudinal outer loop . . . . .	50
5.3.2.1	Altitude step response . . . . .	51
5.3.2.2	Step in airspeed . . . . .	51
5.3.3	Lateral model . . . . .	52
5.3.3.1	Lateral inner loop stability margins . . . . .	52
5.3.3.2	Step in heading angle . . . . .	53
5.3.4	Lateral outer loop . . . . .	54
5.3.4.1	Lateral step response . . . . .	54
<b>6</b>	<b>Analysis of the resulting controller in terms of the applied methodology</b>	<b>56</b>
6.1	Non-linear simulation observing performance criteria . . . . .	56
6.2	Non-linear simulation of an engine failure . . . . .	56
6.3	Non-linear simulation observing ride quality and safety criteria . . . . .	58
6.4	Non-linear simulation under moderate turbulence conditions . . . . .	59
6.5	Non-linear simulations observing robustness criteria . . . . .	61
6.6	Nonlinear simulations with controller with proportional action on the output error . . . . .	66
<b>7</b>	<b>Results of the Automated Evaluation Procedure</b>	<b>71</b>
7.1	Introduction . . . . .	71
7.1.1	A general view of the results . . . . .	71
7.1.2	Segment I: The effect of engine failure . . . . .	72
7.1.3	Segment II: 90 degrees turn . . . . .	73
7.1.4	Segment III: The descent phase . . . . .	74
7.1.5	Segment IV: Final approach . . . . .	75
7.1.6	Numerical results . . . . .	77
7.2	Results using the controller with proportional action on the output error	78
	<b>Conclusions</b>	<b>81</b>
	<b>References</b>	<b>82</b>
<b>A</b>	<b>Software used</b>	<b>84</b>
A.1	Function EIGENAS . . . . .	84
A.2	Function SSINTEG . . . . .	87
A.3	Function MXSSV . . . . .	88
A.4	Function GFMAR . . . . .	90
A.5	Function TRTS . . . . .	91

**B Designer's background and design environment**

**92**

**List of figures**

2.1	Feedback system . . . . .	8
3.1	The overall controller structure . . . . .	14
3.2	Longitudinal controller . . . . .	16
3.3	Longitudinal inner loop controller . . . . .	16
3.4	Lateral controller . . . . .	18
3.5	Lateral inner loop controller . . . . .	18
5.1	Response of the linearised system to a step in commanded flight path angle	31
5.2	Response of the linearised system to a step in commanded airspeed . . .	31
5.3	Response of the linearised system to a step in air velocity . . . . .	32
5.4	Longitudinal inner loop singular values of the input sensitivity functions	33
5.5	Longitudinal inner loop singular values of the output sensitivity functions	34
5.6	Root locus for longitudinal outer loop design . . . . .	36
5.7	Response of the linearised system to a step in commanded altitude . . .	37
5.8	Response of the linearised system to a step in commanded airspeed . . .	37
5.9	Response of the linearised system to a step in inertial track angle . . . .	43
5.10	Lateral inner loop singular values of the input sensitivity functions . . .	44
5.11	Lateral inner loop singular values of the output sensitivity functions . .	44
5.12	Root locus for lateral outer loop design . . . . .	46
5.13	Closed loop lateral response of the linear model to a lateral command .	47
5.14	Output feedback controller with integral action on the error of commanded outputs (structure 1) . . . . .	48
5.15	Output feedback controller with integral and proportional actions on the error of commanded outputs (structure 2) . . . . .	48
5.16	Longitudinal inner loop singular values of the input sensitivity functions (structure 2) . . . . .	49
5.17	Longitudinal inner loop singular values of the output sensitivity functions (structure 2) . . . . .	50
5.18	Response of the linearised system to a step in commanded flight path angle (structure 2) . . . . .	51
5.19	Longitudinal outer loop controller (structure 2) . . . . .	51
5.20	Response of the linearised system to a step in commanded altitude (structure 2) . . . . .	52
5.21	Response of the linearised system to a step in commanded airspeed (structure 2) . . . . .	52
5.22	Lateral inner loop singular values of the input sensitivity functions (structure 2) . . . . .	53
5.23	Lateral inner loop singular values of the output sensitivity functions (structure 2) . . . . .	53

---

5.24	Response of the linearised system to a step in heading angle (structure 2)	54
5.25	Lateral outer loop controller (structure 2)	55
5.26	Response of the linearised system to a step in lateral deviation	55
6.1	Response of the non-linear model to command signals	57
6.2	Response of the non-linear model to an engine failure	58
6.3	Ride quality criteria observation	58
6.4	Safety criteria observation	59
6.5	Control activity under moderate turbulence conditions	61
6.6	Responses under moderate turbulence conditions of angles $\phi$ , $\beta$ , $\psi$ and $\chi$	62
6.7	Lateral, altitude, heading, flight-path, airspeed and wind step response, and airspeed-altitude cross coupling, at the design speed	63
6.8	Roll and heading at engine failure at the design speed	64
6.9	Lateral, altitude, heading, flight-path, airspeed and wind step response, and airspeed-altitude cross coupling, at nominal speed and at maximal flap speed	65
6.10	Roll and heading at engine failure, at nominal speed and at maximal flap speed	66
6.11	Lateral, altitude, heading, flight-path, airspeed and wind step response, and airspeed-altitude cross coupling, using the controller calculated at nominal velocity	67
6.12	Roll and heading at engine failure, using the controller calculated at nominal velocity	68
6.13	Ride quality criteria observation with controller structure 2	68
6.14	Safety criteria observation with controller structure 2	69
6.15	Lateral, altitude, heading, flight-path, airspeed and wind step response, and airspeed-altitude cross coupling, at the design speed, with controller structure 2	70
7.1	The trajectory response of the controlled RCAM model	71
7.2	Segment I: The effect of engine failure with bounds	72
7.3	Segment II: Plan view of the 90 degrees turn with bounds	73
7.4	Segment II: Lateral deviations during the 90 degrees turn with bounds	74
7.5	Segment III: Side view of the -6 and -3 degrees glideslope captures with bounds	74
7.6	Segment III: Vertical deviations during the -6 and 3 degrees glidslope with bounds	75
7.7	Segment IV: Side view of the final approach with wind shear and bounds	76
7.8	Segment IV: Vertical deviations during the final approach with bounds	76
7.9	Segment I: The effect of engine failure with bounds	78
7.10	Segment II: Lateral deviations during the 90 degrees turn with bounds	79

7.11 Segment III: Vertical deviations during the -6 and 3 degrees glidslope with bounds . . . . .	79
7.12 Segment IV: Vertical deviations during the final approach with bounds .	80

**List of tables**

2.1	Modes of the open loop system . . . . .	11
2.2	Absolute value of the components of the eigenvectors of the open loop system . . . . .	11
2.3	Absolute value of the components of the vectors $Cv_i$ . . . . .	11
2.4	Absolute value of the components of the vectors $w_i^T B$ . . . . .	12
2.5	Desired closed loop eigenvalues . . . . .	12
2.6	Eigenvalues and absolute values of the normalised eigenvectors for the closed loop system . . . . .	13
3.1	Longitudinal measurements used . . . . .	15
3.2	Lateral measurements used . . . . .	17
5.1	Modes of the open loop system including actuators . . . . .	25
5.2	Absolute value of the components of the eigenvectors of the open loop system including actuators . . . . .	25
5.3	Absolute value of the components of the vectors $Cv_i$ including actuators . . . . .	26
5.4	Absolute value of the components of the vectors $w_i^T B$ including actuators . . . . .	27
5.5	Desired eigenstructure of the longitudinal closed loop system . . . . .	28
5.6	Inner closed loop eigenvalues and absolute values of the components of vectors $Cv_i$ . . . . .	30
5.7	Open loop absolute values of the components of vectors $Cv_i$ . . . . .	30
5.8	Longitudinal inner loop stability margins at the inputs . . . . .	33
5.9	Longitudinal inner loop stability margins at the outputs . . . . .	34
5.10	Modes of the open loop system including actuators . . . . .	39
5.11	Absolute value of the components of the eigenvectors of the open loop system including actuators . . . . .	39
5.12	Absolute value of the components of the vectors $Cv_i$ including actuators . . . . .	40
5.13	Absolute value of the components of the vectors $w_i^T B$ including actuators . . . . .	40
5.14	Desired eigenstructure of the lateral closed loop system . . . . .	41
5.15	Inner closed loop eigenvalues and absolute values of the components of vectors $Cv_i$ . . . . .	42
5.16	Open loop absolute values of the components of vectors $Cv_i$ . . . . .	43
5.17	Lateral inner loop stability margins at the inputs . . . . .	45
5.18	Lateral inner loop stability margins at the outputs . . . . .	45
5.19	Longitudinal inner loop stability margins at the inputs (structure 2) . . . . .	49
5.20	Longitudinal inner loop stability margins at the outputs (structure 2) . . . . .	50
5.21	Lateral inner loop stability margins at the inputs (structure 2) . . . . .	54
5.22	Lateral inner loop stability margins at the outputs (structure 2) . . . . .	54
6.1	RMS of the errors in angles $\phi$ , $\beta$ , $\psi$ and $\chi$ in open and closed loop . . . . .	60
7.1	Numerical results of the evaluation procedure . . . . .	77

7.2 Numerical results of the evaluation procedure . . . . . 78

## List of symbols and abbreviations

### Symbols

The symbols used are according to the nomenclature defined in the Communication Handbook [1].

### Abbreviations

ALN	Alenia Aeronautica
AVRO	Avro International Aerospace
BAeDD	MATRA - British Aerospace Defence Dynamics
BAe-MA	British Aerospace Military Aircraft
CCL	Cambridge Control
CERT	Centre d'Etudes et de Recherches de Toulouse
CIRA	Centro Italiano Ricerche Aerospaziali
CUN	Cranfield University
DASA	Daimler-Benz Aerospace Airbus
DE	Germany
DLR	Deutsche Forschungsanstalt für Luft- und Raumfahrt
DRA	Defence Research Agency
DUT-AE	Delft University of Technology, Department of Aerospace Engineering
DUT-EE	Delft University of Technology, Department of Electrical Engineering
ES	Spain
FFA	The Aeronautical Research Institute of Sweden
FMAG	Flight Mechanics Action Group
FM-GoR	Flight Mechanics, Systems and Integration Group of Responsables
FMV	Defense Material Administration
FR	France
GARTEUR	Group for Aeronautical Research and Technology in EUROpe
INTA	Instituto Nacional de Técnica Aeroespacial
IT	Italy
LAAS	Laboratoire d'Analyse et d'Architecture des Systemes
LiTH	Linköping University
LUT	Loughborough University
NL	The Netherlands
NLR	National Aerospace Laboratory
ONERA	Office National d'Etudes et de Recherches Aérospatiales
SE	Sweden



SMA	Saab AB, Saab Military Aircraft
UCAM	University of Cambridge
UCM	Universidad Complutense Madrid
UK	United Kingdom
ULES	University of Leicester
UNAP	Università degli Studi di Napoli Federico II
UNED	Universidad Nacional de Educación a Distancia



## 1 Introduction

The eigenstructure technique has been widely applied to the design of flight control systems and it is a well known-fact that its use requires an in-depth knowledge of the system to be controlled [4]. The main characteristic of this method is that it allows the designer to directly satisfy specifications in terms of transient response and mode decoupling. Although such a method is not intended to deal with robustness, many robustification procedures have been proposed. Here the eigenstructure is chosen so that good multiloop gain and phase stability margins are obtained. Our design aims to get a controller that is robust enough to keep the performance criteria in the whole flight envelope and at the same time reduces or avoids scheduling.

The document is organised in the following way:

Chapter 2 gives a brief introduction to the eigenstructure assignment method. In order to keep it simple, only those aspects relevant to the design are expounded. More details may be found in the references.

Chapter 3 describes the used controller structure. The controller has been decoupled into the longitudinal and the lateral channels. Both have been designed according to an inner/outer loop control structure. The inner loop controllers are designed following the eigenstructure method. A constant matrix gain is used in both channels. The outer loop only uses an scalar gain that is calculated by means of the root locus method.

Chapter 4 deals with the way the RCAM design criteria are translated into the desired eigenstructure.

Chapter 5 describes the design cycle. The linear model of the plant is analysed and the most appropriate eigenstructure is chosen. Next, the feedback controller is obtained and the performance of the closed loop system for the linear models is analysed. Multiloop gain and phase margins are used to measure robustness and to guide in the eigenstructure choice. Two controller structures are considered, without and with feedforward action.

In chapter 6 we present the verification of all the design specifications with the non-linear system. Simulations for the worst possible combinations of delay mass and centre of gravity are given.

In chapter 7 the results of the automated evaluation procedure are given.

Next section is devoted to concluding remarks. Finally, Appendix A contains a set of MATLAB m-files we have developed for this project, and Appendix B contains the desing environment and the designer's background prior to starting the project.

## 2 Eigenstructure Assignment Method

### 2.1 Theoretical Aspects

#### 2.1.1 Global Goal

This method is the multivariable extension of the root locus method. The behaviour of a MIMO system is characterised by its eigenvalues and eigenvectors. The eigenvalues determine the stability and the eigenvectors characterise the shapes and coupling of different modes. This method allows the designer to directly satisfy damping, settling time and decoupling specifications by directly choosing the eigenvalues and eigenvectors.

The eigenstructure assignment technique does not cope directly with robustness but may be adapted so we can take into account certain parameter variations and unmodelled dynamics to improve robustness.

This technique has been extensively implemented in aerospace control applications due to its ability to directly incorporate aircraft handling design criteria.

#### 2.1.2 System Model

Let us consider a linear time invariant system described by

$$\dot{x} = Ax + Bu \tag{2.1}$$

$$y = Cx \tag{2.2}$$

where the number of states is  $n$ , the number of inputs is  $n_u$ , and the number of outputs is  $n_y$ .  $A$ ,  $B$  and  $C$  are matrices of appropriate dimensions. Attention should be drawn to our assuming the direct transmission matrix  $D$  of the system to be zero for the sake of simplicity. This assumption is often satisfied, since most time-invariant plants have a strictly proper transfer matrix, and this will be the case of the linear systems we are dealing with.

Exogenous signals and noise do not affect the eigenstructure and thus they are taken to be zero.

The following standard assumptions should be made:

- $B$  and  $C$  are of full rank
- $(A, B)$  is controllable and  $(A, C)$  is observable.

However, the controllable assumption may be removed, and the designer may alter eigenvectors which correspond to uncontrollable eigenvalues, [17].

## 2.1.3 Brief account of the transient time response

As is very well known, the solution of 2.1 is

$$x(t) = e^{At} x_0 + \int_0^t e^{A(t-\tau)} B u(\tau) d\tau \quad (2.3)$$

$$y(t) = C e^{At} x_0 + \int_0^t C e^{A(t-\tau)} B u(\tau) d\tau \quad (2.4)$$

A much more telling representation of the solution of 2.1 can be re-written in terms of the eigenvalues and eigenvectors of the matrix  $A$ . If we suppose that  $A$  has  $n$  distinct eigenvalues  $\{\lambda_i\}_{i=1}^n$  with corresponding eigenvectors  $\{v_i\}_{i=1}^n$ , then the  $n * n$  matrices are defined

$$V = [v_1, v_2, \dots, v_n] \quad (2.5)$$

$$\Lambda = \text{diag} [\lambda_1, \lambda_2, \dots, \lambda_n] \quad (2.6)$$

If so, then

$$AV = V\Lambda \quad (2.7)$$

The  $V$  matrix is called the modal matrix. The  $n$  eigenvectors make up a linear independent family so that they form a basis for the complex  $n$  dimensional space. It may be said that  $A$  has a basis of  $n$  eigenvectors or right eigenvectors. Without loss of generality it can be assumed that the eigenvectors are normalised to constant unity length.

The  $A$  matrix has also a basis of left eigenvectors  $\{w_i\}_{i=1}^n$  so that

$$W = [w_1, w_2, \dots, w_n]^H \quad (2.8)$$

$$WA = \Lambda W \quad (2.9)$$

where

$$WV = I = VW \quad (2.10)$$

Thus the solution given by equations 2.3 and 2.4 may be re-written as

$$x(t) = \sum_{i=1}^n e^{\lambda_i t} v_i \left[ w_i^H x_0 + \int_0^t e^{-\lambda_i \tau} w_i^H B u(\tau) d\tau \right] \quad (2.11)$$

$$y(t) = \sum_{i=1}^n e^{\lambda_i t} C v_i \left[ w_i^H x_0 + \int_0^t e^{-\lambda_i \tau} w_i^H B u(\tau) d\tau \right] \quad (2.12)$$

The transfer function matrix for system 2.1 may be written as

$$G(s) = \sum_{i=1}^n (s - \lambda_i)^{-1} C v_i w_i^H B \quad (2.13)$$

If we pay attention to the homogeneous solution of 2.11, or zero input response of the system, we are entitled to write

$$x(t) = \sum_{i=1}^n \alpha_i e^{\lambda_i t} v_i \quad (2.14)$$

where  $\alpha_i$  are the scalars  $w_i^H x_0$ ,  $i = 1..n$ . This clearly shows that this response is a composition of very simple motions along the eigenvectors of the matrix  $A$ . Those motions are called *system modes*. In every mode the eigenvalue determines the decay/growth rate of the response, whereas the eigenvectors determine the strength of the coupling of this mode with the state.

The numbers  $\alpha_1 .. \alpha_n$  are the coefficients expressing how the initial state  $x_0$  is decomposed along the vectors  $v_1 .. v_n$ . A particular mode is *excited* by assuming the initial state  $x_0$  has a component  $\alpha_i$  along the corresponding eigenvector.

From 2.12 we can see that the coupling of the  $i$ -th mode with the output is given by  $Cv_i$ . If  $Cv_i = 0$ , then equations 2.12 and 2.13 show that the  $i$ -th mode does not contribute to the output.

In 2.11  $w_i^H B$  measures the coupling between the vector input and the  $i$ -th mode; for instance if  $w_i^H B u = 0$ , then the  $i$ -th mode is not excited by that particular input.

#### 2.1.4 Controller Structure

As control mechanism, we may choose static output feedback, or state feedback, or dynamic compensation. As a rule the static output feedback is chosen because eigenstructure assignment through either state feedback or dynamic compensation can be re-formulated as an output feedback problem.

#### 2.1.5 Design Specification

Our aim is to find such a feedback system that the closed-loop eigenstructure is as desired. More precisely, the problem can be stated as follows: given a set of desired eigenvalues  $\{\lambda_i^d, i = 1, \dots, n_y\}$  and a corresponding set of desired eigenvectors  $\{v_i^d, i = 1, \dots, n_y\}$ , we try to find a  $n_u * n_y$  matrix  $K$  such that the eigenvalues of the closed-loop system matrix  $(A - BKC)$ , obtained when using the output feedback control equation

$$u = -Ky, \quad (2.15)$$

include  $\{\lambda_i^d\}$  as a subset, and the corresponding eigenvectors of  $A - BKC$  are as close as possible to the respective members of the set  $\{v_i^d\}$ .

#### 2.1.6 Analysis Information

If the pair  $(A, B)$  is controllable, then the feedback gain matrix  $K$  will exactly assign  $\max\{n_u, n_y\}$  eigenvalues. It will also partially assign  $\max\{n_u, n_y\}$  eigenvectors with

$\min \{n_u, n_y\}$  elements in each vector arbitrarily chosen.

It is assumed that, as is usually the case in aircraft problems, the following is valid:

$$n_u < n_y < n \quad (2.16)$$

Then,  $n_y$  eigenvalues can be assigned and  $n_u$  elements of each eigenvector can be arbitrarily chosen. However it is not possible to ascertain that stable open loop eigenvalues do not move into the right-half of the complex plane when an eigenstructure assignment output feedback controller is made use of [17].

### 2.1.7 Controller Synthesis

Let  $\lambda_i, v_i$  be an eigenvalue-eigenvector pair of the closed-loop system, then

$$\lambda_i v_i = (A - BKC)v_i \quad (2.17)$$

or

$$v_i = -(\lambda_i I - A)^{-1} BKC v_i \quad (2.18)$$

If we define the  $L_i$  matrices as

$$L_i = (\lambda_i I - A)^{-1} B \quad (2.19)$$

and the  $z_i$  auxiliary vectors as

$$z_i = -KC v_i \quad (2.20)$$

then the closed-loop eigenvectors comply with

$$v_i = L_i z_i \quad (2.21)$$

It is obvious from the above equation that a desired eigenvector  $v_i^d$  must lie in the subspace spanned by the columns of the matrix  $L_i, i = 1, \dots, n_y$ . This subspace is of  $n_u$  dimension. Therefore, once the eigenvalues have been chosen, the range space of matrices  $L_i$  constrains the selection of the closed-loop eigenvectors. In general, the eigenvectors  $v_i^d$  desired, whose selection should be made in terms of response shaping and decoupling, do not reside in the prescribed eigenvector and, hence, cannot be arrived at. In order to have the resulting eigenvector as close as possible to the desired one, an optimum choice is made: the projection of the desired eigenvector onto the achievable subspace,  $z_i$ , is found by minimising

$$J_i = \min_{z_i} \left[ v_i^d - L_i z_i \right]^T R_i \left[ v_i^d - L_i z_i \right], i = 1, \dots, n_y \quad (2.22)$$

where  $R_i$  is a weighting matrix whose range is at least  $n_u$ .

The optimal  $z_i$  are calculated as

$$z_i = (L_i^T R_i L_i)^{-1} L_i^T R_i v_i^d, i = 1, \dots, n_y \quad (2.23)$$

and the achievable eigenvectors  $v_i^a$  are given by

$$v_i^a = L_i z_i, i = 1, \dots, n_y \quad (2.24)$$

To find the output feedback gain matrix  $K$  a similarity transformation  $T$  is chosen so that the  $B$  matrix is a lead block identity matrix

$$T = \begin{bmatrix} B & P \end{bmatrix} \quad (2.25)$$

where  $P$  is any matrix that makes  $T$  full rank. Note that this can be always done since we have assumed the  $B$  matrix is of full rank. Applying  $T$  to the original system 2.1 the following transformed system is obtained:

$$\begin{aligned} \bar{B} &= \begin{bmatrix} I \\ 0 \end{bmatrix} = T^{-1}B & (2.26) \\ \bar{A} &= \begin{bmatrix} \bar{A}_1 \\ \bar{A}_2 \end{bmatrix} = T^{-1}AT \\ \bar{C} &= CT & (2.27) \end{aligned}$$

where  $\bar{A}$  has been partitioned into the first  $n_u$  rows and the last  $n - n_u$  rows.

The state, eigenvalues and achievable eigenvectors of the transformed system are given by

$$\begin{aligned} \bar{x} &= T^{-1}x \\ \bar{\lambda}_i &= \lambda_i & (2.28) \\ \bar{v}_i^a &= \begin{bmatrix} \bar{s}_i \\ \bar{w}_i \end{bmatrix} = T^{-1}v_i^a & (2.29) \end{aligned}$$

where  $\bar{v}_i^a$  has also been partitioned into the first  $n_u$  rows and the last  $n - n_u$  rows. We can see that the eigenvalues of the new system are equal to the eigenvalues of the original system.

The gain matrix  $K$  is then given by:

$$K = -(\bar{S} - \bar{A}_1 \bar{V})(\bar{C} \bar{V})^{-1} \quad (2.30)$$

where

$$\bar{S} = \begin{bmatrix} \lambda_1^d \bar{s}_1, \dots, \lambda_{n_y}^d \bar{s}_{n_y} \end{bmatrix} \quad (2.31)$$

$$\bar{V} = \begin{bmatrix} \bar{v}_1^a, \dots, \bar{v}_{n_y}^a \end{bmatrix} \quad (2.32)$$



### 2.1.8 Practical Aspects of Implementation

As has been already said,  $n_u$  elements in each eigenvector can be arbitrarily chosen. In many practical situations some components of the desired eigenvectors are not known or required so they should not induce any drawback in the cost function. Therefore, if only  $n_u$  elements in eigenvector  $v_i^d$  are specified, then  $R_i$  is a diagonal matrix with 1 value in the entries corresponding to the specified elements, and zeroes elsewhere.

Mode decoupling is another important aspect to be considered in the eigenvector selection. This property allows the independent implementation of the control. If we want the  $i$ -th mode to have no influence on some components of the vector state, the corresponding entries in the  $i$ -th eigenvector should be specified as zeroes.

The eigenvectors selection bears on the sensitivity of the eigenvalues to perturbations, since the sensitivity of the eigenvalues of a matrix decreases as the orthogonality of the corresponding eigenvectors increases [10].

In some cases the modal interactions may be coupled with the demanded control effort and with the system robustness, so some iterations in the selection of eigenvectors may be needed.

In [4], [18] and in [12] a method for choosing the elements of the gain matrix which can be suppressed to zero with a minimal effect on the eigenstructure is proposed.

[12] illustrates the way in which static decoupling between each component of the output vector and a corresponding component of step input command can be achieved.

Numerically, the best method for computing the output feedback gain matrix is obtained through the singular value decomposition of the matrices  $B$  and  $CV$ :

$$B = \begin{bmatrix} U_{b0} & U_{b1} \end{bmatrix} \begin{bmatrix} \Sigma_b V_b^T \\ 0 \end{bmatrix} \quad (2.33)$$

$$CV = \begin{bmatrix} U_{n_y0} & U_{n_y1} \end{bmatrix} \begin{bmatrix} \Sigma_{n_y} V_{n_y}^T \\ 0 \end{bmatrix} \quad (2.34)$$

where  $V$  is the matrix whose columns are the achievable eigenvectors; all the  $U$  and  $V$  matrices are orthogonal and the  $\Sigma$  matrices are non singular. The output feedback matrix can now be re-written as:

$$K = -V_b \Sigma_b^{-1} U_{b0}^T (V \Lambda - AV) V_{n_y} \Sigma_{n_y}^{-1} U_{n_y0}^T \quad (2.35)$$

where  $\Lambda$  is an  $n_y \times n_y$  diagonal matrix whose entries are the desired eigenvalues.

The subspace in which the achievable eigenvector  $v_i^a$  must reside is also given by the null space of  $U_{b1}^T (\lambda_i^d I - A)$ . The preferred method for computing the achievable eigenvectors consists in taking the orthogonal projection of the desired eigenvectors onto the null space of this matrix.

### 2.1.9 Measure of Robustness

The criterium we shall use in the eigenstructure selection is a measure of the loop robustness. So, we shall give a brief summary of several possible measures.

Let us consider the control diagram of figure 2.1

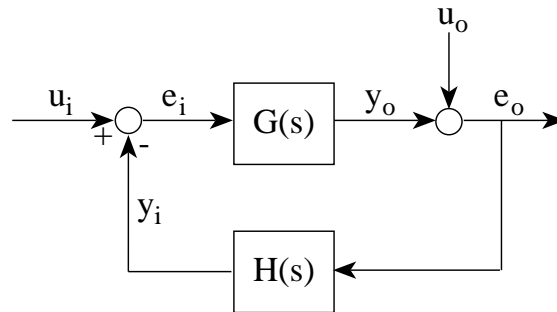


Fig.2.1 Feedback system

where  $G(s)$  is the plant transfer function matrix,  $H(s)$  is the controller transfer function matrix;  $u_i$  and  $u_o$  are external input vectors;  $y_i$  and  $y_o$  are the plant output vector and the controller output vector, respectively; and  $e_i$ ,  $e_o$  are error signal vectors.

The singular values of the sensitivity function  $S = (I+L)^{-1}$ , the complementary sensitivity function  $T = L(I+L)^{-1}$  and the balanced sensitivity function  $S + T$ , where  $L$  is the open loop gain matrix, can be used to measure the stability margins for multiloop feedback control systems [11], [8] and [5].

Functions  $S$  and  $T$  may be calculated at the actuator inputs or at the sensor outputs. For the input  $L = HG$  and for the output  $L = GH$ . Usually the open loop transfer matrix at the input and at the output are different because matrix multiplication is not commutative and, therefore, both cases should be taken into consideration.

The sensitivity function is the transfer matrix from the summing junction input  $u$  to the summing junction output  $e$  ( $u_i$ ,  $e_i$  for the input node and  $u_o$ ,  $e_o$  for the output node). The complementary sensitivity function is the transfer matrix from the summing junction input  $u$  to the correspondig loop return signal  $y$  ( $u_i$ ,  $y_i$  for the input node and  $u_o$ ,  $y_o$  for the output node). The balanced sensitivity function is the transfer matrix from  $u$  to  $e + y$ . The peak value of the maximun singular value ( $\bar{\sigma}$ ) of  $S$ ,  $T$  or  $S + T$  gives a robustness guarantee for all frequencies.

The formulae applied to computing the gain margin  $GM$  and the phase margin  $PM$  using the sensitivity function are the following:

Function  $S$ :

$$K_m = 1/\bar{\sigma}(S)$$

$$\begin{aligned}
 GM &= [1/(1 + K_m), 1/(1 - K_m)] \\
 PM &= \pm 2 \sin^{-1}(K_m/2)
 \end{aligned}
 \tag{2.36}$$

where  $K_m \leq 1$ . The interpretation of 2.36 is as follows: the gains of the loops may be perturbed simultaneously by gains  $\Delta_i$  satisfying  $1/(1 + K_m) < \Delta_i < 1/(1 - K_m)$  without destabilising the closed loop system. That is, the upward gain margin is at least as large as  $1/(1 - K_m)$  and the gain reduction margin as small as  $1/(1 + K_m)$ . Similarly, the feedback loops may be perturbed simultaneously by phases  $\phi_i$  satisfying  $|\phi_i| < 2 \sin^{-1}(K_m/2)$  without destabilising the closed loop system. The best possible gain and phase margins are obtained when  $\bar{\sigma}(S) = 1$ , in this case the gain margin is  $[-6 \text{ dB}, +\infty \text{ dB}]$  and the phase margin is  $\pm 60^\circ$ .

The formulae applied to computing the gain margin  $GM$  and the phase margin  $PM$  using the complementary sensitivity function are the following:

Function  $T$ :

$$\begin{aligned}
 K_m &= 1/\bar{\sigma}(T) \\
 GM &= [1 - K_m, 1 + K_m] \\
 PM &= \pm 2 \sin^{-1}(K_m/2)
 \end{aligned}
 \tag{2.37}$$

where  $K_m \leq 1$ . The interpretation is similar to the  $S$  sensitivity function case. The best possible gain margin is now  $[-\infty \text{ dB}, 6 \text{ dB}]$  when  $\bar{\sigma}(T) = 1$ , and the best possible phase margin is  $\pm 60^\circ$ .

Finally, the formulae applied to computing the gain margin  $GM$  and the phase margin  $PM$  using the balanced sensitivity function are the following:

Function  $S + T$ :

$$\begin{aligned}
 K_m &= 1/\bar{\sigma}(S + T) \\
 GM &= [(1 - K_m)/(1 + K_m), (1 + K_m)/(1 - K_m)] \\
 PM &= \pm 2 \tan^{-1}(K_m)
 \end{aligned}
 \tag{2.38}$$

where  $K_m \leq 1$ . The interpretation is similar to the sensitivity function case. Here the best possible gain margin is  $[-\infty \text{ dB}, \infty \text{ dB}]$  when  $\bar{\sigma}(S + T) = 1$ , and the best possible phase margin is  $\pm 90^\circ$ .

Those margins are known to be conservative, a better approach could be obtained by replacing the maximum singular value  $\bar{\sigma}$  with the structured singular value  $\mu$  [5].

## 2.2 Applications

Sobel et al. (1994) [17] apply the eigenstructure method to the linearized lateral dynamics of the F-18 High Angle of Attack Research Vehicle (HARV). They use MATLAB for computing the achievable eigenvectors. In their work they also study the design of a robust sampled data controller for the yaw pointing/lateral translation manoeuvre of the

Flight Propulsion Control Coupling (FPCC) aircraft. In order to get a robust design they use the design method of Piou et al. (1992) [16]. MATLAB is used in the optimisation process.

In Lin (1994) [12] the lateral model of the L-1011 aircraft at the cruise flight condition is controlled. An iterative procedure is applied to increase the robustness of the system yielding small improvements in robustness.

In White (1993) [20] several algorithms for eigenstructure assignment are outlined and their realisations in MATLAB are given. The algorithms are applied to the control of a linear model of the lateral motion of an MS760 Paris fighter-trainer aircraft.

In Patton et al. (1994) [15] a parameter insensitive design method using eigenstructure assignment and the method of inequalities is submitted. Such a method is applied to the lateral dynamics of the L-1011 aircraft corresponding to a certain cruise flight condition. Better insensitivity to perturbations is achieved.

In Burrows et al. (1989) [7] two methods for eigenstructure assignment are made use of the Ctrl-C software package. They use the lateral motion of a light aircraft as an example application.

## 2.3 A Simple Design Example

### 2.3.1 Model

We give a simple example using the longitudinal directional dynamics of the RCAM model linearised around the following conditions:  $V = 80$  m/s,  $h = 1000$  m, mass = 120000 kg,  $cg_x = 0.23$  and  $cg_z = 0.1$ . Equation 2.39 represents the model where no dynamics for the actuators has been included.

$$\begin{bmatrix} \dot{q} \\ \dot{\theta} \\ \dot{u}_B \\ \dot{w}_B \end{bmatrix} = \begin{bmatrix} -0.981 & 0 & -0.0007 & -0.0153 \\ 1.0000 & 0 & 0 & 0 \\ -2.2343 & -9.7754 & -0.0325 & 0.0744 \\ 77.3559 & -0.7727 & -0.2261 & -0.6685 \end{bmatrix} \begin{bmatrix} q \\ \theta \\ u_B \\ w_B \end{bmatrix} + \begin{bmatrix} -2.4360 & 0.6131 \\ 0 & 0 \\ 0.1871 & 19.6200 \\ -6.4784 & 0 \end{bmatrix} \begin{bmatrix} \delta_T \\ \delta_{TH} \end{bmatrix} \quad (2.39)$$

$$\begin{bmatrix} q \\ n_z \\ w_V \\ V_A \end{bmatrix} = \begin{bmatrix} 1.0000 & 0 & 0 & 0 \\ -0.2661 & 0 & -0.0230 & -0.0681 \\ 0 & -79.8667 & -0.0289 & 0.9996 \\ 0 & 0 & 0.9996 & 0.0295 \end{bmatrix} \begin{bmatrix} q \\ \theta \\ u_B \\ w_B \end{bmatrix} \quad (2.40)$$

The four state variables are the pitch rate  $q$ , the pitch angle  $\theta$ , the  $x$  component of the inertial velocity in body-fixed reference frame  $u_B$ , and the  $z$  component of the inertial velocity in body-fixed reference frame  $w_B$ . The two control variables are the tailplane deflection  $\delta_T$  and the throttle position  $\delta_{TH}$ . The latter variable is the sum of the individual engine commands,  $\delta_{TH} = \delta_{TH1} + \delta_{TH2}$ . We take into account four measurements: the pitch rate  $q$ , the vertical load factor  $n_z$ , the  $z$  component of vertical velocity in the vehicle-carried vertical frame  $w_V$  and the airspeed  $V_A$ .

## 2.3.2 Analysis

Typically an open loop linear aircraft model with a classical configuration exhibits two longitudinal modes: the short period and the phugoid. The former is fast and oscillatory and takes place at nearly constant speed. It is dominated by angle of attack and pitch rate response [3]. The phugoid is slow, oscillatory and lightly damped and takes place at nearly constant angle of attack. It can be interpreted as a gradual interchange of potential and kinetic energy about the equilibrium altitude and airspeed. It is dominated by  $u_B$ .

	Mode 1	Mode 2
Eigenvalues	$-0.0115 \pm 0.1237i$	$-0.8299 \pm 1.0797i$
Damping	0.0925	0.6094
Freq.(rad/s)	0.1242	1.3618
Rise time (s)	7.94	1.34
Settling time (s)	401.18	5.83

Table 2.1 Modes of the open loop system

Table 2.1 gives the eigenvalues of model 2.39 and some associated parameters. Table 2.2 gives for every eigenvalue the absolute values of the components of the corresponding normalised eigenvector. We can see that mode 1 is strongly coupled with  $u_B$  and much less so with  $w_B$ . Mode 2 is strongly coupled with  $w_B$  and slightly with  $u_B$ . Obviously, we can associate mode 1 with the phugoid and mode 2 with the short period.

Eigenvalue	$-0.0115 \pm 0.1237i$	$-0.8299 \pm 1.0797i$
$q$	0.0016	0.0140
$\theta$	0.0129	0.0103
$u_B$	0.9887	0.0154
$w_B$	0.1496	0.9997

Table 2.2 Absolute value of the components of the eigenvectors of the open loop system

We analyse next the coupling of the modes with the inputs and the outputs. In equation 2.12 the vectors  $Cv_i$  and  $w_i^T B$  represent the strength of the coupling of the  $i$ th-mode with the output and the input, respectively. Table 2.3 shows the absolute values of the vectors  $Cv_i$ .

	Phugoid	Short Period
Outputs	$-0.0115 \pm 0.1237i$	$-0.8299 \pm 1.0797i$
$q$	0.0016	0.0140
$n_z$	0.0130	0.0680
$w_V$	1.0022	0.4948
$V_A$	0.9838	0.0447

Table 2.3 Absolute value of the components of the vectors  $Cv_i$

If we pay attention to the rows of Table 2.3, we can see that  $n_z$  undergoes a stronger influence from the short period than from the phugoid;  $w_V$  is highly influenced by both modes, but somewhat more by the phugoid; and finally,  $V_A$  is affected almost exclusively by the phugoid.

Table 2.4 shows the coupling of the modes with the input. On examining the columns we see that the throttle input has almost the same coupling with both the phugoid and the short period, but the tailplane input has a stronger coupling with the short period than with the phugoid. If we pay attention to the rows, we can see that the tailplane input has a larger influence on the modes than the throttle input, specially in the short period.

Modes	$\delta_T$	$\delta_{TH}$
$-0.0115 \pm 0.1237i$	33.4	14.4
$-0.8299 \pm 1.0797i$	87.5	21.0

Table 2.4 Absolute value of the components of the vectors  $w_i^T B$

### 2.3.3 Controller design

An output feedback gain matrix is now computed by using eigenstructure assignment. Since there are four outputs and two inputs, we are able to modify the four closed loop eigenvalues and to assign two elements to each of the four eigenvectors.

Table 2.5 gives the desired closed loop poles and some associated parameters.

	Phugoid	Short Period
Eigenvalues	$\lambda_{1,2} = -0.4376 \pm 0.0624i$	$\lambda_{3,4} = -0.9059 \pm 0.4388i$
Damping	0.990	0.900
Freq. (rad/s)	0.44	1.00
Rise time (s)	7.8	3.0
Settling time (s)	15.0	6.0

Table 2.5 Desired closed loop eigenvalues

The desired eigenvectors are shown below where the symbol "x" means an unspecified component. We chose the phugoid eigenvectors  $v_1, v_2$  so that they couple pitch angle  $\theta$  and perturbed forward velocity  $u_B$  while keeping perturbed vertical velocity  $w_B$  constant. The short period eigenvectors  $v_3, v_4$  are chosen so that they couple  $q$  and  $w_B$  while keeping  $u_B$  constant. Thus we get a satisfactory degree of decoupling between these modes.

Phugoid:

$$v_1 = \begin{bmatrix} x \\ x \\ 1 \\ 0 \end{bmatrix} \quad v_2 = \begin{bmatrix} x \\ 1 \\ x \\ 0 \end{bmatrix} \quad (2.41)$$

Short Period:

$$v_3 = \begin{bmatrix} x \\ x \\ 0 \\ 1 \end{bmatrix} \quad v_4 = \begin{bmatrix} 1 \\ x \\ 0 \\ x \end{bmatrix} \quad (2.42)$$

The feedback gain can be computed with the following commands

```
E =[-0.4376 - 0.0624i
     -0.4376 + 0.0624i
     -0.9059 - 0.4388i
     -0.9059 + 0.4388i];
```

```
x=-1;
```

```
Ev=[x x x 1
     x 1 x x
     1 x 0 0
     0 0 1 x];
```

```
K=eigenas(E,Ev,A,B,C)
```

```
K=
```

```
-0.4055  0.1802  0.0096 -0.0051
-2.2142  0.4781  0.0427 -0.0229
```

where A, B and C are the matrices of the model given in 2.39 and 2.40. The MATLAB function `eigenas` can be found in appendix A.

The closed loop eigenvalues as obtained and the absolute value of the normalised eigenvectors are given in Table 2.6. We can see that the eigenvalues we obtain are the desired ones and that an exact decoupling between  $u_B$  and  $w_B$  has been achieved.

	Phugoid	Short Period
Eigenvalue	$-0.4376 \pm 0.0624i$	$-0.9059 \pm 0.4388i$
$q$	0.0023	0.0066
$\theta$	0.0052	0.0066
$u_B$	1.0000	0.0000
$w_B$	0.0000	1.0000

Table 2.6 Eigenvalues and absolute values of the normalised eigenvectors for the closed loop system

### 3 Controller architecture

#### 3.1 Introduction

We make use of the classical approach consisting in splitting up the controller into two parts: a longitudinal and a lateral controller. Both of them have been designed in two stages: the inner loop and the outer loop. The function of the inner loop is to make the aircraft easy and pleasant to fly, and it is often called a stability augmentation system. However, the outer loop function is to replace the pilot for certain flight manoeuvres such as maintaining height and speed, turning onto a specified heading, climbing at a specified rate, etc.

The overall controller architecture is shown as a SIMULINK diagram in Figure 3.1. Figures 3.2 and 3.3 show the structure of the longitudinal controller; and figures 3.4 and 3.5 show the structure of the lateral controller.

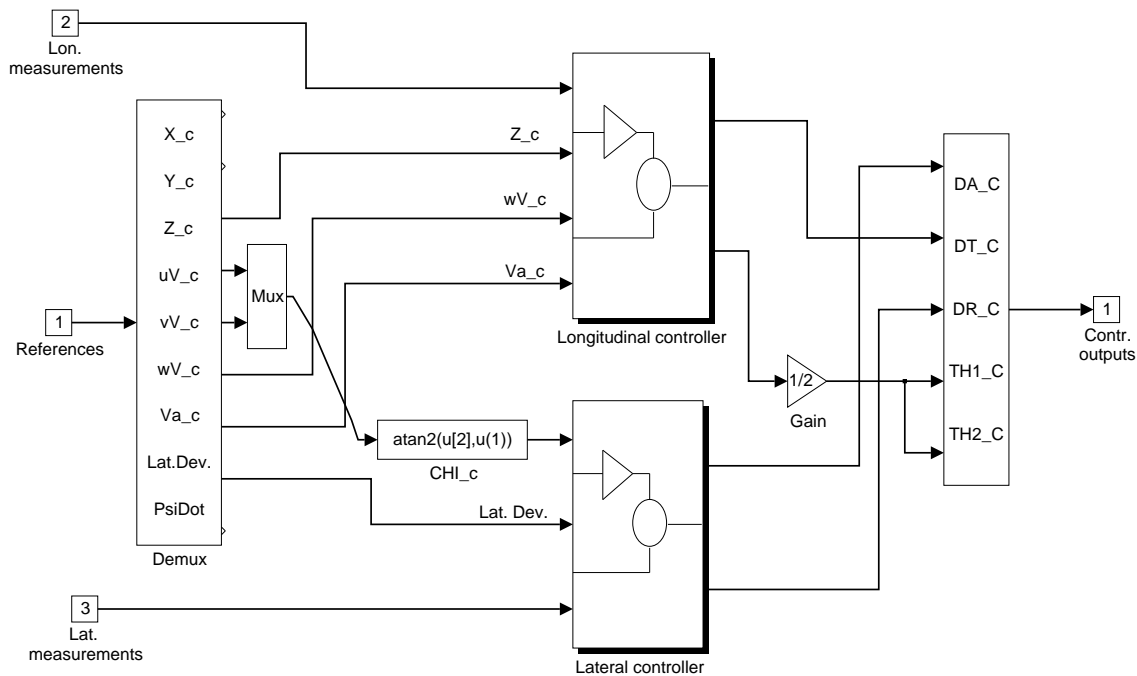


Fig.3.1 The overall controller structure

#### 3.2 Longitudinal Controller

The choice of the signals to be used in a design is based on the analysis of the system, the specifications and the design method.



### 3.2.1 Measurement Signals

The longitudinal model has 7 measurements available, but in designing the controller we have not taken into account the total inertial velocity. Table 3.1 shows the measurements as used by the longitudinal controller.

Inner Loop controller	
$q$	Pitch rate
$n_x$	Horizontal load factor
$n_z$	Vertical load factor
$w_V$	$z$ component of inertial velocity
$V_A$	Air speed
Outer Loop controller	
$z$	$z$ position of aircraft CoG

Table 3.1 Longitudinal measurements used

Although in the inner loop only four measurements are needed to assign four eigenvalues, two for the short period and two for the phugoid, we make use of five in order to prevent one eigenvalue of the actuators from becoming unstable. In section 5.1 such a selection is accounted for in full detail.

Lastly, the outer loop provides altitude tracking by adding a feedback of the altitude  $z$ .

### 3.2.2 Actuator Signals

These signals are the elevator deflection or tailplane deflection  $\delta_T$ , and throttle position  $\delta_{TH}$ .

### 3.2.3 Reference Signals

The selection of signals chosen as references has been guided by the specifications given as design criteria, see section 4.2. The selected ones have been the reference velocity  $w_{Vc}$  and the reference airspeed  $V_{Ac}$  for the inner loop, and the reference position  $z_C$  for the outer loop.

### 3.2.4 Controller Structure

The inner loop controller has two parts: a static gain acting on the five chosen measured signals and a static gain acting on the integral of the errors in the commanded variables  $w_V$  and  $V_A$  to eliminate steady state errors. The two integrators result in two additional states that must be incorporated into the linear model for the controller design.

The outer loop has a proportional action acting on the altitude error. No integral action is

needed here to avoid steady state errors relating to altitude step commands or disturbances since the altitude dynamics include a pole at the origin. The output of the outer loop acts as a reference for  $w_V$ .

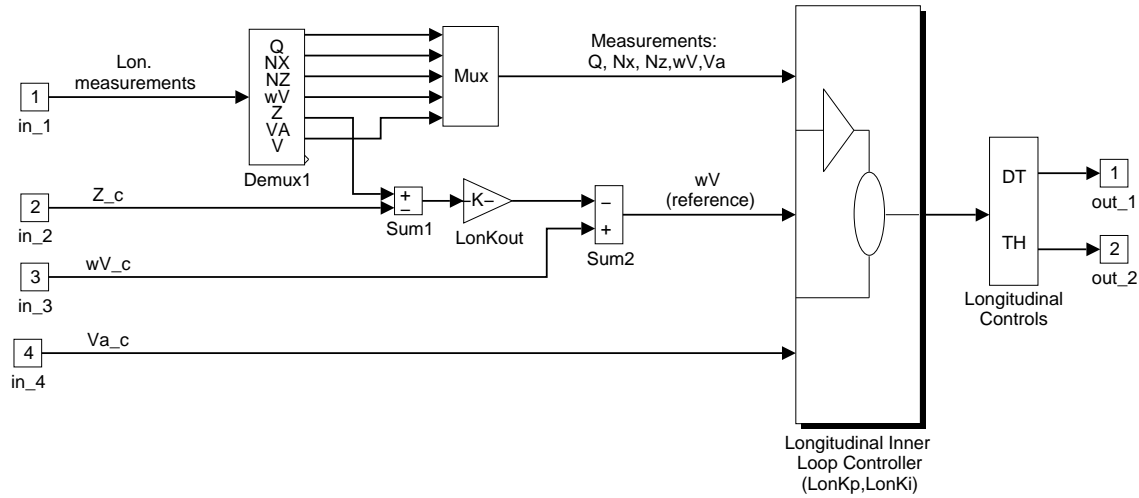


Fig.3.2 Longitudinal controller

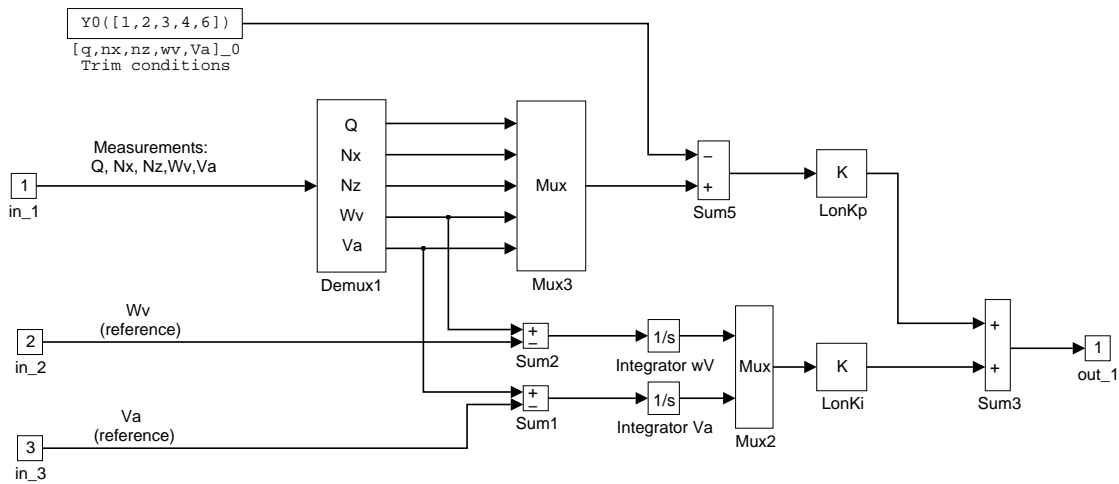


Fig.3.3 Longitudinal inner loop controller

### 3.3 Lateral Controller

The lateral controller has a structure analogous to the longitudinal controller.

#### 3.3.1 Measurement Signals

The longitudinal model has 8 measurements available, but in designing the controller we made use of only 5 for the inner loop, and the lateral deviation of the aircraft for the outer loop. Table 3.2 shows the measurements as used by the lateral controller.

Inner Loop controller	
$\beta$	Angle of sideslip
$p$	Roll rate
$r$	Yaw rate
$\phi$	Roll angle
$\chi$	Inertial track angle
Outer Loop controller	
$\Delta y$	Lateral deviation

Table 3.2 Lateral measurements used

#### 3.3.2 Actuator Signals

These signals are the aileron deflection  $\delta_a$ , and rudder deflection  $\delta_R$ .

#### 3.3.3 Reference Signals

The selection of references has been guided by the specifications given as design criteria, see section 4.2. Those selected have been the reference position  $y_C$  for the outer loop, and the inertial track angle  $\chi_C$  and sideslip angle  $\beta_C$  for the inner loop.  $\chi_C$  is not given as a reference signal but it is obtained from the reference velocity components  $u_C$  and  $v_C$  as  $\text{atan}(v_C/u_C)$ .  $\beta_C$  has a null constant reference value in order to keep always  $\beta$  close to zero.

#### 3.3.4 Controller Structure

The inner loop controller has two parts: a static gain acting on the five chosen signals measured and a static gain acting on the integral of the errors in the commanded variables  $\chi$  and in the sideslip angle to eliminate steady state errors. The introduction of two integrators results in two additional states that must be incorporated into the linear model for the controller design.

The outer loop has a proportional action acting on the lateral error. No integral action is required here to avoid steady state errors relating to lateral step commands or disturbances since the lateral dynamics include a pole at the origin. The output of the outer loop acts as a reference for the inertial track angle.

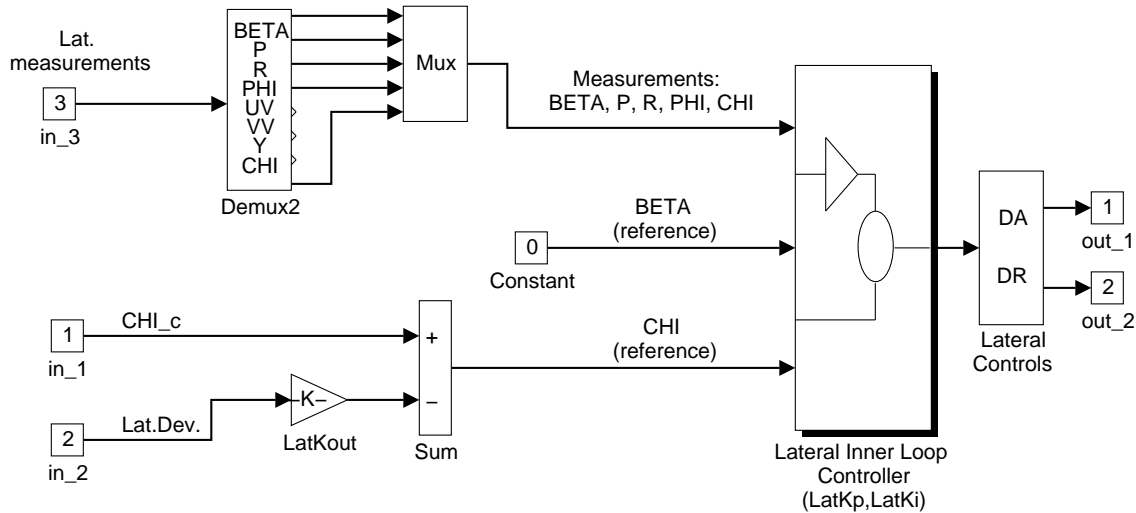


Fig.3.4 Lateral controller

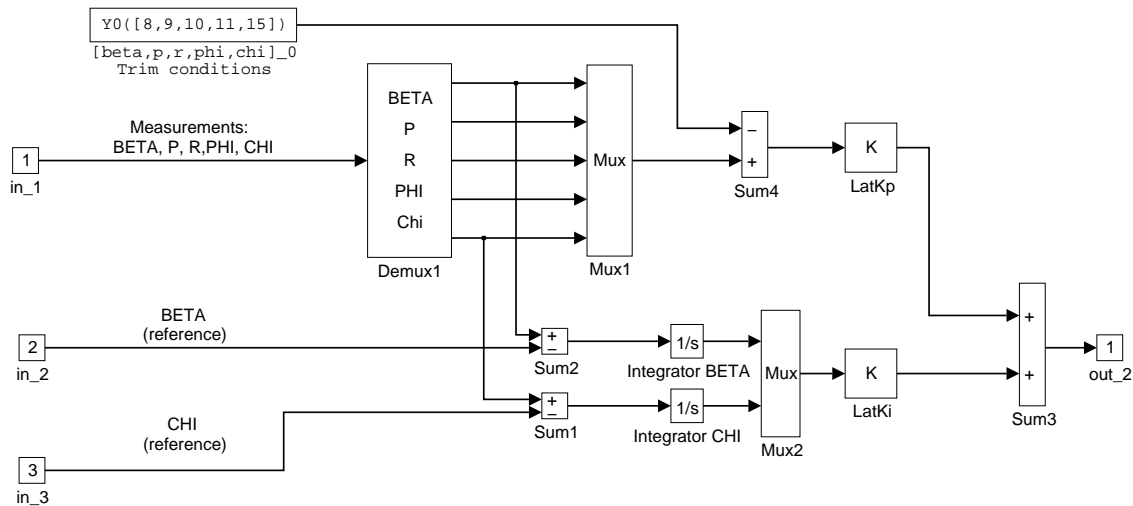


Fig.3.5 Lateral inner loop controller

## 4 The Translation of RCAM design criteria into method dependent objectives

### 4.1 Introduction

Out the five classes of design criteria given in [2] for the RCAM design, the performance criteria are the most significant. These criteria are given in terms of transient response characteristics to command signals and cross coupling constraints. The main characteristic of the eigenstructure assignment method is that it allows the designer to directly satisfy specifications in terms of transient response and mode decoupling. Then, these are the most suitable criteria to be used as a guide in the design phase.

Our design has been based only on these criteria, but we made use of linear and non-linear closed loop time responses and robust analysis tools as a guide in the selection of the eigenstructure.

### 4.2 Performance Criteria

The performance criteria can be classified into two groups: longitudinal and lateral. We discuss separately for every group the way in which the specifications have been incorporated into the design.

#### 4.2.1 Longitudinal Specifications

There are command response specifications in terms of overshoot, rise time and settling time for three commanded signals: airspeed, flight path angle and altitude. These specifications provide a lower limit for the damping ratio and natural frequency of second order modes and for the time constant of first order modes coupled with the signals. There are additional specifications that we give separately.

##### 4.2.1.1 Airspeed

- Design criteria.
  - The controlled system airspeed,  $V_A$ , should be able to track speed commands,  $V_{Ac}$ , with  $t_r < 12$  s,  $t_s < 45$  s and  $M_p < 5$  %.
  - In the presence of a wind step with an amplitude of 13 m/s there should be no deviation in the airspeed larger than 2.6 m/s after 15 s.
  - There should be no steady state error due to constant wind disturbances.

As can be seen in table 5.3, the airspeed is strongly coupled with the phugoid mode and very lightly coupled with the short period mode, so that we translate the transient response specifications to a speed command and to a wind step perturbation into specifications for the desired phugoid mode.

An airspeed error integrator is introduced to avoid steady state errors just in case of wind step disturbances.

#### 4.2.1.2 Flight path angle

- Design criteria.
  - The commanded flight path angle,  $\gamma_c$ , should be tracked by the actual flight path angle,  $\gamma$ , with  $t_r < 5$  s,  $t_s < 20$  s and  $M_p < 5$  %.

The flight path angle  $\gamma$  is neither available as an output nor as a reference signal. To cope with such a problem we use the relation  $\sin(\gamma) = -w_V/V$ , where  $V$  is the total inertial velocity. In the linearised model  $V = V_A$ ; therefore for constant airspeed the flight path angle may be controlled by means of  $w_V$ . We are thus lead to interpret the specifications in terms of commands in  $w_{Vc}$ .

As may be seen in table 5.3 the  $w_V$  output signal is strongly coupled with both the short period and the phugoid modes. But the short period is dominated by pitch rate and angle of attack and it is lightly coupled with  $V_A$ . Consequently, the flight path angle transient response to a step command imposes limits on the desired short period mode.

We add a vertical velocity error integrator state to get good low-frequency tracking.

#### 4.2.1.3 Altitude

- Design criteria.
  - The controlled system should be able to track altitude commands,  $h_c$ , with  $t_r < 12$  s,  $t_s < 45$  s and  $M_p < 5$  %.

We add an outer loop for tracking the reference altitude. A signal proportional to the altitude error is used as a reference signal for  $w_V$ . The proportional gain is calculated using the root locus method, in such a way that it fulfils the transient criteria. The altitude is not included in the inner loop because there exists a similar state with a faster dynamics: the velocity error integrator state.

#### 4.2.1.4 Cross coupling between airspeed $V_A$ and altitude $h$

- Design criteria.
  - For a step in commanded altitude  $h_c$  of 30 m,  $|V_A - V_{Ac}| < 0.5$  m/s.
  - For a step in commanded airspeed  $V_{Ac}$  of 13 m/s,  $|h - h_c| < 10$  m.

This specification may be obtained by decreasing cross-coupling between  $V_A$  and  $w_V$ .

#### 4.2.2 Lateral Specifications

There are now two command signals specifications in terms of transient response characteristics that may be transformed into bounded eigenvalues. The remaining specifications are given in terms of behaviour in case of engine failure and under disturbances.

##### 4.2.2.1 Heading angle response

- Design criteria.
  - The commanded heading angle,  $\psi_c$ , should be tracked by the actual heading angle,  $\psi$ , with  $t_r < 10$  s,  $t_s < 30$  s and  $M_p < 5$  %.

The heading angle is a lateral motion state but it is neither available as an output nor as a reference. Instead we make use of the inertial track angle that is an output signal and is related to the heading angle by means of the equation  $\chi = \psi + \beta_V$ . Although there is no reference signal for  $\chi$  such a signal may be obtained from the reference velocity components  $u_C$  and  $v_C$  by means of equation  $\chi_C = \tan^{-1}(v_C/u_C)$ .

An integrator is introduced to eliminate sideslip errors, where the command signal for  $\beta$  is chosen as 0. In so doing we cope with the safety criteria of keeping  $\beta$  minimised at every time.

An inertial track angle error integrator is also introduced in order to avoid heading angle steady state errors.

##### 4.2.2.2 Lateral deviations

- Design criteria.
  - The controlled aircraft's lateral deviation, defined as the difference between the actual and commanded lateral aircraft position,  $e_{yb} = y(t) - y_c(t)$ , should be reduced to 10 % within 30 s.
  - In response to a unit step in lateral command signal  $M_p < 5$  %.
  - There should be no steady state error due to constant lateral wind disturbances.

The lateral deviation is controlled in the outer loop. A signal proportional to the lateral error is used as a reference signal for the inertial track angle. The proportional gain is calculated using the root locus method, in such a way that it fulfils the transient criteria. No integral action to avoid steady state error in the presence of constant disturbances is needed here, because the heading state already introduces an integrator into the loop.

##### 4.2.2.3 Engine failure

- Design criteria.

- In case of engine failure in still air  $\phi$  should not exceed 10 *deg*; its maximum steady state deviation should not exceed 5 *deg*. When the failed engine is restarted the roll angle should be reduced to zero with  $M_p < 50\%$ .
- Sideslip angle  $\beta$  should be minimised.
- The maximum heading rate,  $\dot{\psi}$ , should be less than 3 *deg/sec*.

These requirements can not be easily interpreted in terms of eigenvalues and eigenvectors specifications and shall not be tested before the phase of analysis of simulation results. However, the requirement of keeping sideslip angle to a minimum in case of engine failure can be translated into a specification of decoupling between the eigenvalues related with the roll motion and those related with the lateral velocity.

### 4.3 Robustness Criteria

The eigenstructure method is not a robust control method and, although many different algorithms have been proposed to enhance the robustness, no method will be used here. However, we make use of the stability margins given in section 2.1.9 to measure the robustness of the feedback system. For a chosen eigenstructure the stability margins are measured and the eigenstructure changed to get better stability margins. After a few steps a suitable eigenstructure is selected.

The ride quality criteria, safety criteria and control activity criteria can not be incorporated in an *ad hoc* manner into the eigenstructure method. As done with robustness, they will be analysed in the course of the analysis of results phase and physical relations between their behaviour and the eigenstructure achieved will be established to try to cope with them. In the election of the eigenvalues we should have in mind to assign the mode values close to the open loop aircraft modes to minimise the control activity.



## 5 The description of the design cycle

The design cycle is summarised in the following schema

1. Analysis of the linear and non-linear model of the plant.
2. Selection of the eigenstructure and gain calculation.
3. Analysis of the open and closed loop system (linear and non linear model).
4. Robustification procedure (iterate).
5. Iterate 1 - 4.

As we have seen in the previous section, among all the design criteria only those of the performance criteria related to the transient response of the system can be interpreted almost directly in terms of eigenstructure. The rest of them must be analysed after an eigenstructure has been chosen and the controller found. From this analysis another eigenstructure will be chosen and so on. That will be the most consuming time task. A robustification procedure or any other form of "optimal" solution may help to break the iterative procedure.

We explain now the method we have used to select an eigenstructure.

- we analyse the design criteria and the coupling of the modes of the plant with the states, the inputs and the outputs. This analysis is used as a guide in choosing the outputs for feedback and the eigenstructure. After selecting the outputs to be used for feedback the integrators are added to the loop.
- we chose a set of eigenvalues that fulfil the transient response limits in accordance with the requirements and are close to the natural aircraft modes. After that, their associated eigenvectors are chosen to get the desired decoupling between the modes.
- With the eigenstructure chosen we compute the feedback gain and analyse:
  - the stability (since one of the non assigned eigenvalues might become unstable or badly damped) and the stability margins
  - the time response of the system
  - the decoupling of the obtained modes

Now the cycle begins. New outputs and/or eigenstructure must be chosen to improve the results obtained. We have first selected an eigenstructure that provides acceptable design criteria. We have tested different eigenvalues with fixed eigenvectors. Once the eigenvalues that give better stability margins have been chosen, the eigenvectors have been changed trying to improve robustness and, when necessary, decoupling. After a few steps we convinced ourselves that the eigenvectors chosen could not be improved.

## 5.1 Longitudinal controller

### 5.1.1 Analysis of the linear longitudinal model of the plant

#### 5.1.1.1 Longitudinal model

The non-linear model is used to generate linear models for control law design and to generate non-linear time histories for evaluating control designs. Once a trim condition is established for the non-linear aircraft model within the simulation environment, a linear model is generated to capture the perturbational dynamics around the equilibrium point. Equation 5.1 shows the longitudinal linear model obtained when it is linearised around the following states:  $V = 80 \text{ m/s}$ ,  $h = 1000 \text{ m}$ ,  $mass = 120000 \text{ kg}$ ,  $cgx = 0.23$  and  $cgz = 0.1$ . The aerodynamic model is augmented with first order actuator models. The states are the pitch rate  $q$ , the pitch angle  $\theta$ , the  $x$  component of the inertial velocity in body-fixed reference frame  $u_B$ , the  $z$  component of the inertial velocity in body-fixed reference frame  $w_B$ , the state corresponding to the first order tailplane model  $X_T$  and the state corresponding to the first order engine model  $X_{TH}$ . This last state is the sum of the individual engine commands,  $X_{TH} = X_{TH1} + X_{TH2}$ .

$$\begin{aligned}
 \begin{bmatrix} \dot{q} \\ \dot{\theta} \\ \dot{u}_B \\ \dot{w}_B \\ \dot{X}_T \\ \dot{X}_{TH} \end{bmatrix} &= \begin{bmatrix} -0.9817 & 0 & -0.0007 & -0.0153 & -2.4360 & 0.6131 \\ 1.0000 & 0 & 0 & 0 & 0 & 0 \\ -2.2343 & -9.7754 & -0.0325 & 0.0744 & 0.1871 & 19.6200 \\ 77.3559 & -0.7727 & -0.2261 & -0.6685 & -6.4784 & 0 \\ 0 & 0 & 0 & 0 & -6.6667 & 0 \\ 0 & 0 & 0 & 0 & 0 & -0.6667 \end{bmatrix} \begin{bmatrix} q \\ \theta \\ u_B \\ w_B \\ X_T \\ X_{TH} \end{bmatrix} + \begin{bmatrix} 0 & 0 \\ 0 & 0 \\ 0 & 0 \\ 0 & 0 \\ 6.67 & 0 \\ 0 & 0.67 \end{bmatrix} \begin{bmatrix} \delta_T \\ \delta_{TH} \end{bmatrix} \\
 \begin{bmatrix} q \\ n_x \\ n_z \\ w_V \\ V_A \end{bmatrix} &= \begin{bmatrix} 1.0000 & 0 & 0 & 0 & 0 & 0 \\ 0.0077 & 0 & -0.0033 & 0.0076 & 0.0191 & 2.0000 \\ -0.2661 & 0 & -0.0230 & -0.0681 & -0.6604 & 0 \\ 0 & -79.8667 & -0.0289 & 0.9996 & 0 & 0 \\ 0 & 0 & 0.9996 & 0.0295 & 0 & 0 \end{bmatrix} \begin{bmatrix} q \\ \theta \\ u_B \\ w_B \\ X_T \\ X_{TH} \end{bmatrix} \quad (5.1)
 \end{aligned}$$

These system matrices will be represented as  $A$ ,  $B$  and  $C$ . Matrix  $D$  is a 5-by-2 matrix of zeros and has been left out.

There are seven measured signals available as inputs to the controller. However only five are shown in 5.1 since in the linearised model one of them, the  $z$  position of aircraft centre of gravity in earth-fixed reference frame is always zero, and the total inertial velocity  $V$  is equal to the air speed measurement.

The remaining measurements are: pitch rate  $q$ , horizontal load factor  $n_x$ , vertical load factor  $n_z$ ,  $z$  component of vertical velocity in the vehicle-carried vertical frame  $w_V$  and air speed  $V_A$ .

Table 5.1 gives the eigenvalues and some associated parameters of model 5.1. There are four modes. Modes 1 and 2 correspond, as we have already seen in section 2.3, to the phugoid and the short period, respectively, and modes 3 and 4 correspond to the actuators (throttle and tailplane, respectively).

Useful information for the design phase can be obtained by studying the coupling of the plant modes with the states, the outputs and the inputs signals.

	Mode 1	Mode 2	Mode 3	Mode 4
Eigenvalues	$-0.0115 \pm 0.1237i$	$-0.8299 \pm 1.0797i$	-0.6667	-6.6667
Damping	0.0926	0.6094	-	-
Freq.(rad/s)	0.1242	1.3618	-	-
Rise time(s)	7.9	1.30	3.30	0.33
Settling time(s)	400	5.83	6.91	0.69

Table 5.1 Modes of the open loop system including actuators

### 5.1.1.2 Coupling of the modes with the states

Table 5.2 gives, for every eigenvalue  $\lambda_i$ , the absolute values of the components of the corresponding normalised right eigenvector,  $v_i$ . Looking at the column of a selected mode we get information about the coupling of this mode with the state components. But if a row of the table is examined, we get information about the coupling of every mode with the selected component.

Mode	Phugoid	Short Period	Throttle	Tailplane
$q$	0.0016	0.0140	0.0018	0.0940
$\theta$	0.0129	0.0103	0.0026	0.0141
$u_B$	0.9887	0.0154	0.6155	0.0154
$w_B$	0.1496	0.9997	0.7879	0.9695
$X_T$	0	0	0	0.2253
$X_{TH}$	0	0	0.0180	0

Table 5.2 Absolute value of the components of the eigenvectors of the open loop system including actuators

We can see in the table that:

- The phugoid is strongly coupled with  $u_B$  and less so with  $w_B$  (in the ratio of 7)
- The short period is strongly coupled with  $w_B$  and slightly with  $u_B$  (in the ratio of 650)
- $q$  has a stronger coupling with the short period than with the phugoid (in the ratio of 9)
- $\theta$  has almost the same coupling with both modes
- The throttle has almost the same coupling with both  $u_B$  and  $w_B$ , so it has almost the same coupling with the short period than with the phugoid
- The tailplane has a stronger coupling with  $w_B$  than with  $u_B$ , so it has a stronger coupling with the short period than with the phugoid.

We may conclude that the phugoid is mainly an aerodynamic velocity mode and the short period dominates the angle of attack and the pitch rate.

### 5.1.1.3 Coupling of the modes with the outputs and the inputs

Table 5.3 shows the absolute values of the vectors  $Cv_i$ .

Mode	Phugoid	Short Period	Throttle	Tailplane
$q$	0.0016	0.0140	0.0018	0.0940
$n_x$	0.0044	0.0075	0.0440	0.0024
$n_z$	0.0130	0.0680	0.0390	0.1081
$w_V$	1.0022	0.4948	0.5952	0.1560
$V_A$	0.9838	0.0447	0.5920	0.0132

Table 5.3 Absolute value of the components of the vectors  $Cv_i$  including actuators

We can see in this table that:

- The phugoid is strongly coupled with  $w_V$  and  $V_A$ , with practically the same strength; but, while the short period is slightly coupled with  $V_A$ , it is strongly coupled with  $w_V$ .
- $n_z$  has a stronger coupling with the short period than the phugoid has (in the ratio of 5), and with the tailplane than with the throttle (in the ratio of 2.8).
- $n_x$  has almost the same coupling with both the short period and the phugoid (in the ratio of 1.7), and has a stronger coupling with the throttle than with the tailplane (in the ratio of 18).

We might conclude that the best representatives of the short period would be  $q$  and  $n_z$ , and that the best representative of the phugoid would be  $V_A$ , whereas  $w_V$  and  $n_x$  show rather similar coupling with both modes. After analysing tables 5.2 and 5.3 we are tempted to translate the limits in the transient response specifications on the airspeed into specifications for the desired phugoid mode, and the limits in the transient response specifications on the flight path angle into specifications for the desired short period mode, and at the same time the required decoupling between airspeed and altitude can be achieved by reducing the coupling of  $w_V$  with the phugoid mode.

Of course, this is the result of a primary analysis but we shall have to wait and see the results to ascertain that our conclusions are right.

Finally, table 5.4 shows the coupling of the modes with the input. Examining the columns we can see that the throttle input has almost the same coupling with both the phugoid and the short period, but the tailplane input has a stronger coupling with the short period than with the phugoid (these conclusions were also obtained from table 5.2). Moreover, we can see that the tailplane input has a larger influence on the modes than the throttle input has.

Modes	$\delta_T$	$\delta_{TH}$
Phugoid	33.4	14.4
Short Period	98.2	12.8
Throttle	0	36.9
Tailplane	29.6	0

Table 5.4 Absolute value of the components of the vectors  $w_i^T B$  including actuators

#### 5.1.1.4 Outputs selection

As has been said in section 2.6.1 we can specify as many closed loop eigenvalues as outputs for feedback are used. Therefore, only four measurements are needed to specify the phugoid and short period modes. If the five measurements are used, one of the actuators modes may be specified.

At first, we chose for feedback four measurements ( $q$ ,  $n_z$ ,  $w_V$  and  $V_A$ ) in order to specify only the eigenvalues of the short period and the phugoid modes. However, we found that the slower mode of the actuators (that of the throttle) had become unstable, and this also happened for any other choice of four outputs measurements for feedback. Therefore, in the final design we make use of five output measurements and, in addition to the short period and phugoid eigenstructures, we specify the closed loop eigenvalue and eigenvector of the throttle mode.

#### 5.1.1.5 Integrators selection

For the longitudinal motion the performance criteria require the control system to track step commands for altitude, flight path angle and airspeed. The first will be handled in the outer loop, and the last two are handled by introducing integral action on the errors of the commanded variables (section 4.2). Therefore, two integrated error states are added to the linearised model, one for  $w_V$  to cope with flight path angle commands, and another for  $V_A$ . The number of outputs is now increased by two and the eigenvalues for the modes of the integrators may be specified.

#### 5.1.2 Inner loop controller design

Before calculating the feedback static gain matrix, the maximum allowed transport time delay of 0.10 s is added to the model with a first order Padé approximation. Then, we augment the open loop system matrices with the two integrated error states. To do that we use the MATLAB function `SSINTEG`, that can be found in the appendix. In this function the input parameters are the original system and a vector specifying the outputs where the integrators are going to be placed; the outputs are the matrices of the augmented system.

```
lon=pck(A,B,C,D);
[numdel,dendel]=pade(.1,1);
```

```

delay1=nd2sys(numdel,dendel);
lon1=mmult(lon,daug(delay1,delay1));
[A1,B1,C1,D1]=unpck(lon1);
[A2,B2,C2,D2]=ssinteg(A1,B1,C1,D1,[4 5]);
    
```

Mode	Phugoid	Short Period	Throttle	$\int w_V$	$\int V_A$
Eigenvalues	-0.4376 $\pm 0.0624i$	-0.9059 $\pm 0.4388i$	-0.5	-2.0000	-1.9000
$q$	x x	1 x	x	x	x
$\theta$	x 1	x x	x	x	x
$u_B$	1 x	0 0	x	0	x
$w_B$	0 0	x 1	x	x	0
$X_T$	x x	x x	x	x	x
$X_{TH}$	x x	x x	1	x	x
$delay \delta_T$	x x	x x	x	x	x
$delay \delta_{TH}$	x x	x x	x	x	x
$\int w_V$	0 0	x x	x	1	0
$\int V_A$	x x	0 0	x	0	1

Table 5.5 Desired eigenstructure of the longitudinal closed loop system

Table 5.5 shows the eigenstructure chosen for the system. The short period and the phugoid modes are those given in section 2.3. The desired closed loop mode for the throttle is chosen a little smaller than its open loop value. The integral tracking modes have been chosen faster than the other modes. Of course, these values are not the first we tested, but the result of testing different values in the way explained in the introduction. The eigenvectors have been chosen so that  $V_A$  and  $w_V$  are as uncoupled as possible:

- In the phugoid eigenvectors the pitch angle and the forward velocity are coupled together while vertical velocity and  $w_V$  integrated error are set to zero.
- In the short period eigenvectors the vertical velocity and the pitch rate are coupled together while the forward velocity and  $V_A$  integrated error are set to zero.
- In the throttle eigenvector its state component is emphasised and the remainder are unspecified.
- In the  $w_V$  integral tracking mode its state component is emphasised while, like in the short period mode, forward velocity and  $V_A$  integrated error are set to zero.
- In the  $V_A$  integral tracking mode its state component is emphasised while, as in the phugoid mode, vertical velocity and  $w_V$  integrated error are set to zero.

The feedback gain matrix is computed by means of eigenstructure assignment algorithm to be found in the MATLAB function **EIGENAS** given in Appendix A.

The inputs to the functions are the desired eigenstructure and the system matrices. The eigenstructure is introduced by means of a vector with the desired eigenvalues and a matrix with the desired eigenvectors as shown in table 5.5.

The inner loop controller gain is then determined by

```

E =[-0.4376 - 0.0624i
     -0.4376 + 0.0624i
     -0.9059 - 0.4388i
     -0.9059 + 0.4388i
     -0.5000
     -2.0000
     -1.9000];

x = -1;
Ev=[x  x  1  x  x  x  x
     x  1  x  x  x  x  x
     1  x  0  0  x  0  x
     0  0  x  1  x  x  0
     x  x  x  x  x  x  x
     x  x  x  x  1  x  x
     x  x  x  x  x  x  x
     x  x  x  x  x  x  x
     0  0  x  x  x  1  0
     x  x  0  0  x  0  1];

K=eigenas(E,Ev,A2,B2,C2);

K=
  0.4755    0.0532   -0.0838   -0.0169   -0.0055   -0.0033   -0.0014
  0.0455   -1.3063   -0.3047   -0.0152   -0.1221    0.0004   -0.0227

```

The gains of the inner loop controller in figure 3.3 are:

```

LonKp = K(:,1:5);
LonKi = K(:,6:7);

```

### 5.1.3 Analysis of the closed inner loop

Table 5.6 shows the eigenvalues of the closed loop system and the way the obtained closed loop eigenvectors appear in the outputs, and Table 5.7 shows the absolute values of the components of  $Cv_i$  for the open loop. Before comparing both tables we must note that the introduction of the integrators has changed the way the coupling between the phugoid and the short period becomes apparent. In Table 5.3 (which shows the coupling before introducing the integrated error states) there is a strong coupling of both modes with  $w_V$ , and we can see in Table 5.7 that there is a strong coupling of both modes with  $w_V$  integrated error state,  $\int w_V$ .

Comparing the results given in Table 5.6 with those given in Table 5.7, we can see that the coupling of the phugoid with  $\int w_V$  has been greatly reduced and so has the coupling with  $w_V$ , while the coupling with  $V_A$  and  $\int V_A$  has been increased. Moreover, the effect of

Mode	Phugoid	Short Period	Throttle	$\int w_V$	$\int V_A$	Tailplane
Eigenvalues	-0.4376 $\pm 0.0624i$	-0.9059 $\pm 0.4388i$	-0.5	-2.0000	-1.9000	-2.4880
$q$	0.0007	0.0056	0.0003	0.0181	0.0008	0.0252
$n_x$	0.0196	0.0057	0.0183	0.0060	0.1708	0.0127
$n_z$	0.0014	0.0539	0.0138	0.0533	0.0066	0.0464
$w_V$	0.0166	0.5291	0.2814	0.2658	0.0083	0.1878
$V_A$	0.4014	0.0126	0.3386	0.0234	0.8804	0.0042
$\int w_V$	0.0376	0.5257	0.5628	0.1329	0.0044	0.0755
$\int V_A$	0.9081	0.0125	0.6773	0.0117	0.4634	0.0017

Table 5.6 Inner closed loop eigenvalues and absolute values of the components of vectors  $Cv_i$

Mode	Phugoid	Short Period	Throttle	$\int w_V$	$\int V_A$	Tailplane
$q$	0.0001	0.0132	0.0011	0	0	0.0939
$n_x$	0.0004	0.0071	0.0274	0	0	0.0024
$n_z$	0.0011	0.0639	0.0243	0	0	0.1081
$w_V$	0.0883	0.4648	0.3701	0	0	0.1560
$V_A$	0.0867	0.0420	0.3682	0	0	0.0132
$\int w_V$	0.7109	0.3413	0.5552	1	0	0.0234
$\int V_A$	0.6978	0.0308	0.5523	0	1	0.0020

Table 5.7 Open loop absolute values of the components of vectors  $Cv_i$

the short period on  $V_A$ , and  $\int V_A$  has been reduced, and the coupling with  $w_V$  and with  $\int w_V$  has been increased.

This analysis may be useful when comparing the results obtained in dealing with different eigenstructures. However, time responses of the system to step inputs in airspeed and vertical velocity may be more revealing about the coupling between the modes.

### 5.1.3.1 Step in flight path angle

Figure 5.1 shows the response of the linearised closed loop system to a step of 4.2 m/s in commanded vertical velocity  $w_{Vc}$ , corresponding to -3 deg in commanded flight path angle. There is very little cross coupling with airspeed: the maximum deviation in airspeed is smaller than 0.13 m/s. There is no overshoot and the settling time is shorter than the specified 15 s, but the rise time is slightly longer than the specified 5 s and the vertical acceleration  $n_z$  surpasses the specified 0.05g. Decreasing the damping factors of the short period and phugoid modes in order to reduce the rise time leads to higher vertical acceleration and smaller robustness, so the selected eigenvalues are an attempt at establishing a compromise between both aspects.

### 5.1.3.2 Step in airspeed

Figure 5.2 shows the response of the linearised closed loop system to a step of 13 m/s in commanded airspeed  $V_{Ac}$ . The response satisfies all the requirements. The cross coupling to  $w_V$  is very small: the maximum deviation in flight path angle is smaller than 0.2 deg. There is no overshoot, the settling time is well below the specified 45 s, the rise time is



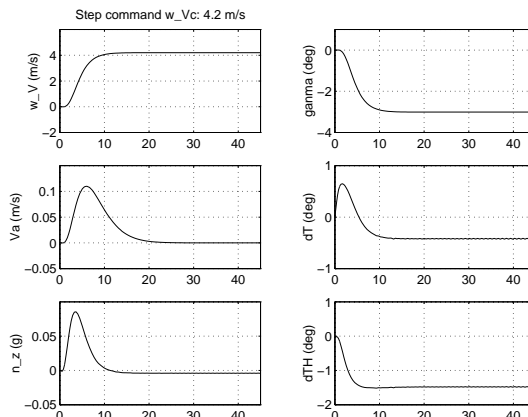


Fig.5.1 Response of the linearised system to a step in commanded flight path angle

shorter than the required 12 s, and the vertical acceleration  $n_z$  remains smaller than the specified  $0.05g$ .

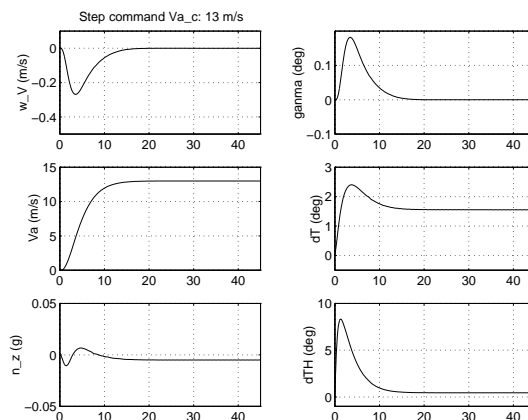


Fig.5.2 Response of the linearised system to a step in commanded airspeed

Figure 5.3 shows the response to a wind step with an amplitude of 13 m/s. The deviation in airspeed is smaller than 2.6 m/s well within 15 s. However the throttle exceeds the saturation limits; therefore in the non-linear model a higher time response may be expected.

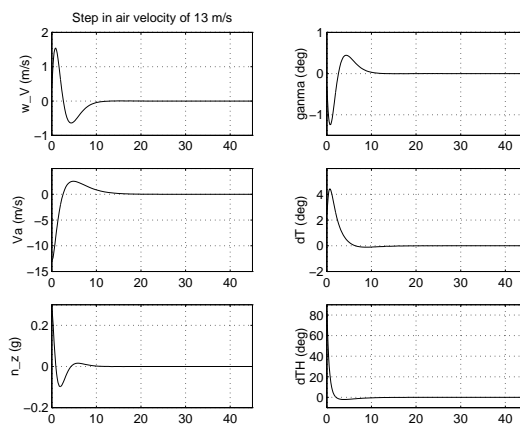


Fig.5.3 Response of the linearised system to a step in air velocity

### 5.1.3.3 Loop stability margins

To obtain a measure of the stability margins the method of section 2.1.9 will be used. Now, in the control diagram of figure 2.1,  $G(s)$  represents the transfer function, from the inputs  $\delta_T, \delta_{TH}$  to the outputs  $w_V, V_A$ , of the linearised longitudinal model with static gain feedback (LonKp) of the output signals.  $H(s)$  represents the transfer function of the integral controller from the commanded output errors ( $\int \Delta w_V, \int \Delta V_A$ ) to the actuators inputs ( $\delta_T, \delta_{TH}$ ).

We make use of the MATLAB function `MXSSV` to compute the maximum singular values of the sensitivity functions  $S, T$  and  $S + T$  at the actuators input and at the sensors output, then we compute the gain and phase margins by means of the function `GFMAR`. Both functions are given in the Appendix A.

```
[mxsi,mxti,mxsti,mxso,mxto,mxsto]=mxssv(A1,B1,C1,LonKp,LonKi,[4 5]);
[lonmgi,lonmfi]=gfmar(mxsi,mxti,mxsti);
[lonmgo,lonmfo]=gfmar(mxso,mxto,mxsto);
```

The results as obtained at the input of the actuators and at the output of the sensor are summarised in table 5.8 and table 5.9, respectively. Figures 5.4 and 5.5 show the singular values plots of the sensitivity functions.

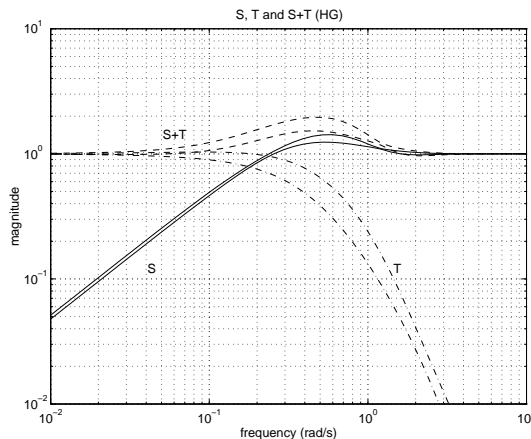


Fig.5.4 Longitudinal inner loop singular values of the input sensitivity functions

Function	$\bar{\sigma}$	$\omega$	$K_m = 1/\bar{\sigma}$	Gain margin (dB)	Phase margin (deg)
$S$	1.42	0.57	0.70	[-4.6,10.6]	$\pm 41.2$
$T$	1.03	0.09	0.98	[-29.7,5.9]	$\pm 57.8$
$S + T$	1.96	0.48	0.51	[-9.8,9.8]	$\pm 54.1$

Table 5.8 Longitudinal inner loop stability margins at the inputs

Good stability margins are obtained, however we must remember that those margins are conservative, therefore even better stability margins should be expected.

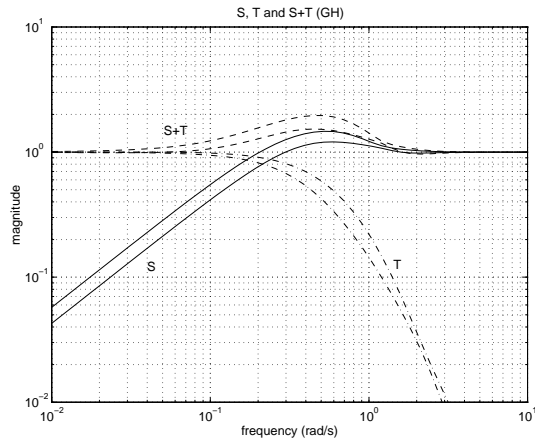


Fig.5.5 Longitudinal inner loop singular values of the output sensitivity functions

Function	$\bar{\sigma}$	$\omega$	$K_m = 1/\bar{\sigma}$	Gain margin(dB)	Phase margin deg)
<i>S</i>	1.47	0.54	0.68	[-4.5,10.0]	$\pm 39.9$
<i>T</i>	1.00	0.02	1.00	[-54.4,6.0]	$\pm 59.9$
<i>S + T</i>	1.96	0.46	0.51	[-9.8,9.8]	$\pm 54.1$

Table 5.9 Longitudinal inner loop stability margins at the outputs

## 5.1.4 Outer loop controller

The closed inner loop has been designed for decoupling  $V_A$  and  $w_V$  and for tracking the flight path angle and airspeed references. Now we add an outer loop for tracking the reference altitude.

The altitude error is multiplied by a constant gain and used as a reference signal for the flight path angle. First, the transfer function from the vertical velocity command  $w_{Vc}$  to altitude  $h$  is extracted and the constant gain is obtained through a root locus analysis. In MATLAB

```
Cqnxnz = C1(1:3,:); Cwva = C1(4:5,:);          % Outputs without and with integrators
Ai=[0 0;0 0]; Bi=[1 0;0 1];Ci=LonKi; Di=Ai;    % Integral controller
pi1=pck(Ai,Bi,Ci,Di);
lonrea=pck(A1+B1*LonKp*C1,B1,Cwva,zeros(size(Cwva,1),size(B1,2)));

% We build the closed loop system

double=[eye(2,2);eye(2,2)];
closed=starp(mmuint(pi1,double'),mmuint(double,lonrea),2,2);
lonh=mmuint(nd2sys(1,[1 0]),sel(closed,1,1));
% an integrator is used to get altitude
[Ahla,Bhla,Chla,Dhla]=unpck(lonh);
[numh,denh]=ss2tf(Ahla,Bhla,Chla,Dhla);
numh=numh(5:12); % Eliminate leading zeroes
rlocus(-numh,denh); sgrid
axis([-1 1 -1 1])
[LonKout,poles]=rlocfind(-numh,denh);
```

Choosing LonKout = 0.1027 the eigenvalues of the closed loop system are

```
damp(poles)
Eigenvalue      Damping      Freq. (rad/sec)
-22.0496        1.0000        22.0496
-16.0253        1.0000        16.0253
-2.4459         1.0000        2.4459
-2.1171         1.0000        2.1171
-1.8999         1.0000        1.8999
-0.9795 + 0.5859i  0.8582        1.1413
-0.9795 - 0.5859i  0.8582        1.1413
-0.4367 + 0.0590i  0.9910        0.4407
-0.4367 - 0.0590i  0.9910        0.4407
-0.1399 + 0.1381i  0.7116        0.1966
-0.1399 - 0.1381i  0.7116        0.1966

trts(poles)
```

Root	Rise time	Settling time
-22.0496	0.0996	0.2089
-16.0253	0.1371	0.2874
-2.4459	0.8983	1.8828
-2.1171	1.0379	2.1753
-1.8999	1.1565	2.4238
-0.9795 + 0.5859i	2.4452	5.3825
-0.9795 - 0.5859i	2.4452	5.3825
-0.4367 + 0.0590i	7.8329	15.1500
-0.4367 - 0.0590i	7.8329	15.1500
-0.1399 + 0.1381i	11.0943	35.4454
-0.1399 - 0.1381i	11.0943	35.4454

We can see that the slower roots have a rise time lower than the specified rise time for an altitude command (15 s) and a settling time well below the required 45 s.

Figure 5.6 shows the root locus with two different scales. In Figure 5.6 the open loop poles are marked with **x**, the open zeros with **o** and the chosen closed loop roots with **+**.

The gain margin for the outer loop is 13 dB at  $w = 0.35 \text{ rad/s}$  and the phase margin is 63 deg at  $w = 0.1 \text{ rad/s}$ .

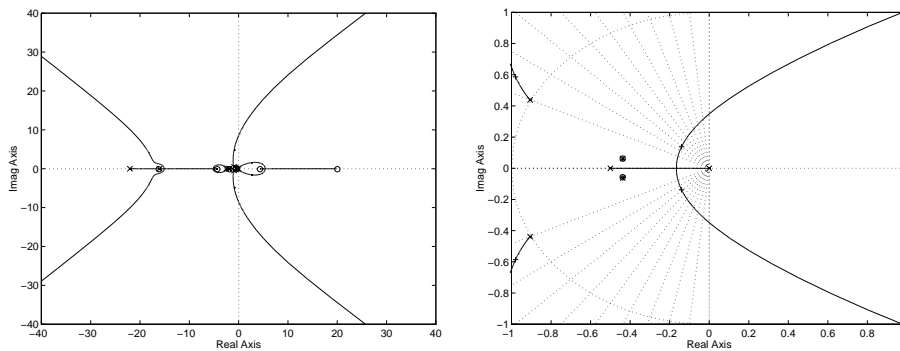


Fig.5.6 Root locus for longitudinal outer loop design

#### 5.1.4.1 Altitude step response

Figure 5.7 shows the response of the linearised system to a command in altitude. The overshoot is slightly smaller than the specified 5% and cross coupling to airspeed (less than 0.1 m/s) is much smaller than the specified 0.5 m/s. The rise time is about the specified 12 s but settling time is smaller than the 45 s. The vertical acceleration slightly exceeds the specified 0.05g.

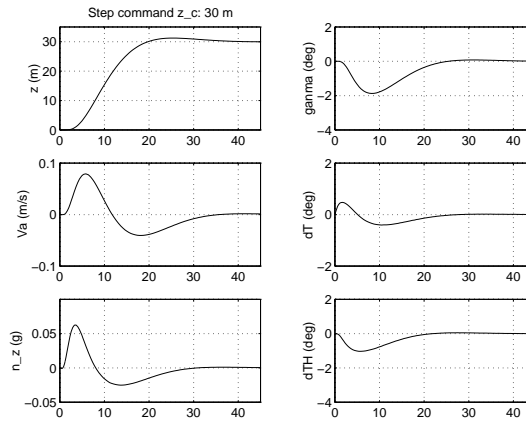


Fig.5.7 Response of the linearised system to a step in commanded altitude

### 5.1.4.2 Step in airspeed

Figure 5.8 shows the response of the linearised closed loop system to a step of 13 m/s in commanded airspeed  $V_{Ac}$ . The response is different from figure 5.2 since the outer loop has been added. All the requirements are satisfied. The obtained cross coupling to altitude is smaller than 1.5 m while the maximum allowed is 10 m.

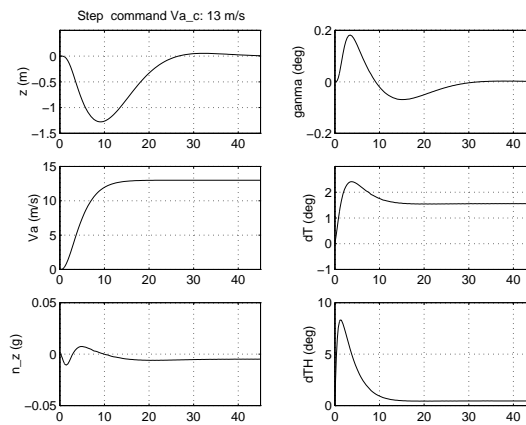


Fig.5.8 Response of the linearised system to a step in commanded airspeed

## 5.2 Lateral controller

### 5.2.1 Analysis of the linear lateral model of the plant

#### 5.2.1.1 Lateral model

The procedure followed in dealing with the lateral model is analogous to the one used with the longitudinal model.

A linear model is generated from the same trim condition used to obtain the linearised longitudinal model. Equation 5.2 shows the lateral linear model we have extracted from the complete linearised model.

$$\begin{bmatrix} \dot{p} \\ \dot{r} \\ \dot{\phi} \\ \dot{\psi} \\ \dot{v}_B \\ \dot{X}_A \\ \dot{X}_R \end{bmatrix} = \begin{bmatrix} -1.2667 & 0.5498 & 0 & 0 & -0.0214 & -0.8402 & 0.2568 \\ 0.0522 & -0.5207 & 0 & 0 & 0.0046 & -0.0176 & -0.3332 \\ 1.0000 & 0.0289 & 0 & 0 & 0 & 0 & 0 \\ 0 & 1.0004 & 0 & 0 & 0 & 0 & 0 \\ 2.3097 & -79.9666 & 9.7896 & 0 & -0.1699 & 0 & 2.0384 \\ 0 & 0 & 0 & 0 & 0 & -6.6667 & 0 \\ 0 & 0 & 0 & 0 & 0 & 0 & -3.3333 \end{bmatrix} \begin{bmatrix} p \\ r \\ \phi \\ \psi \\ v_B \\ X_A \\ X_R \end{bmatrix} + \begin{bmatrix} 0 & 0 \\ 0 & 0 \\ 0 & 0 \\ 0 & 0 \\ 0 & 0 \\ 6.67 & 0 \\ 0 & 3.33 \end{bmatrix} \begin{bmatrix} \delta_A \\ \delta_R \end{bmatrix}$$

$$\begin{bmatrix} \beta \\ p \\ r \\ \phi \\ \chi \end{bmatrix} = \begin{bmatrix} 0 & 0 & 0 & 0 & 0.0125 & 0 & 0 \\ 1.0000 & 0 & 0 & 0 & 0 & 0 & 0 \\ 0 & 1.0000 & 0 & 0 & 0 & 0 & 0 \\ 0 & 0 & 1.0000 & 0 & 0 & 0 & 0 \\ 0 & 0 & -0.0288 & 1.0000 & 0.0125 & 0 & 0 \end{bmatrix} \begin{bmatrix} p \\ r \\ \phi \\ \psi \\ v_B \\ X_A \\ X_R \end{bmatrix} \quad (5.2)$$

The system matrices will be represented as *Alat*, *Blat*, *Clat* and *Dlat*. *Dlat* is a 5-by-2 matrix of zeros and has been left out. The actuator dynamics have been added to the linear model by augmenting it with corresponding states  $X_A, X_R$ . Now the model has seven states ( $p, r, \phi, \psi, v_B, X_A, X_R$ ): roll rate  $p$ , roll angle  $\phi$ , heading angle  $\psi$ ,  $y$  component of inertial velocity in body-fixed reference frame  $v_B$ , aileron deflection  $X_A$  and rudder deflection  $X_R$ . Out the eight measured signals available we have chosen the following five ( $\beta, p, r, \phi, \chi$ ): angle of sideslip  $\beta$ , roll rate  $p$ , yaw rate  $r$ , roll angle  $\phi$  and inertial track angle  $\chi$ . The remaining three are the  $y$  position, that is used in outer loop,  $u_V$  and  $v_V$ , that we don't use.

Table 5.10 shows the eigenvalues and some associated parameters of model 5.2. Table 5.11 shows, for every eigenvalue, the absolute values of the component of the corresponding eigenvectors. The strength of the coupling of the modes with the output is given in table 5.12. The coupling between the different states and the different outputs in a column allows us to associate the eigenvalues with the typical modes of the lateral dynamics. Such an association is pointed out at the head of the tables. As expected, dutch roll and spiral modes dominate  $v_B$  and the sideslip response, and the roll subsidence mode dominates roll rate and roll angle response. The heading mode has influence exclusively on the inertial track angle.

Table 5.13 shows the strength of the coupling of the modes with the input. It can be seen that the rudder has the strongest influence on the dutch roll and the spiral modes. The



aileron also has a strong influence on the dutch roll and spiral modes, but such an influence is smaller than the one from rudder (particularly in the dutch roll), and dominates the effect on the roll subsidence mode. Both actuators have almost the same influence on the heading mode.

	Mode 1	Mode 2	Mode 3	Mode 4	Mode 5	Mode 6
Eigenvalues	0	-0.2512 $\pm 0.5953i$	-0.1537	-1.3012	-6.6667	-3.3333
Damping	-	0.3888	-	-	-	-
Freq.(rad/s)	-	0.6461	-	-	-	-
Rise time(s)	-	1.9793	14.2991	1.6886	0.3296	0.6592
Settling time(s)	-	18.6590	29.9695	3.5390	0.6908	1.3816

Table 5.10 Modes of the open loop system including actuators

Mode	Heading	Dutch roll	Spiral	Roll Sub.	Aileron	Rudder
Eigenvalues	0	-0.2512 $\pm 0.5953i$	-0.1537	-1.3012	-6.6667	-3.3333
$p$	0	0.0170	0.0140	0.7897	0.1536	0.0524
$r$	0	0.0057	0.0103	0.0524	0.0015	0.0467
$\phi$	0	0.0262	0.0894	0.6057	0.0230	0.0153
$\psi$	1	0.0089	0.0673	0.0402	0.0002	0.0140
$v_B$	0	0.9995	0.9936	0.0712	0.0011	0.9143
$X_A$	0	0	0	0	0.9879	0
$X_R$	0	0	0	0	0	0.3984

Table 5.11 Absolute value of the components of the eigenvectors of the open loop system including actuators

### 5.2.1.2 Inner loop controller design

The lateral inner controller is designed analogously to the longitudinal controller. Before calculating the feedback static gain matrix we add a 0.10 s delay with a first order Padé approximation, and then we add the two integrated error states.

```
lat=pck(Alat,Blat,Clat,Dlat);
[numdel,dendel]=pade(.1,1);
delay1=nd2sys(numdel,dendel);
lat1=mmult(lat,daug(delay1,delay1));
[Alat1,Blat1,Clat1,Dlat1]=unpck(lat1);
[Alat2,Blat2,Clat2,Dlat2]=ssinteg(Alat1,Blat1,Clat1,Dlat1,[1 5]);
```

Table 5.14 shows the eigenstructure chosen. The time constant for the roll subsidence mode has been chosen smaller than its open loop value and equal to 1 sec., which is

	Heading	Dutch roll	Spiral	Roll Sub.	Aileron	Rudder
Outputs	0	-0.2512 $\pm 0.5953i$	-0.1537	-1.3012	-6.6667	-3.3333
$\beta$	0	0.0125	0.0124	0.0009	0.0000	0.0114
$p$	0	0.0170	0.0140	0.7897	0.1536	0.0524
$r$	0	0.0057	0.0103	0.0524	0.0015	0.0467
$\phi$	0	0.0262	0.0894	0.6057	0.0230	0.0153
$\chi$	1.0000	0.0035	0.0575	0.0568	0.0004	0.0030

Table 5.12 Absolute value of the components of the vectors  $Cv_i$  including actuators

Modes	$\delta_A$	$\delta_R$
Heading	0.4933	0.6742
Dutch roll	4.6841	26.8198
Spiral	9.3696	13.7765
Roll sub.	1.3080	0.0096
Aileron	6.7485	0
Rudder	0	8.3678

Table 5.13 Absolute value of the components of the vectors  $w_i^T B$  including actuators

the maximum value of the equivalent roll mode time constant for level 1 flying qualities given in [13]. The dutch roll frequency has been chosen equal to 1 *rad/sec*, which is the minimum value given in [13] for level 1, and the damping has been chosen equal to 0.8 so that there is very little overshoot to track angle command step responses. In the same way the other modes have been chosen to fulfil the performance criteria and to yield suitable flying qualities. The eigenvectors selection is well documented [4], and have been chosen to produce the necessary decoupling between the states and the outputs:

- In the dutch roll mode the yaw rate and the lateral velocity  $v_B$  are coupled together while roll angle and roll rate coupling are suppressed.
- In the roll mode the roll is emphasised while yaw rate and  $v_B$  are set to zero.
- In the spiral mode the roll angle is emphasised and the  $v_B$  is set to zero to avoid sideslip in steady turns.
- In the heading mode its state component is emphasised and  $v_B$  is set to zero to avoid sideslip in steady turns.
- In the sideslip integrated error mode its state component is emphasized and roll rate and roll angle are set to zero.
- In the  $\chi$  integrated error mode its state component is emphasised and this mode is required not to appear in  $v_B$ .

The inner loop controller gain is determined by using the function **EIGENAS**:

Mode	Dutch roll	Spiral	Roll Sub.	Heading	$\int \beta$	$\int \chi$
Eigenvalues	$-0.8 \pm 0.6i$	-0.4	-1	-0.8	-1.5	-1.4
p	0 0	x	1	x	0	x
r	1 x	x	0	x	x	x
$\phi$	0 0	1	x	x	0	x
$\psi$	x x	x	x	1	x	x
$v_B$	x 1	0	0	0	x	0
$X_A$	x x	x	x	x	x	x
$X_R$	x x	x	x	x	x	x
Delay $\delta_a$	x x	x	x	x	x	x
Delay $\delta_r$	x x	x	x	x	x	x
$\int \beta$	x x	x	x	x	1	x
$\int \chi$	x x	x	x	x	x	1

Table 5.14 Desired eigenstructure of the lateral closed loop system

```
E = [-0.8 - 0.6i
-0.8 + 0.6i
-1.0
-0.4
-0.8
-1.5
-1.4];
```

```
Ev=[0 0 1 x x 0 x
1 x 0 x x x x
0 0 x 1 x 0 x
x x x x 1 x x
x 1 0 0 0 x 0
x x x x x x x
x x x x x x x
x x x x x x x
x x x x x 1 x
x x x x x x 1];
```

```
K=eigenas(E,Ev,Alat2,Blat2,Clat2)
```

```
K =
```

```
-3.6246 1.7016 2.9057 3.0480 13.1933 0.6869 2.2288
-1.5216 -0.0782 2.4251 -0.2268 1.0320 -0.7237 0.1820
```

The gains of the inner loop controller are:

```
LatKp=K(:,1:5);
LatKi=K(:,6:7);
```

### 5.2.2 Analysis of the closed inner loop

Table 5.15 shows the eigenvalues of the closed loop system and the way the obtained closed loop eigenvectors appear on the outputs, and Table 5.16 shows the absolute values of the components of  $Cv_i$  for the open loop. The latter table is different from 5.12 since the outputs of the integrated error states have been included. Before comparing the coupling of the open and closed loop modes with the outputs we will examine how introducing the integrated error states modifies the coupling of the modes with the outputs. When comparing table 5.16 with table 5.12 we may see that introducing the integrated error states has had almost no effect on the coupling of the modes with the outputs  $\beta$ ,  $p$ ,  $r$  and  $\phi$ ; however the heading mode does not appear now coupled with  $\chi$  but with  $\int \chi$ . Paying attention to the coupling of the modes with the new outputs  $\int \beta$  and  $\int \chi$ , we can see that: there is a strong coupling of the spiral mode with  $\int \chi$ , and  $\int \beta$  has its strongest coupling with the spiral mode and with the dutch roll mode.

Let us compare now the results given in Table 5.15 with those given in Table 5.16. We can see that:

- the coupling of the dutch roll with  $p$  and  $\phi$  has been reduced dramatically
- there is almost no coupling of the modes heading, spiral, roll subsidence and inertial track angle integrated error with the outputs  $\beta$  and  $\int \beta$
- the heading and the inertial track angle integrated error mode have now a strong coupling with the roll rate and the roll angle

Mode	Heading	Dutch Roll	Spiral	Roll Sub.	Aileron	Rudder	$\int \beta$	$\int \chi$
Eigenvalues	-0.8000	-0.8000	-0.4000	-1.0000	-3.0478	-0.6075	-1.5000	-1.4000
		$\pm 0.6000i$						
$\beta$	0.0000	0.0125	0.0000	0.0000	0.0014	0.0124	0.0125	0.0000
$p$	0.5727	0.0002	0.2825	0.6789	0.4154	0.0625	0.0002	0.8083
$r$	0.0695	0.0113	0.0745	0.0625	0.0004	0.0047	0.0183	0.0473
$\phi$	0.7134	0.0002	0.7090	0.6771	0.1363	0.1026	0.0002	0.5764
$\chi$	0.1075	0.0020	0.2088	0.0821	0.0054	0.0230	0.0003	0.0504
$\int \beta$	0.0000	0.0125	0.0000	0.0000	0.0004	0.0203	0.0083	0.0000
$\int \chi$	0.1344	0.0020	0.5219	0.0821	0.0018	0.0379	0.0002	0.0360

Table 5.15 Inner closed loop eigenvalues and absolute values of the components of vectors  $Cv_i$

#### 5.2.2.1 Step in heading angle

Figure 5.9, shows the response of the linearised closed loop system to a step of 20 deg in heading angle. The step is given through a command in inertial track angle, since this is the reference input for the inner loop. We can see that the cross coupling to sideslip

Mode	Heading	Dutch Roll	Spiral	Roll Sub.	Aileron	Rudder	$\int \beta$	$\int \chi$
Eigenvalues	0	-0.2512 $\pm 0.5953ii$	-0.1537	-1.3012	-6.6667	-3.3333	0.0	0.0
$\beta$	0.0000	0.0125	0.0116	0.0009	0.0000	0.0114	0	0
$p$	0.0000	0.0170	0.0131	0.7890	0.1536	0.0524	0	0
$r$	0.0000	0.0057	0.0097	0.0523	0.0015	0.0467	0	0
$\phi$	0.0000	0.0262	0.0835	0.6052	0.0230	0.0153	0	0
$\chi$	0.0000	0.0035	0.0537	0.0568	0.0004	0.0030	0	0
$\int \beta$	0.0000	0.0193	0.0755	0.0007	0.0000	0.0034	1.0000	0
$\int \chi$	0.1344	0.0054	0.3492	0.0436	0.0001	0.0009	0	1.0000

Table 5.16 Open loop absolute values of the components of vectors  $Cv_i$

is very small: the maximum deviation in  $\beta$  is lower than  $0.3 \text{ deg}$ . So, there is almost no difference between the inertial track angle and the heading angle. The response satisfies all the requirements for a heading angle command: there is no overshoot, the rise time is smaller than the specified  $10 \text{ s}$ , and the settling time is well below the specified  $30 \text{ s}$ .

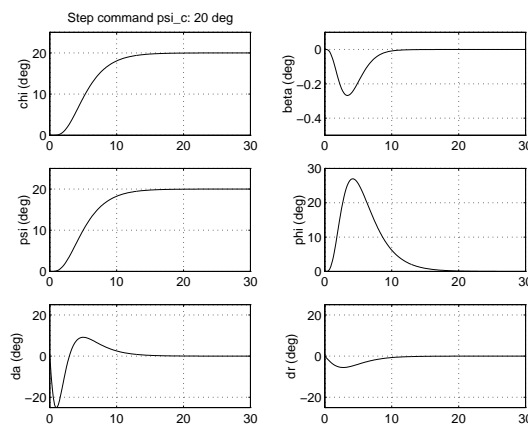


Fig.5.9 Response of the linearised system to a step in inertial track angle

### 5.2.2.2 Loop stability margins

Again, the method of section 2.1.9 will be used to obtain a measure of the stability margins. Now, in the control diagram of figure 2.1,  $G(s)$  represents the transfer function, from the inputs  $\delta_a$ ,  $\delta_r$  to the outputs  $\beta$ ,  $\chi$ , of the linearised lateral model with static gain feedback (LatKp) of the output signals.  $H(s)$  represents the transfer function of the integral controller from the commanded output errors ( $\int \Delta\beta$ ,  $\int \Delta\chi$ ) to the actuator inputs ( $\delta_a$ ,  $\delta_r$ ).

The gain and phase margins at the actuators input and at the sensors output are calculated as follows:

```
[mxsi,mxti,mxsti,mxso,mxto,mxsto]=mxssv(Alat1,Blat1,Clat1,LatKp,LatKi,[1 5]);
```

```
[latmgi,latmfi]=gfmar(mxsi,mxti,mxsti);  
[latmgo,latmfo]=gfmar(mxso,mxto,mxsto);
```

The results obtained at the input of the actuators and at the output of the sensor are summarised in Table 5.17 and Table 5.18, respectively. Figures 5.10 and 5.11 show the singular values plots of the sensitivity functions.

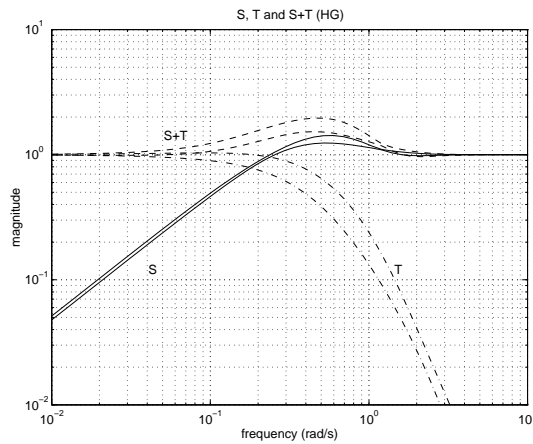


Fig.5.10 Lateral inner loop singular values of the input sensitivity functions

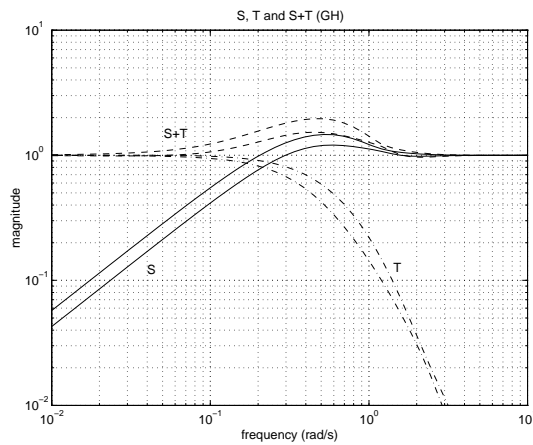


Fig.5.11 Lateral inner loop singular values of the output sensitivity functions

### 5.2.3 Outer loop design

The outer loop is designed for tracking commanded lateral aircraft position. The lateral deviation is multiplied by a constant gain and is used as a reference signal for the inertial

Function	$\bar{\sigma}$	$\omega$	$K_m = 1/\bar{\sigma}$	Gain margin (dB)	Phase margin (deg)
$S$	1.43	0.65	0.70	[-4.6,10.4]	$\pm 40.8$
$T$	1.18	0.21	0.85	[-16.2,5.3]	$\pm 50.0$
$S + T$	2.19	0.46	0.46	[-8.6,8.6]	$\pm 49.2$

Table 5.17 Lateral inner loop stability margins at the inputs

Function	$\bar{\sigma}$	$\omega$	$K_m = 1/\bar{\sigma}$	Gain margin(dB)	Phase margin deg)
$S$	1.71	0.50	0.59	[-4.0,7.7]	$\pm 34.1$
$T$	1.01	0.04	0.99	[-43.3,6.0]	$\pm 59.5$
$S + T$	2.19	0.46	0.46	[-8.6,8.6]	$\pm 49.2$

Table 5.18 Lateral inner loop stability margins at the outputs

track angle.

The present procedure is similar to the one used in the longitudinal channel. First, the transfer function from the inertial track angle command  $\chi_c$  to lateral position  $y$  is extracted and the gain is obtained by means of a root locus analysis. To obtain the lateral position we must integrate the output  $v_V$  ( $y$  component of inertial velocity in vehicle-carried vertical frame), so we consider now the linear system with outputs:  $\beta, p, r, \phi, \chi$  and  $v_V$  (in that order). In MATLAB we add to matrices  $Clat1$  and  $Dlat1$  a row corresponding to the output  $v_V$ .

```

Clatv=[Clat1; 0 0 -2.3059 79.8667 1.0000 0 0 0 0];
Dlatv=[Dlat1; 0 0];
Cprfi=Clatv(2:4,:); % Outputs without integrators
Cbechiv=Clatv([1 5 6],:); % Outputs with integrators and v_V
Ai=[0 0;0 0]; Bi=[1 0;0 1]; % Integral controller
Ci=LatKi; Di=[0 0;0 0];
pi1=pck(Ai,Bi,Ci,Di);

% We build the closed loop system

latreah=pck(Alat1+Blat1*LatKp*Clat1,Blat1,Cbechiv,zeros(size(Cbechiv,1),size(Blat1,2)));
latlah=mmult(latreah,pi1);
%
% latlah has:
% 2 inputs (beta_ref,chi_ref)
% 3 outpus (beta,chi,v_V)
% beta_ref is not used in the outer loop
%
link1=[0 1 0;-1 0 1];
innercl=starp(link1,latlah,2,2); % inner closed loop
%
% An integrator is added to get lateral position

```

```

integrador=nd2sys([1],[1 0]);
inner1=mmult(integrador,innerc1);
[Ainner1,Binner1,Cinner1,Dinner1]=unpck(inner1);
[num,den]=ss2tf(Ainner1,Binner1,Cinner1,Dinner1);
num=num(5:13); rlocus(num,den); sgrid
axis([-1,1,-1,1]);
[LatKout,polos]=rlocfind(num,den)
    
```

Choosing LatKout = 0.001 the eigenvalues of the closed loop system are

Eigenvalue	Damping	Freq. (rad/sec)
-21.2744	1.0000	21.2744
-20.3275	1.0000	20.3275
-3.0453	1.0000	3.0453
-1.5309	1.0000	1.5309
-1.4994	1.0000	1.4994
-0.8015 + 0.6003i	0.8004	1.0014
-0.8015 - 0.6003i	0.8004	1.0014
-0.9231 + 0.3704i	0.9281	0.9946
-0.9231 - 0.3704i	0.9281	0.9946
-0.6037	1.0000	0.6037
-0.1134 + 0.1043i	0.7360	0.1541
-0.1134 - 0.1043i	0.7360	0.1541

Figure 5.12 shows the root locus with two different scales. In Figure 5.12 the open loop poles are marked with **x**, the open zeros with **o** and the chosen closed loop roots with **+**. The gain margin for the outer loop is 13.9 dB at  $w = 0.29 \text{ rad/s}$  and the phase margin is 63.9 deg at  $w = 0.08 \text{ rad/s}$ .

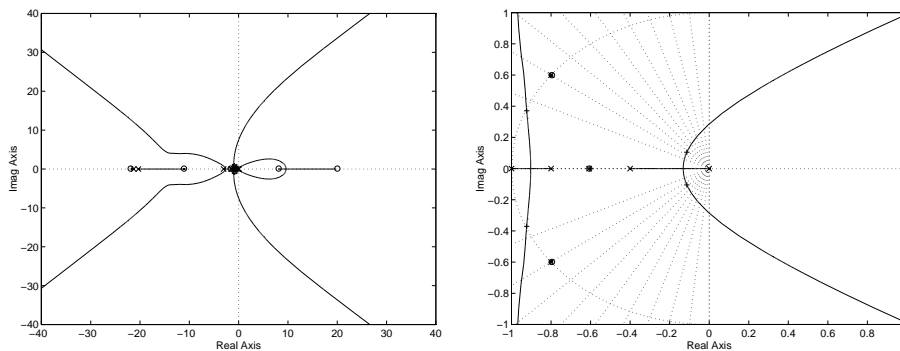


Fig.5.12 Root locus for lateral outer loop design



### 5.2.3.1 Lateral step response

Figure 5.13 shows the response of the linearised system to a lateral command. The overshoot is slightly smaller than the specified 5%. The lateral deviation is reduced to 10%, well below the specified 30%. The cross coupling to sideslip is very small (less than 0.1 deg).

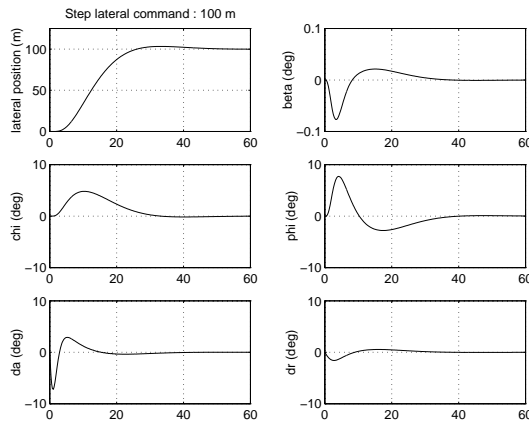


Fig.5.13 Closed loop lateral response of the linear model to a lateral command

### 5.3 Controller with proportional action on the output error

The controllers we made use of in the inner loop of both channels, longitudinal and lateral, have the structure (structure 1) shown in figure 5.14. It is a proportional plus integral controller with integral action on the error of the commanded outputs  $y_c$ , and proportional action on the commanded and non commanded outputs ( $y_n$ ).

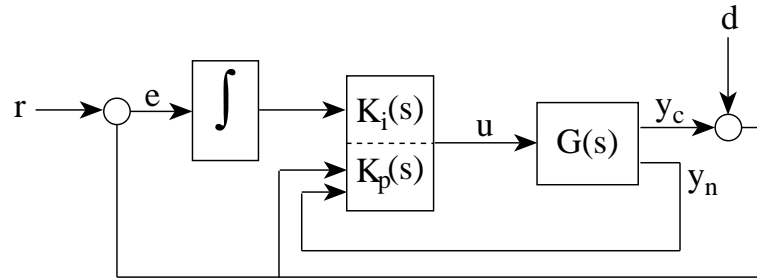


Fig.5.14 Output feedback controller with integral action on the error of commanded outputs (structure 1)

A different structure is shown in figure 5.15 (structure 2), where there is a proportional action acting on the error in addition to the integral action. Both closed loop systems have the same eigenstructure and the same behaviour for process disturbances. However, they have different behaviour for reference input signals since they have different transmission zeros. Thus, changes in the overshoots and rise times of the responses to steps in the reference inputs may be introduced, depending on the zeros positions, but will have little effect on the settling time [9].

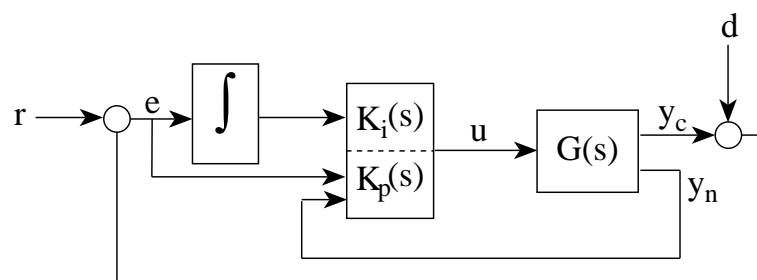


Fig.5.15 Output feedback controller with integral and proportional actions on the error of commanded outputs (structure 2)

We submit now the results arrived at when using the structure 2. In the inner loops the same fixed gains used with the structure 1 are used now. In the outer loops the same gains can also be used, but now a first order filter must be included to cancel a zero that, otherwise, would limit the time responses to command inputs. This zero is introduced by the feedforward action and when canceled the same closed loop as with the previous

controller is obtained.

As we shall see, this controller structure has worse inner loop robustness properties. However the same outer loop stability margins are obtained and, we want to state that in general, better results are obtained in the Evaluation Phase (see chapter 7).

### 5.3.1 Longitudinal model

#### 5.3.1.1 Inner loop stability margins

Figures 5.16 and 5.17 show the singular values plots of the sensitivity functions. We can see that the maxima of the three functions have increased significantly and so have the frequencies at which the maxima occur. That implies higher velocity in the transient responses and also less robustness. Tables 5.19 and 5.20 show the stability margins as obtained. As can be seen the stability margins have been reduced quite a lot.

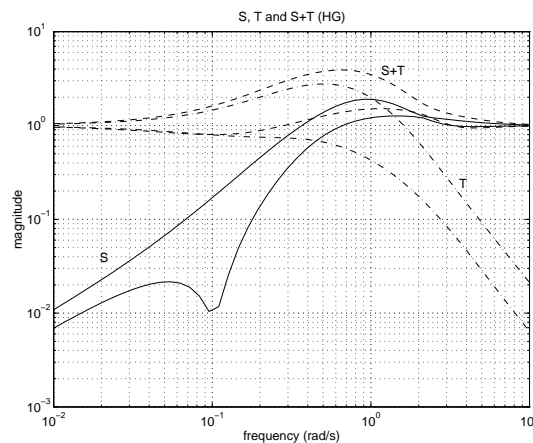


Fig.5.16 Longitudinal inner loop singular values of the input sensitivity functions (structure 2)

Function	$\bar{\sigma}$	$\omega$	$K_m = 1/\bar{\sigma}$	Gain margin (dB)	Phase margin (deg)
$S$	1.91	0.95	0.52	[-3.7,6.5]	$\pm 30.6$
$T$	2.78	0.50	0.36	[-3.9,2.7]	$\pm 20.8$
$S + T$	3.91	0.62	0.25	[-4.6,4.6]	$\pm 28.7$

Table 5.19 Longitudinal inner loop stability margins at the inputs (structure 2)

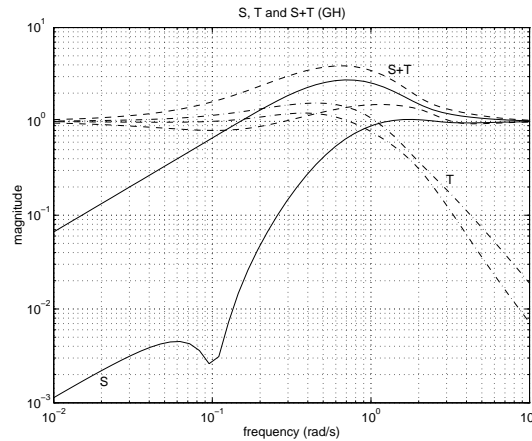


Fig.5.17 Longitudinal inner loop singular values of the output sensitivity functions (structure 2)

Function	$\bar{\sigma}$	$\omega$	$K_m = 1/\bar{\sigma}$	Gain margin(dB)	Phase margin deg)
<i>S</i>	2.77	0.71	0.36	[-2.7,3.9]	$\pm 20.8$
<i>T</i>	1.57	0.45	0.67	[-8.8,4.3]	$\pm 37.2$
<i>S + T</i>	3.91	0.65	0.26	[-4.6,4.6]	$\pm 28.7$

Table 5.20 Longitudinal inner loop stability margins at the outputs (structure 2)

### 5.3.1.2 Step in flight path angle

Figure 5.18 shows the response of the linearised system to a step of  $-3 \text{ deg}$  in commanded flight path angle. There is a big overshoot (about 30 %), but the rise time and settling time are well below the specified 5 s and 20 s, respectively. In comparison with the response obtained with only integral action on the commanded outputs errors (figure 5.1) the rise time has been considerably reduced, but the overshoot, the actuators effort, vertical acceleration and cross coupling with airspeed have been significantly increased.

### 5.3.2 Longitudinal outer loop

In the outer loop, the controller structure has undergone some changes since a first order filter is added at the output of the constant gain (*LonKout*) and its output is now the reference signal for the inner loop (figure 5.19). The aim of the filter is to cancel a zero introduced in the outer loop with the new inner loop structure. If the zero is not cancelled, the response to altitude commands would be slower. The same value is used for *LonKout* and the filter time constant is chosen as 4.7371 s. The same gain and phase margins, and at the same frequencies, than with the previous controller are obtained.

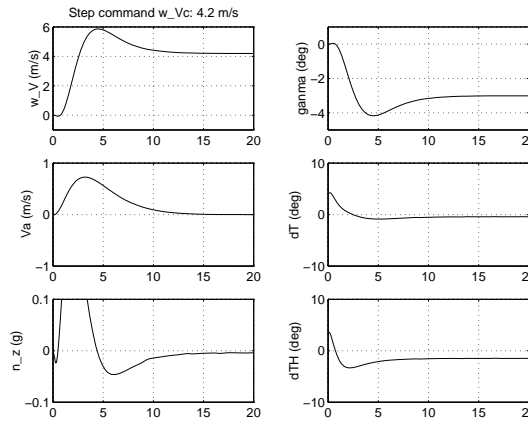


Fig.5.18 Response of the linearised system to a step in commanded flight path angle (structure 2)

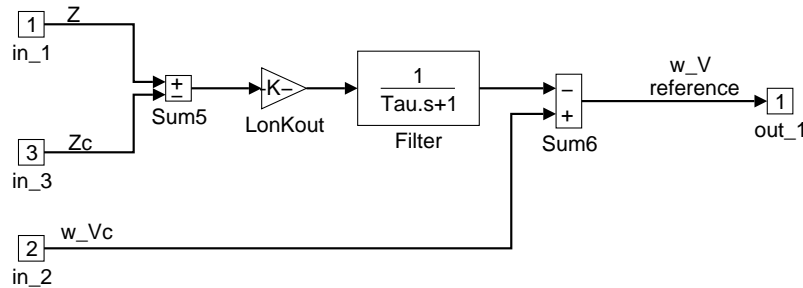


Fig.5.19 Longitudinal outer loop controller (structure 2)

### 5.3.2.1 Altitude step response

The response of the linearised system to a command of altitude is given in figure 5.20. The overshoot is slightly smaller than the specified 5%. The rise time is close to the specified 12 s and the settling time is shorter than the specified 45 s. The cross coupling to airspeed is smaller than the specified 0.5 m/s.

### 5.3.2.2 Step in airspeed

Figure 5.21 shows the response of the linearised closed loop system to a step of 13 m/s in commanded airspeed. The command has been given through a prefilter with a time constant of 1 s in order to reduce the actuator signals. The overshoot is about 15 %, which is higher than the specified 5 %. The rise time and settling time are well below the specified 12 s and 45 s, respectively. The cross coupling with altitude is smaller than the specified 10 m.

The overshoot and the actuator commands can be reduced by increasing the prefilter time constant, for instance with a prefilter with a time constant of 5 s, the time responses are

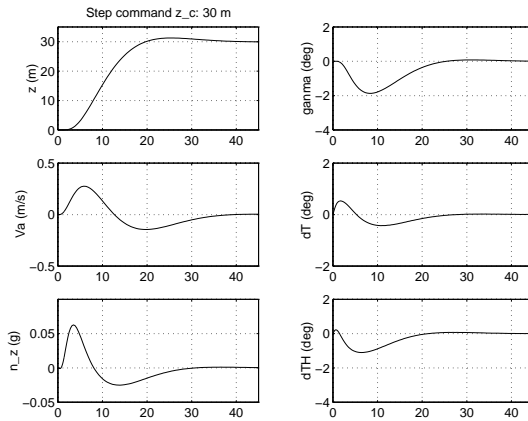


Fig.5.20 Response of the linearised system to a step in commanded altitude (structure 2)

very similar to those of figure 5.2.

The response to a wind step is not included here since, as has already been said, both controller structures have the same behaviour for process disturbances and figure 5.3 is the response of both controllers to a step in wind velocity.

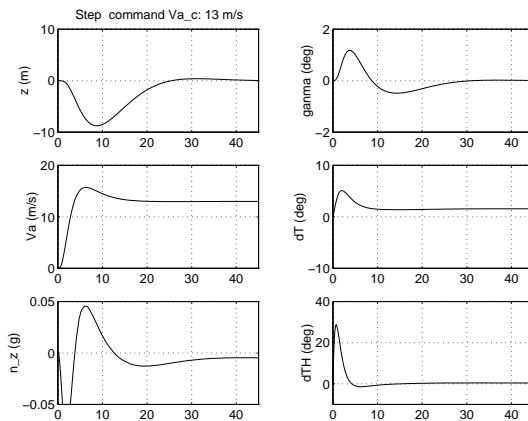


Fig.5.21 Response of the linearised system to a step in commanded airspeed (structure 2)

### 5.3.3 Lateral model

Let us give now the results we obtained in the lateral channel.

#### 5.3.3.1 Lateral inner loop stability margins

Figures 5.22 and 5.23 show the singular values plots of the sensitivity functions and tables 5.21 and 5.22 show the stability margins. Like in the longitudinal model, the maxima of the three sensitivity functions have increased significantly, and because of that the system will have smaller robustness and higher velocity in the transient responses to step

commands.

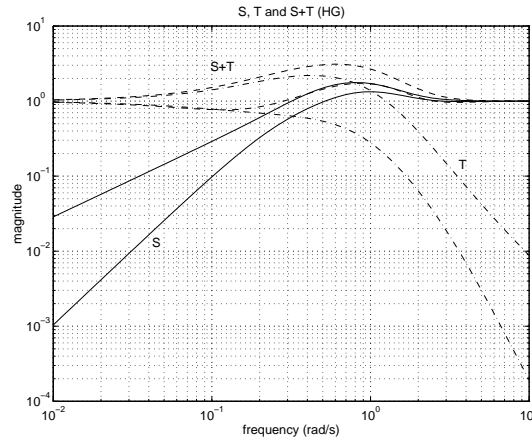


Fig.5.22 Lateral inner loop singular values of the input sensitivity functions (structure 2)

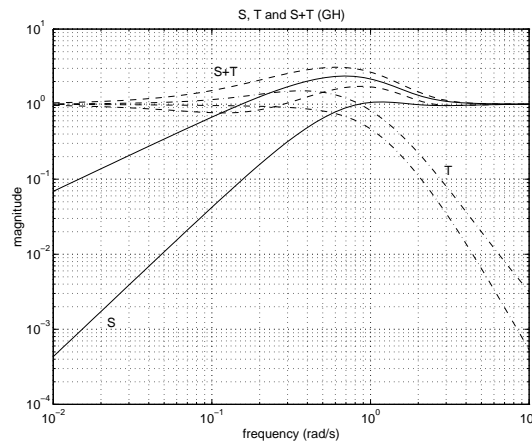


Fig.5.23 Lateral inner loop singular values of the output sensitivity functions (structure 2)

### 5.3.3.2 Step in heading angle

The step is given through an input ramp with a slope of 2 deg/sec in inertial track angle command in order to reduce the actuator signals. We can see that the  $\chi$  and  $\psi$  angles are very similar. There is a big overshoot of about 20%. The cross coupling with  $\beta$  is very small, with a maximum deviation in  $\beta$  of less than 0.3 deg. The rise time is shorter than

Function	$\bar{\sigma}$	$\omega$	$K_m = 1/\bar{\sigma}$	Gain margin (dB)	Phase margin (deg)
<i>S</i>	1.77	0.82	0.57	[-3.9,7.2]	$\pm 32.9$
<i>T</i>	2.19	0.42	0.46	[-5.3,3.3]	$\pm 26.3$
<i>S + T</i>	3.11	0.61	0.32	[-5.8,5.8]	$\pm 35.7$

Table 5.21 Lateral inner loop stability margins at the inputs (structure 2)

Function	$\bar{\sigma}$	$\omega$	$K_m = 1/\bar{\sigma}$	Gain margin (dB)	Phase margin (deg)
<i>S</i>	2.37	0.69	0.42	[-3.1,4.9]	$\pm 24.9$
<i>T</i>	1.51	0.37	0.66	[-9.5,4.4]	$\pm 38.8$
<i>S + T</i>	3.11	0.60	0.32	[-5.8,5.8]	$\pm 35.7$

Table 5.22 Lateral inner loop stability margins at the outputs (structure 2)

the specified 10 s, and the settling time is well below the specified 30 s.

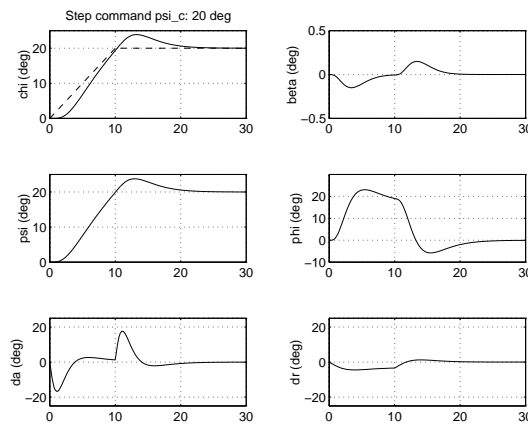


Fig.5.24 Response of the linearised system to a step in heading angle (structure 2)

### 5.3.4 Lateral outer loop

As in the longitudinal model, the outer loop controller structure has undergone some changes since a first order filter is added at the output of the constant gain (*LatKout*) and its output is now the reference signal for the inner loop, Figure 5.25. The aim of the filter is to cancel a zero introduced in the loop with the new inner loop structure. If the zero is not cancelled the response to a lateral deviation command would be worse. The same value is used for *LatKout* and the filter time constant is chosen as 5.8962 s. The same gain and phase margins, and at the same frequencies, than with the previous controller are obtained.

#### 5.3.4.1 Lateral step response

Figure 5.26 shows the response of the linearised system to a step response. The results are quite similar to those obtained with structure 1 (figure 5.13). All the requirements are



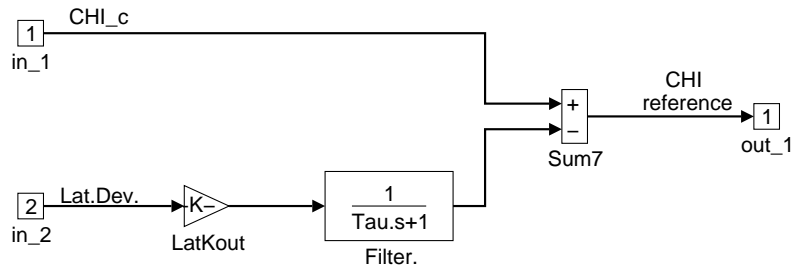


Fig.5.25 Lateral outer loop controller (structure 2)

fulfilled. The overshoot is slightly smaller than the specified 5% and the lateral deviation is reduced to 10%, well below the specified 30 s. The cross coupling with sideslip is lesser than 0.1 deg.

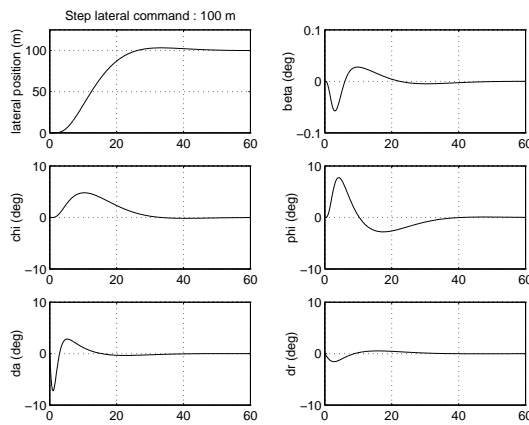


Fig.5.26 Response of the linearised system to a step in lateral deviation

## 6 Analysis of the resulting controller in terms of the applied methodology

The controller was designed by an iterative method considering criteria of performance and robustness in the linear model, without taking into account non linearities. In previous chapters some analyses were made: eigenvalues and eigenvectors analyses, frequency analyses, linear time domain simulations, close loop singular values and other time domain analysis in the open and close loop system. In this chapter we present the verification of all the design specifications with the non-linear system.

All the simulations are made using the following configuration (see section 5.1.1): mass = 120.000 kg,  $\Delta x = 0.23 \bar{c}$ ,  $\Delta y = 0 \bar{c}$  and  $\Delta z = 0.1 \bar{c}$ ; and the main starting conditions are:  $V_A = 80 \text{ m/s}$ , altitude = 1000 m,  $\psi = -90 \text{ deg}$ ,  $\gamma = 0 \text{ deg}$  and  $\alpha = 1.65 \text{ deg}$ .

We will see the results obtained with both controller structures (1 and 2). First the results with structure 1 are given. The results with structure 2 are given in section 6.6.

### 6.1 Non-linear simulation observing performance criteria

The description of the performance criteria has been given in chapter 4.

Figure 6.1 shows the response to lateral deviation, altitude, heading angle, flight path angle and airspeed commands. Those responses are similar to the ones we analyse in chapter 5 by using the linear model and it can be seen that they fulfil nearly all the performance criteria:

**Lateral deviation** A step change of 100 m has an overshoot of 13 %, bigger than in the linear model where the overshoot is smaller than 5 %, and the lateral deviation is reduced to 10 % in less than 30 s, according to specifications.

**Altitude** A step change in altitude command of 30 m is tracked with a  $tr = 11 \text{ s}$ ,  $ts \approx 35 \text{ s}$  and  $Mp = 4.6 \%$ . The coupling with airspeed is smaller than 0.2 m/s.

**Heading angle** A step change of 3 deg in the commanded heading angle  $\psi_c$  is tracked with a  $tr \approx 6 \text{ s}$ ,  $ts < 20 \text{ s}$  and without overshoot.

**Inertial flight path angle** A step change of 3 deg in the commanded flight path angle  $\gamma_c$  is tracked with a  $tr \approx 5 \text{ s}$ ,  $ts < 15 \text{ s}$  and without overshoot

**Airspeed** A step command of 13 m/s in the airspeed is tracked with a  $tr = 6 \text{ s}$ ,  $ts < 20 \text{ s}$  and  $Mp = 3.2 \%$ . The coupling with altitude is smaller than 4 m.

### 6.2 Non-linear simulation of an engine failure

In case of engine failure the following specifications have to be fulfilled:

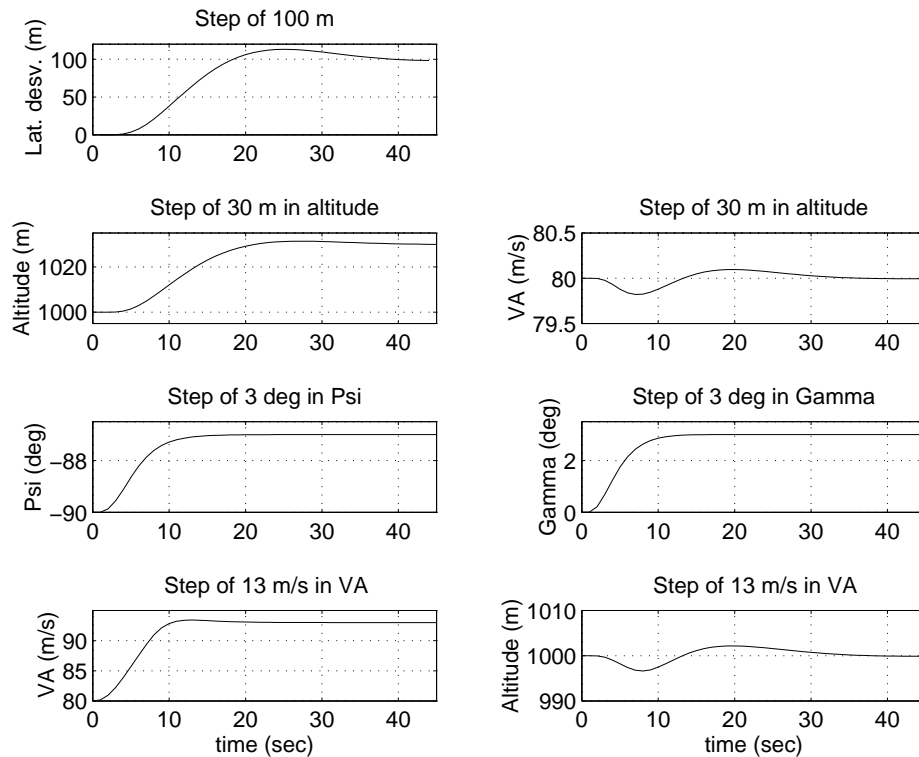


Fig.6.1 Response of the non-linear model to command signals

- In case of engine failure in still air  $\phi$  should not exceed 10 deg; its maximum steady state deviation should not exceed 5 deg. When the failed engine is restarted the roll angle should be reduced to zero with  $M_p < 50\%$ .
- Sideslip angle  $\beta$  should be minimised.
- The maximum heading rate,  $\dot{\psi}$ , should be less than 3 deg/s.

Figure 6.2 shows that:

- $\phi$  is lower than 10 deg, its steady state deviation is 3.7 deg and, when the engine is restarted,  $\phi$  is reduced to zero with an overshoot that exceeds a little the specification of 50 %
- $\beta$  is quickly minimised
- $\dot{\psi}$  has values lower than 1 deg/s

The comfort and safety criteria are also verified:

- the airspeed always higher than 79 m/s, which is much bigger than the specified  $62.2 = 1.2V_{stall}$
- the angle of attack  $\alpha \approx 1.7$  deg is less than the specified 12 deg

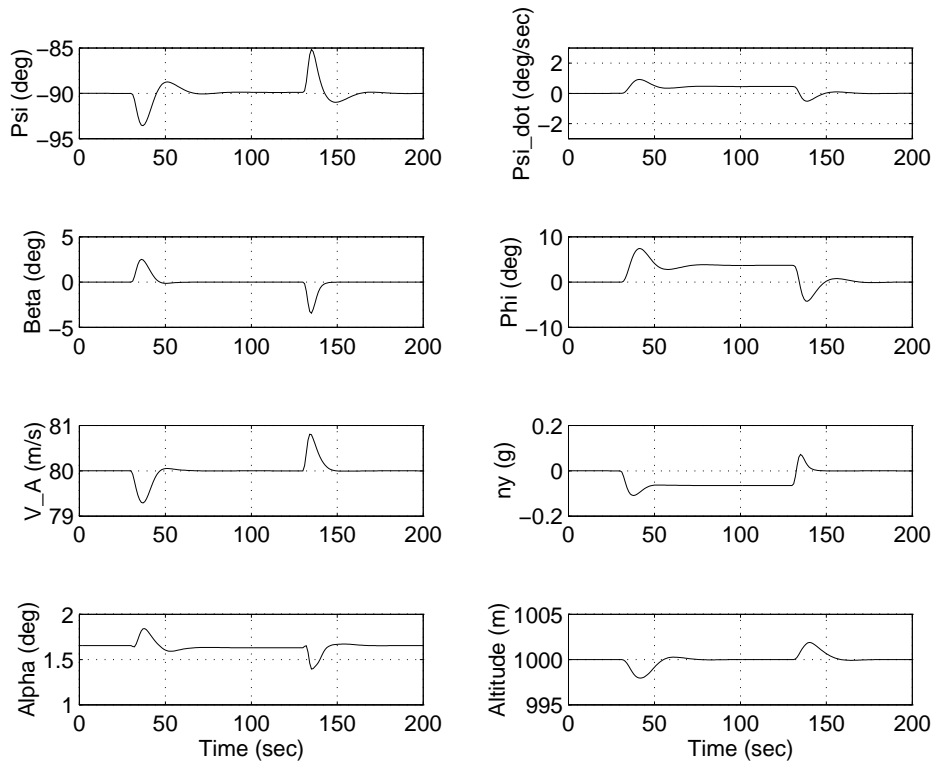


Fig.6.2 Response of the non-linear model to an engine failure

- the lateral acceleration  $n_y$  increases up to  $0.1g$ , that is less than the specified  $0.2g$ .

Finally, the variations in altitude are less than  $2\text{ m}$ .

### 6.3 Non-linear simulation observing ride quality and safety criteria

The specifications for ride quality criteria are a maximum vertical acceleration and a maximum lateral acceleration. Figure 6.3 shows the lateral acceleration in a  $90\text{ deg}$  turn and the vertical acceleration in a change from  $\gamma = 0\text{ deg}$  to  $\gamma = -6\text{ deg}$  and from  $-6\text{ deg}$  to  $-3\text{ deg}$ . These values corresponds to segments II and III of the Automated Evaluation Procedure (chapter 7). It can be seen that lateral acceleration  $n_y$  is always within the limits and the vertical acceleration  $n_z$  surpasses slightly the maximum level.

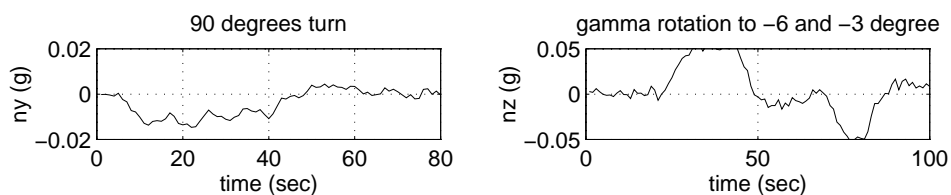


Fig.6.3 Ride quality criteria observation

Figure 6.4 depicts the results of the non-linear simulation showing the safety criteria. The simulations correspond to the landing approach of the evaluation procedure as used in chapter 7, which is a good representation of all possible flight conditions.

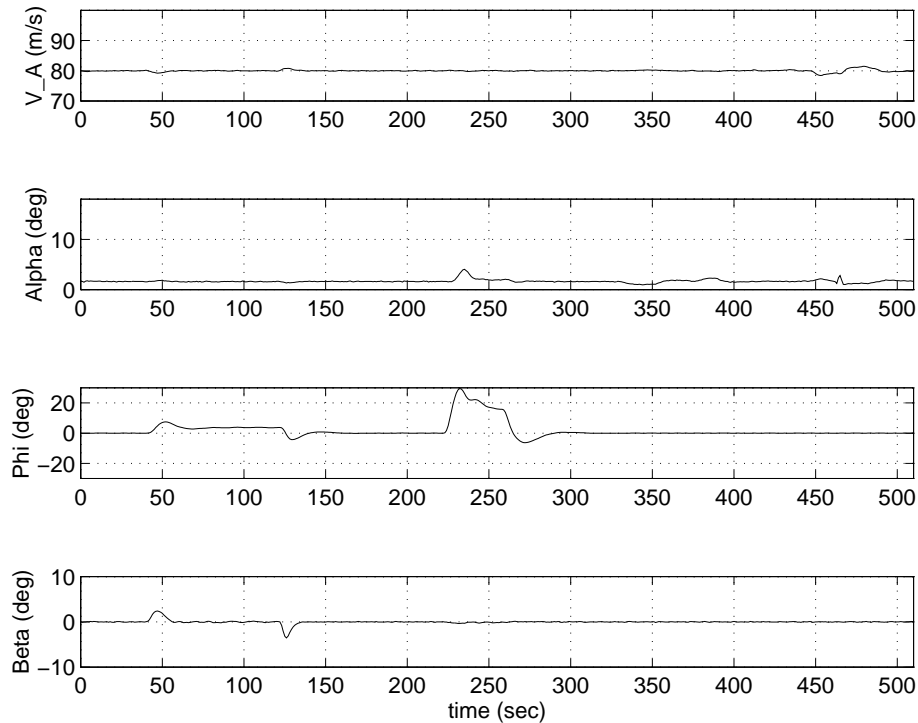


Fig.6.4 Safety criteria observation

The safety criteria are fulfilled since:

- The airspeed is always well above than  $1.2V_{stall} = 62.2m/s$
- The maximum angle of attack  $\alpha$  remains within the limits, its maximum value is observed during the turn, but is well below the limit of  $12\ deg$
- The roll angle  $\phi$  remains also within the limits, but in the turn is near to the limit of  $30\ deg$
- The sideslip angle  $\beta$  is quickly minimised at all times.

Detailed response to a engine failure for airspeed and angle of attack is given in the previous section.

#### 6.4 Non-linear simulation under moderate turbulence conditions

We give an analysis of the non-linear systems under moderate turbulence conditions. The spectra of the turbulence we used in the simulations is described with the following

standard deviation values

$$\sigma_{ug} = \sigma_{vg} = \sigma_{wg} = 0.1W_{20} = 1.54 \text{ m/s} \quad (6.1)$$

and with the following turbulence scale lengths

$$L_{ug} = L_{vg} = L_{wg} = 305 \text{ m} \quad (6.2)$$

For those turbulence conditions, the design criteria are:

- The mean actuator rates for aileron, tailplane and rudder should be less than 33% of the maximum rates (i.e. 8.25 *deg/s* for aileron and rudder and 5 *deg/s* for tailplane)
- The mean throttle rate should be less than 15 % of the maximum rate (i.e. 0.24 *deg/s*)
- $\phi$  should remain smaller than 5 *deg*
- The RMS of  $\beta$  and the RMS of the heading angle error should be less than those in open loop

Figure 6.5 shows the actuators behaviour. All the requirements on the mean of actuators are fulfilled. Moreover, all RMS are lesser than limits:

- The mean aileron rate is 0.42 *deg/s* with a RMS of 7.30 *deg/s*
- The mean tailplane rate is 0.12 *deg/s* with a RMS of 1.03 *deg/s*
- The mean rudder rate is 0.08 *deg/s* with a RMS of 1.97 *deg/s*
- The mean throttle rate is 0.09 *deg/s* with a RMS of 1.50 *deg/s*

Figure 6.6 shows both in the open and closed loop, the roll angle  $\phi$ , the sideslip angle  $\beta$ , the heading angle  $\psi$  and the the inertial track angle  $\chi$  under these moderate turbulence conditions. In the closed loop  $\phi$  always remains within the specification limit of 5 *deg*. Table 6.1 shows the RMS values of the errors in open and closed loop. The closed loop values of  $\phi$ ,  $\beta$  and  $\psi$  are less than their corresponding open loop values, however the RMS of  $\psi$  is higher in closed loop than in open loop.

	$\phi$	$\beta$	$\psi$	$\chi$
Open loop RMS (deg)	2.04	1.06	0.89	0.97
Closed loop RMS (deg)	0.65	0.96	1.45	0.28

Table 6.1 RMS of the errors in angles  $\phi$ ,  $\beta$ ,  $\psi$  and  $\chi$  in open and closed loop

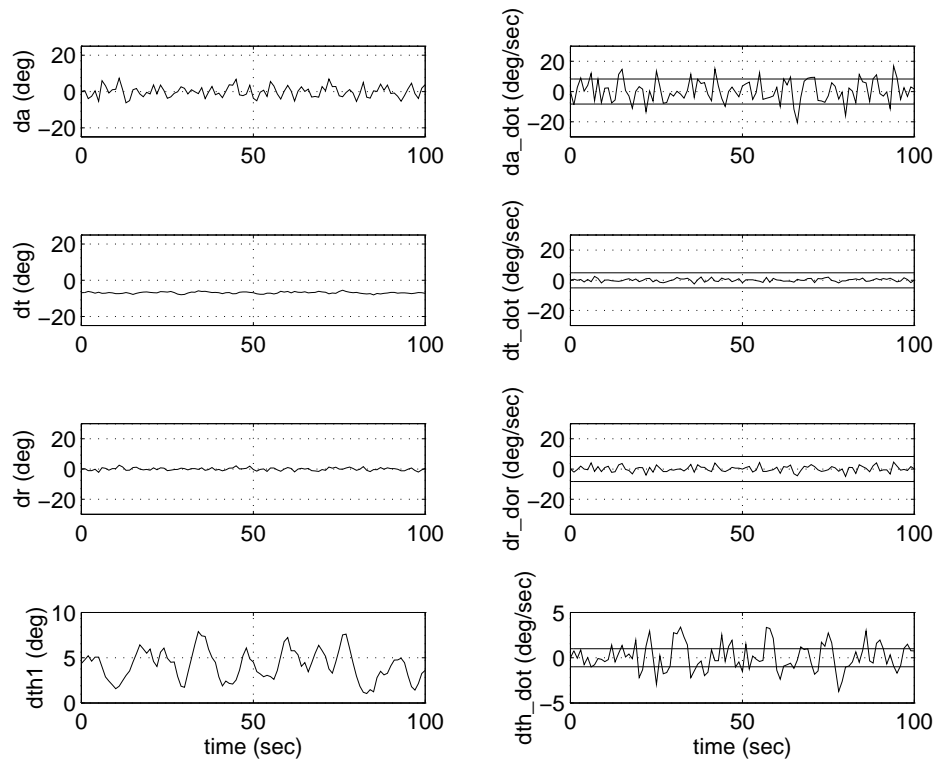


Fig.6.5 Control activity under moderate turbulence conditions

### 6.5 Non-linear simulations observing robustness criteria

The specified robustness criteria are:

stability and sufficient performance should be maintained for

- centre of gravity variations between ( $\bar{c}$ : means aerodynamic chord)
  - $0.15\bar{c} < \Delta x < 0.31\bar{c}$
  - $0.0\bar{c} < \Delta z < 0.21\bar{c}$
- mass variations between  $100000 \text{ Kg} \leq \text{mass} \leq 150000 \text{ Kg}$
- transpor delays from 50 to 100 ms

Figures 6.7 and 6.8 show the simulation results obtained, making use of the Assessment Software for all possible worst conditions of time delay, mass and centre of gravity, and besides at the design airspeed of 80 m/s.

Figure 6.7 shows the lateral and altitude step response, the inner loop response to heading and flight path angle steps, the airspeed step and wind response, and the airspeed-altitude cross-coupling.

With regard to lateral and altitude step response, we can see that there is a very small control activity, there are almost no overshots and the settling times are well below the specified times.

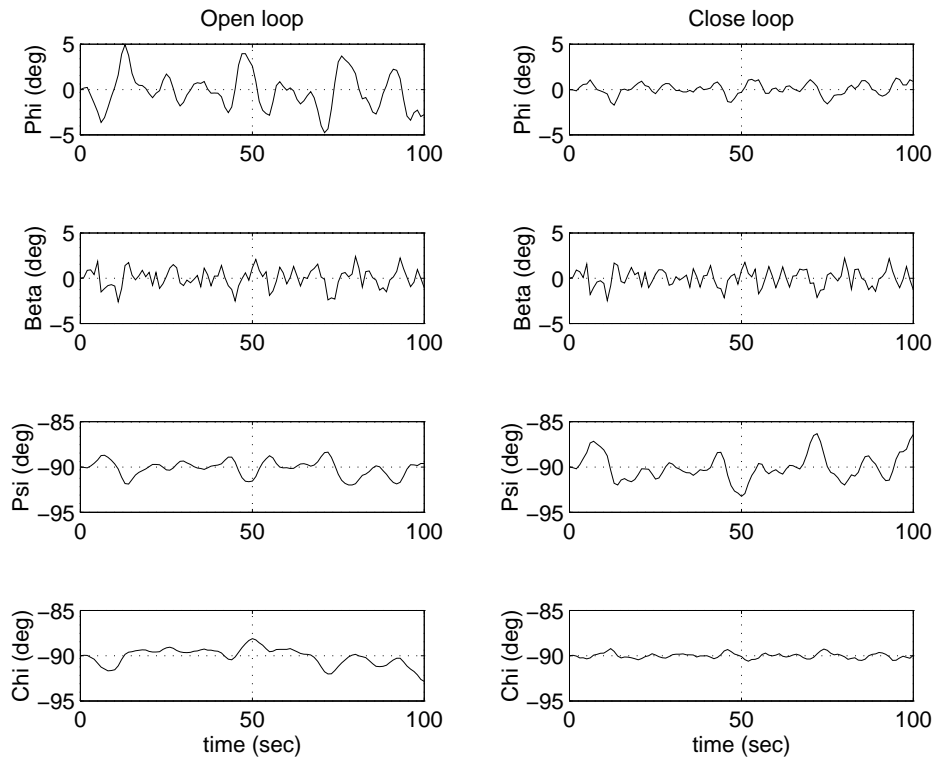


Fig.6.6 Responses under moderate turbulence conditions of angles  $\phi$ ,  $\beta$ ,  $\psi$  and  $\chi$

In respect of the inner loop response to heading and flight path angle steps, we can see that in all cases the overshoot is lower than the specified 5 % and the settling time is less than the specifications.

Regarding the airspeed step and wind response, we can see that all the performance criteria are fulfilled in the airspeed command. In the responses to wind step we can see three different behaviours that correspond to the three different values of the mass which have been considered. In case of minimum and maximum mass values, the deviation in airspeed is larger than 2.6 m/s after 15 s of the step, and in case of nominal mass value the specification is fulfilled.

Regarding the airspeed-altitude cross-coupling, we can see that the deviations are always within the limits.

In Figure 6.8 we can see the roll and heading at engine failure. All the performance criteria are fulfilled: the roll angle never exceeds 10 deg and its steady state deviation does not exceed 5 deg; the heading rate is always well below the specified 3 deg/s, and the sideslip angle is quickly minimised.

Figures 6.9 and 6.10 show the simulation results obtained for all possible worst conditions of time delay, mass and centre of gravity, at nominal speed (63.7 m/s) and at maximal flap speed (90 m/s).

The worst results are obtained in the engine failure at nominal velocity and minimum mass. Consequently a new set of controller gains have been computed using the linearised



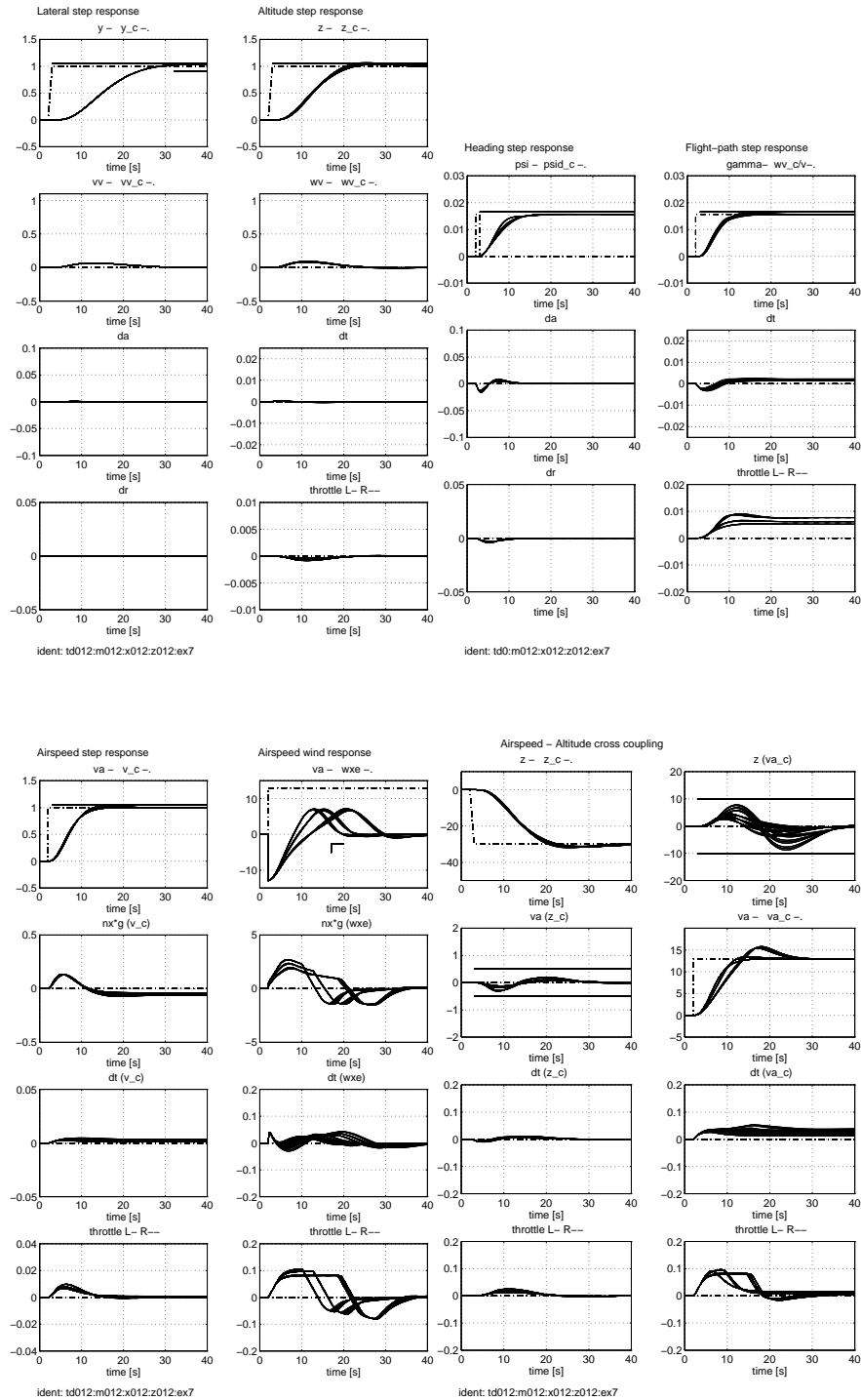


Fig.6.7 Lateral, altitude, heading, flight-path, airspeed and wind step response, and airspeed-altitude cross coupling, at the design speed

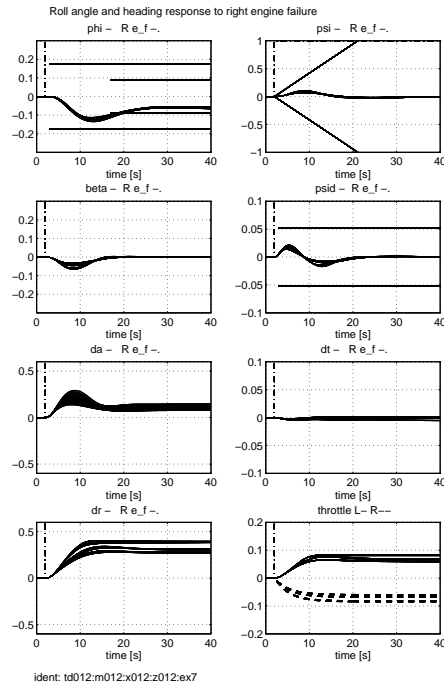


Fig.6.8 Roll and heading at engine failure at the design speed

model at nominal speed velocity but without changing the rest of trimming parameters, and with the same eigenstructure as before. That is, the same MATLAB commands given in chapter 5 should be used now, but changing the system matrices. The resulting controller gains are:

LonKout = 0.1000

LonKp =

0.7475	0.0821	-0.2081	-0.0292	-0.0126
-0.1823	-1.3169	-0.3775	0.0046	-0.1256

LonKi =

-0.0053	-0.0029
0.0068	-0.0221

LatKout = 0.0012

LatKp =

-4.2135	2.7546	4.2865	4.6405	15.7038
-3.0877	-0.1453	4.2337	-0.0083	2.2480

LatKi =

0.6952	2.6083
-0.7415	0.3166

The gain and phase margins obtained with this new controller at the actuator inputs and at the sensor outputs, using the sensitivity function  $S + T$  are:

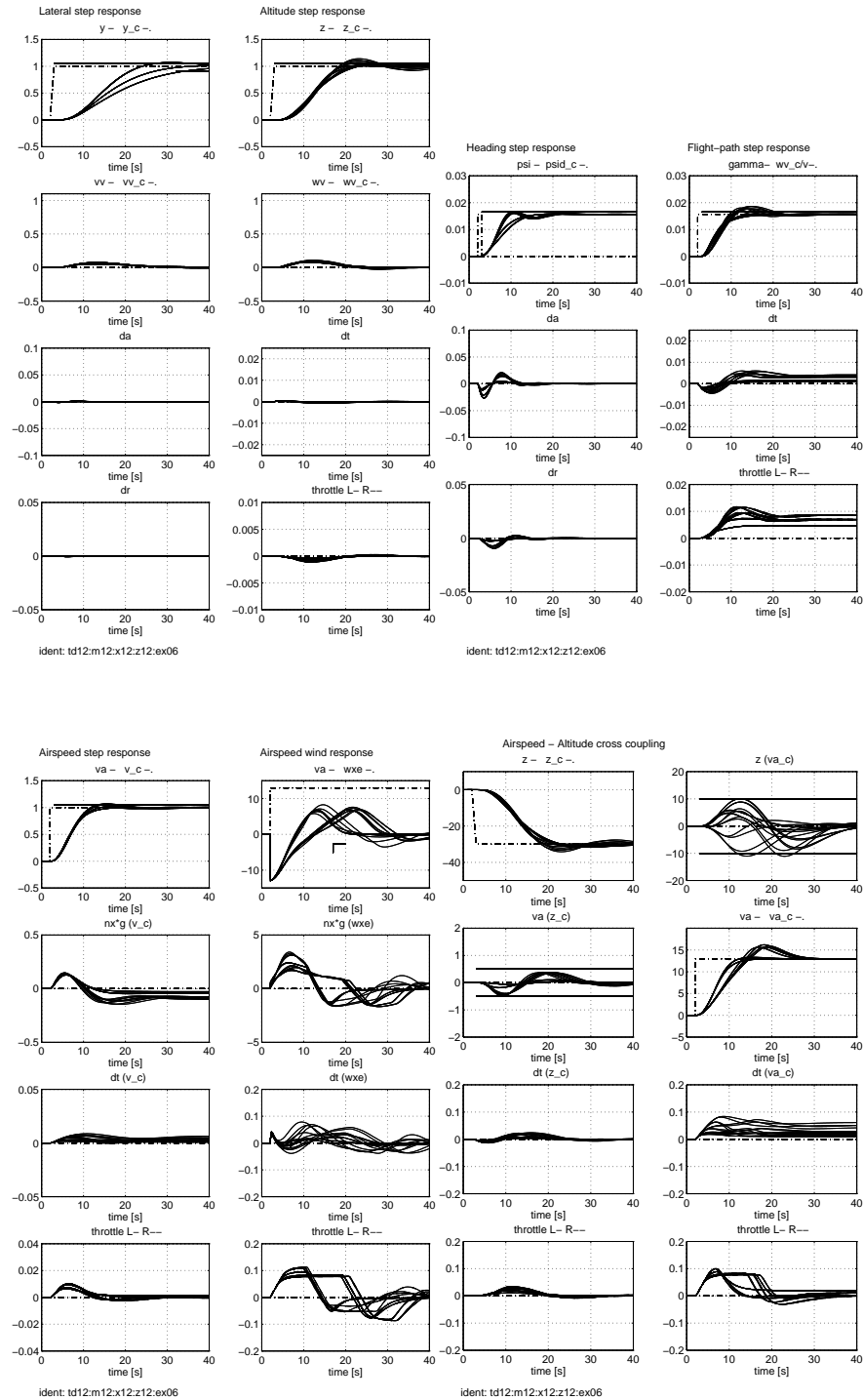


Fig.6.9 Lateral, altitude, heading, flight-path, airspeed and wind step response, and airspeed-altitude cross coupling, at nominal speed and at maximal flap speed

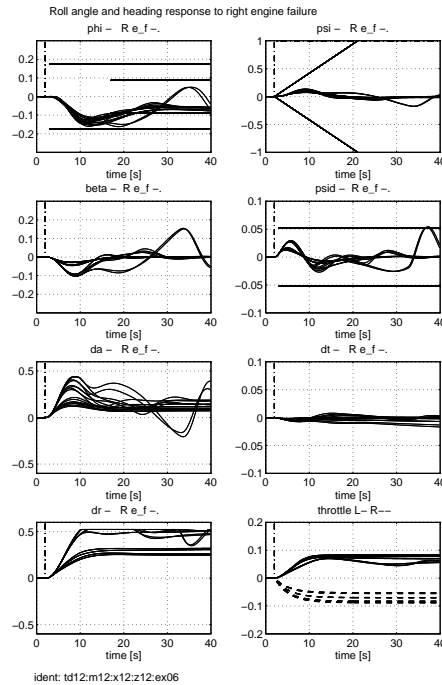


Fig.6.10 Roll and heading at engine failure, at nominal speed and at maximal flap speed

- longitudinal:  $[-10.0, 10.0] dB, \pm 54.9 deg$
- lateral:  $[-9.3, 9.3] dB, \pm 52.3 deg$

Figures 6.11 and 6.12 show the results obtained using this controller when simulating with the nominal velocity and for the worst time delay, mass and centre of gravity. Similar performance and robustness results to those obtained with the controller designed at the original speed of  $80 m/s$  are obtained, thus gain scheduling with respect to velocity should be used.

## 6.6 Nonlinear simulations with controller with proportional action on the output error

Since the only change in this controller structure with respect to the previous one is an added reference feedforward action, the nonlinear simulations results in case of engine failure and in case of moderate turbulence conditions will be the same and because of that are not repeated. We will observe differences in the ride quality criteria and in the safety criteria and in the response to inner loop command inputs.

Figure 6.13 shows the ride quality criteria observation. We can see that the lateral acceleration has increased and the limits are slightly surpassed, with a maximum of  $0.0247g$ . However, the vertical acceleration has almost the same shape.

Figure 6.14 shows the safety criteria observation. We can see that during the turn the

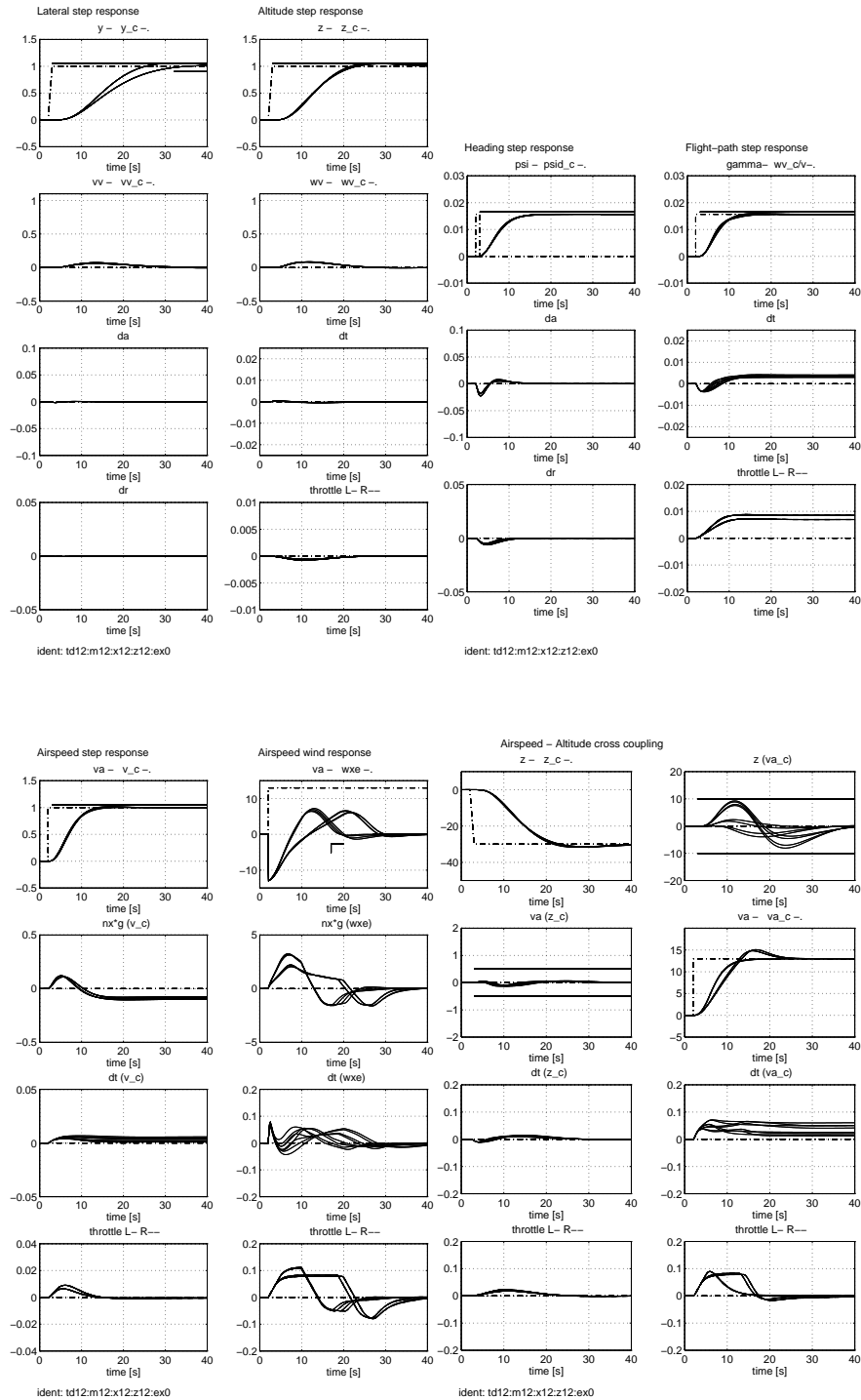


Fig.6.11 Lateral, altitude, heading, flight-path, airspeed and wind step response, and airspeed-altitude cross coupling, using the controller calculated at nominal velocity

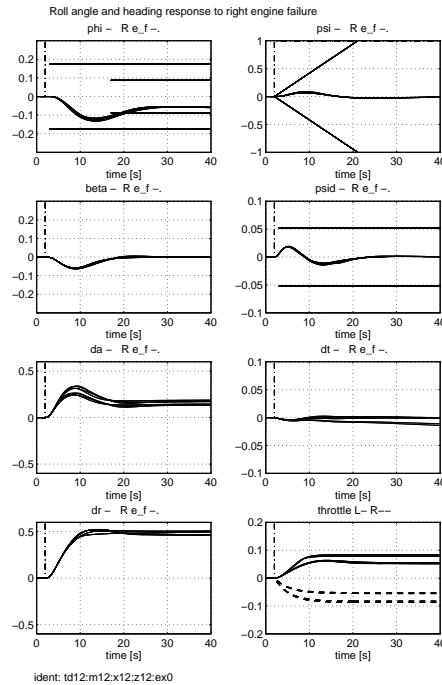


Fig.6.12 Roll and heading at engine failure, using the controller calculated at nominal velocity

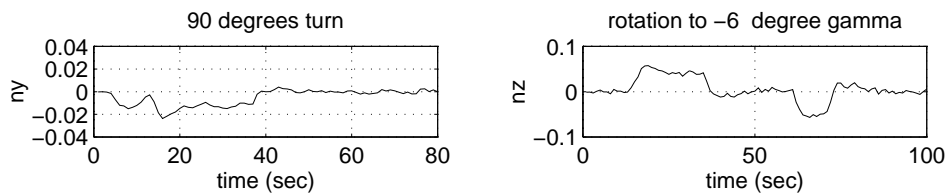


Fig.6.13 Ride quality criteria observation with controller structure 2

angle of attack has increased. However, it remains well below the limit of  $12 \text{ deg}$ . The roll angle surpasses the limit of  $30 \text{ deg}$  during the turn, with a maximum of  $35.4 \text{ deg}$ . The sideslip angle and the airspeed have the same shape as in previous section.

Figure 6.15 shows the simulation results obtained, making use of the Assessment Software for all possible worst conditions of time delay, mass and centre of gravity, and besides at the design airspeed of  $80 \text{ m/s}$ .

Figure 6.15 shows the lateral and altitude step response, the inner loop response to heading and flight path angle steps, the airspeed step and wind response, and the airspeed-altitude cross-coupling.

With regard to lateral and altitude step response, we can see that the same results that with previous controller are obtained.

In respect of the inner loop response to heading and flight path angle steps, we can see

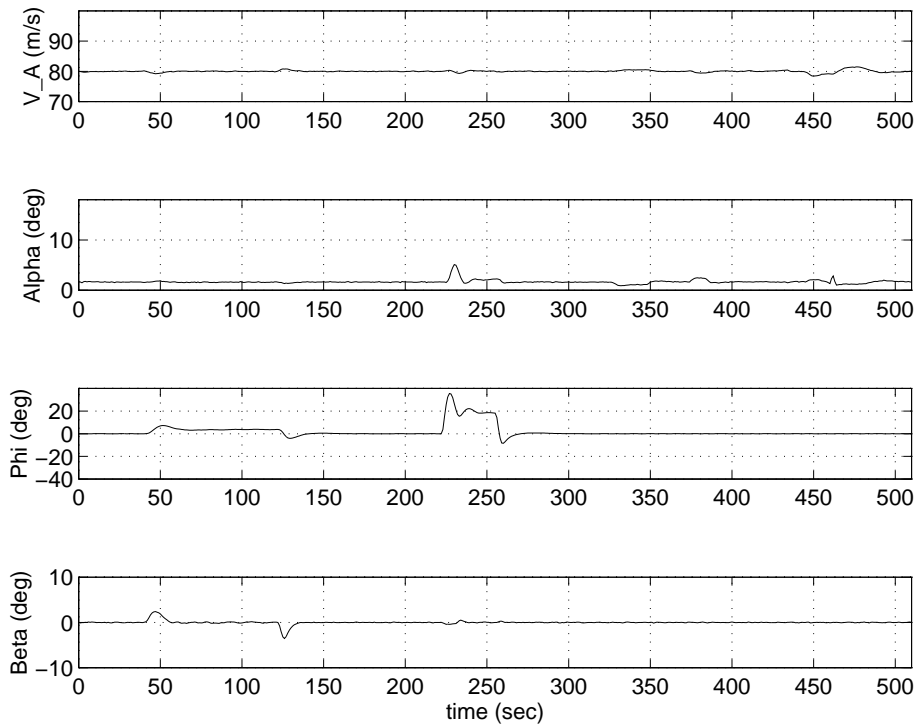


Fig.6.14 Safety criteria observation with controller structure 2

that the overshoot has been greatly increased reducing considerably the rise time and the settling time is less than the specifications.

Regarding the airspeed step and wind response, we can see that in the airspeed command the overshoot has been greatly increased. As expected, the same responses as with the previous controller are observed in the wind step case. Regarding the airspeed-altitude cross-coupling, we can see that the airspeed deviations are always within the limits, however the altitude surpasses the limits. That could be avoided if the airspeed command is introduced through a prefilter, as has already been seen in the linear case.

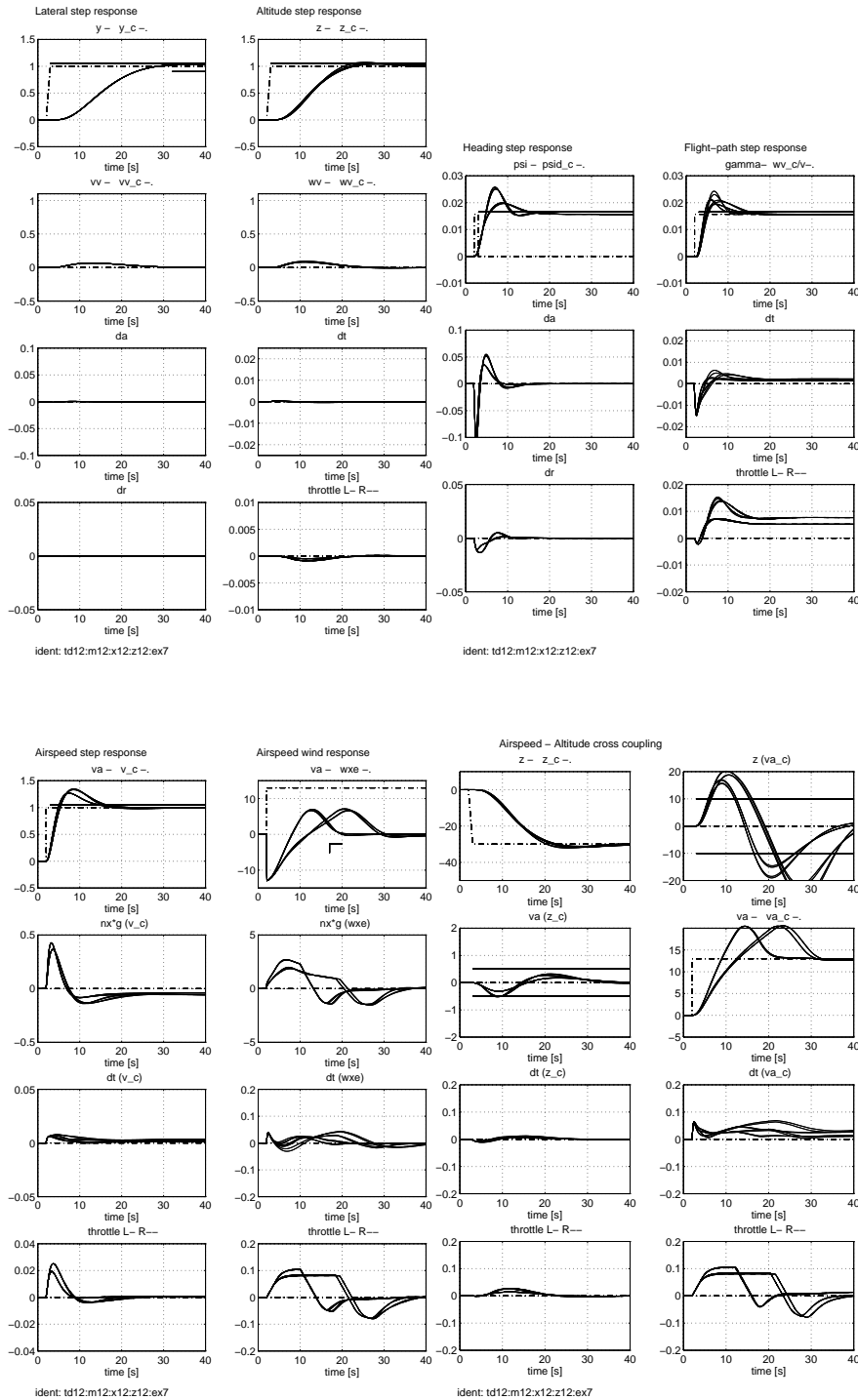


Fig.6.15 Lateral, altitude, heading, flight-path, airspeed and wind step response, and airspeed-altitude cross coupling, at the design speed, with controller structure 2



## 7 Results of the Automated Evaluation Procedure

### 7.1 Introduction

This chapter presents the results for the evaluation procedure as proposed in [2] consisting of a landing approach. It starts at an altitude of 1000 *m*, with a track angle of  $\chi = -90$  *deg* and with a constant airspeed of 80 *m/s*.

In order to check robustness the entire approach is flown with a most forward, a nominal and a most afterward horizontal centre of gravity location. Furthermore, one flight is executed with a nominal centre of gravity location and a time delay of 100 *ms*.

We present the results obtained with both controllers considered in chapter 5. However, the controller with only integral action on the error of the commanded outputs should be considered for the evaluation phase, since it is more robust. First, we present the results with this controller. In the next section the results with the controller with proportional and integral action on the error of the commanded outputs are given.

#### 7.1.1 A general view of the results

The behaviour in the landing approach of the RCAM model using the controller, as proposed in this document, is decomposed into 4 segments that are explained in the next sections of this chapter.

Figure 7.1 plots the trajectory followed by the model, together with the reference trajectory in the landing approach, although they are almost indistinguishable, and it also marks the four flight segments above mentioned.

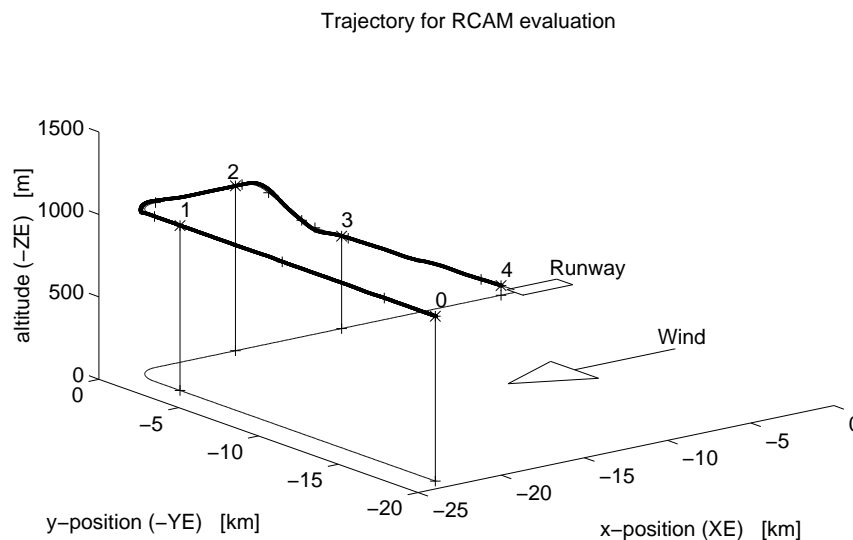
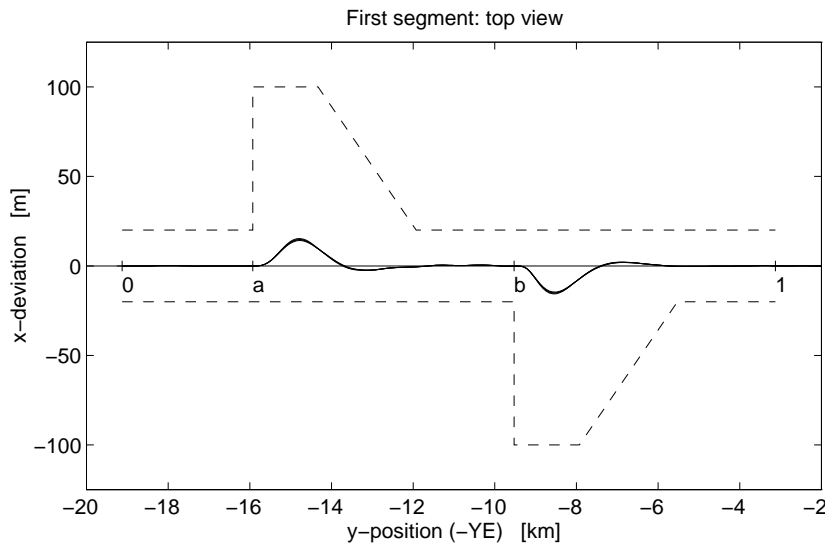


Fig.7.1 The trajectory response of the controlled RCAM model

### 7.1.2 Segment I: The effect of engine failure

During this segment it is possible to investigate some lateral features of the controller by simulating failure of the left engine: the failure occurs at point **a**, after which the engine is restarted at point **b**.



*Fig.7.2 Segment I: The effect of engine failure with bounds*

During the engine failure the specifications allow a maximum lateral deviation of 100 m that should be quickly reduced to less than 20 m at the end of the segment. Also, in order to measure robustness, differences are allowed of 10 % of the maximal allowable lateral deviations.

Figure 7.2 shows the performance of the controller in this segment, and it can be seen that the lateral deviation is always less than 20 m, therefore, the controller complies with the corresponding specification. Moreover, the four plots are almost the same, which means good robustness of the design.

### 7.1.3 Segment II: 90 degrees turn

This segment consists of a commanded co-ordinated turn from points **c** to **d** with a heading rate of  $\dot{\psi} = 3 \text{ deg/sec}$ .

The objectives are to maintain a constant speed of  $80 \text{ m/s}$ , to keep the lateral acceleration close to zero, to restrict the bank angle to  $\phi = 30 \text{ deg}$  with consistent rudder/aileron deflections, not to exceed a lateral deviation of  $200 \text{ m}$  during the entire segment, and not to exceed a lateral deviation of  $20 \text{ m}$  at the end of the segment (point **2** in Figure 7.3). The maximal lateral acceleration  $n_y$  should be limited  $|n_y| < 0.02g$ .

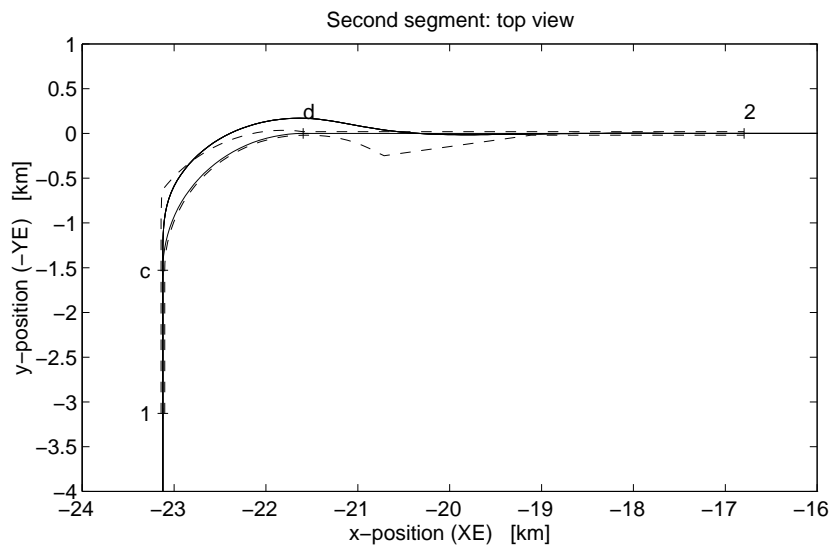


Fig.7.3 Segment II: Plan view of the 90 degrees turn with bounds

Figures 7.3 and 7.4 give the behaviour of the model in this manoeuvre. It can be seen that the trajectory of the model surpasses the bounds marked in the plots but the lateral deviation never exceeds the maximum value of  $200 \text{ m}$  and at the end the lateral deviation is close to zero. The lateral acceleration never surpasses the maximal allowable value (see Figure 6.3). Moreover, the model has a very smooth turn and fulfils all the performance design criteria, so we accept it.

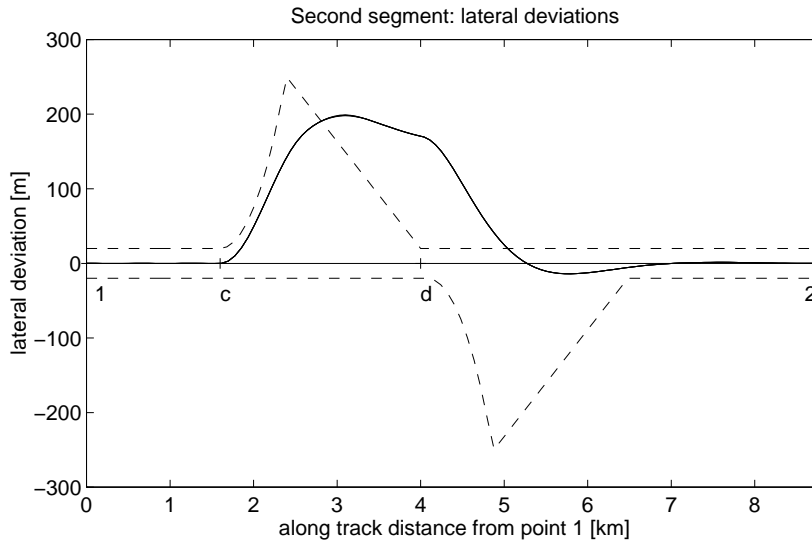


Fig.7.4 Segment II: Lateral deviations during the 90 degrees turn with bounds

7.1.4 Segment III: The descent phase

In this segment, after a short period of level flight at an altitude of 1000 m, the flight path angle is set to  $\gamma = -6 \text{ deg}$  at point e, and to  $\gamma = -3 \text{ deg}$  at point f.

The desired airspeed is 80 m/s, with variations smaller than 5 %, i.e. 4 m/s. Also, the maximum vertical acceleration  $n_z$  should be limited:  $|n_z| < 0.05 g$ ; a maximum vertical deviation of 20 m should not be exceeded during the entire segment, and at the end of the segment (point 3) a deviation of 6 m should not be exceeded.

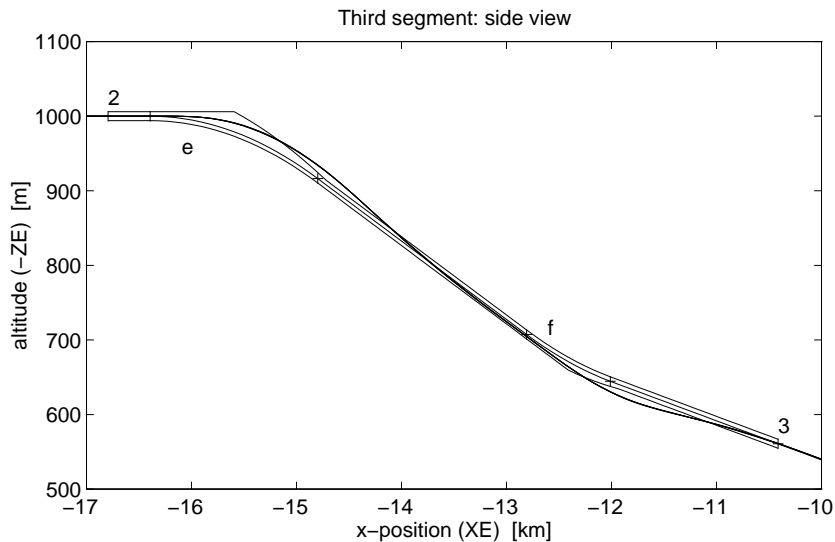


Fig.7.5 Segment III: Side view of the -6 and -3 degrees glideslope captures with bounds

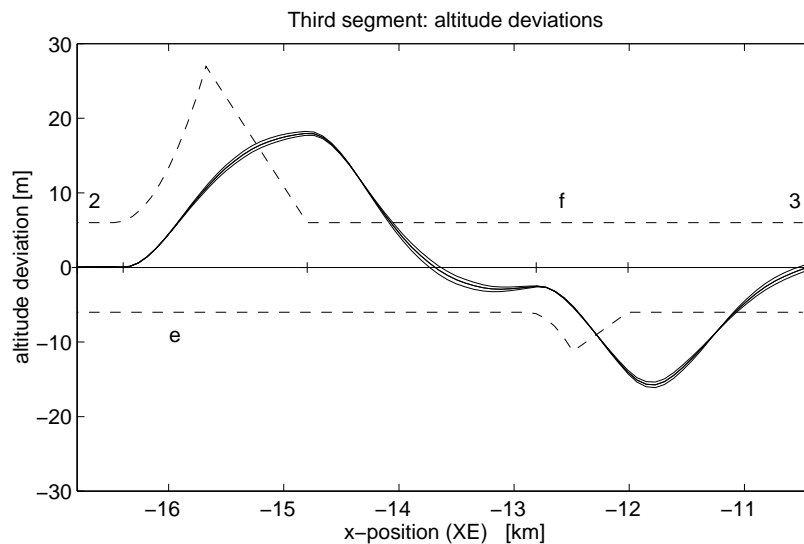


Fig.7.6 Segment III: Vertical deviations during the -6 and 3 degrees glidslope with bounds

Figures 7.5 and 7.6 represent the behaviour of the model in the descent phase. It can be seen that the trajectories of the model surpass the bounds marked in the plots although the vertical deviation never exceeds the maximum value of 20 m and at the end of the segment the deviation is close to zero. In Figure 6.4 we can see that the speed variation is well below the allowable 4 m/s. Moreover, the model has a very smooth transition during the entire segment although the vertical acceleration is a little high at some points. We can see in Figure 6.3 that the vertical acceleration surpasses a little the maximal allowable value. This last trouble is reflected by the comfort index in Table 7.1. Since the rest of the design criteria are fulfilled and our intent to diminish this value produces worse results, we accept it.

#### 7.1.5 Segment IV: Final approach

Along this segment the aircraft is faced with a headwind going up to about  $Wx_E = -7$  m/s, then the windspeed changes to a tailwind of about  $Wx_E = 7$  m/s, combined with a downdraught of about  $Wz_E = 8$  m/s. Obviously, the size of the longitudinal deviation and time until recovery are measures for evaluation of the controller.

During this segment a maximum deviation of 20 m should not be exceeded, and at its end a maximum deviation of 1.5 m is taken into account. Moreover,  $|n_z| < 0.1 g$  and, in order to measure robustness, differences are allowed of 10 % of the maximal allowable vertical deviation.

Figures 7.7 and 7.8 show the behaviour of the model in this segment. It can be seen how the trajectories of the model fall inside the bounds during the entire segment. The rest of specifications are fulfilled by the controller.

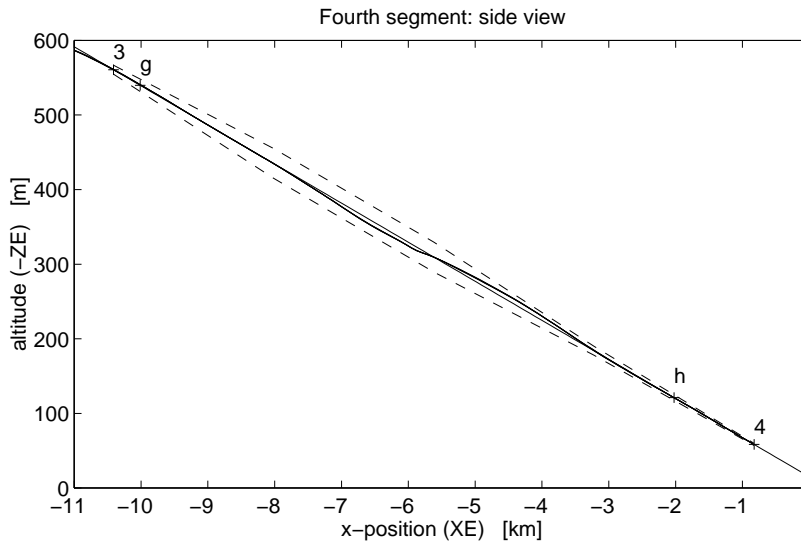


Fig.7.7 Segment IV: Side view of the final approach with wind shear and bounds

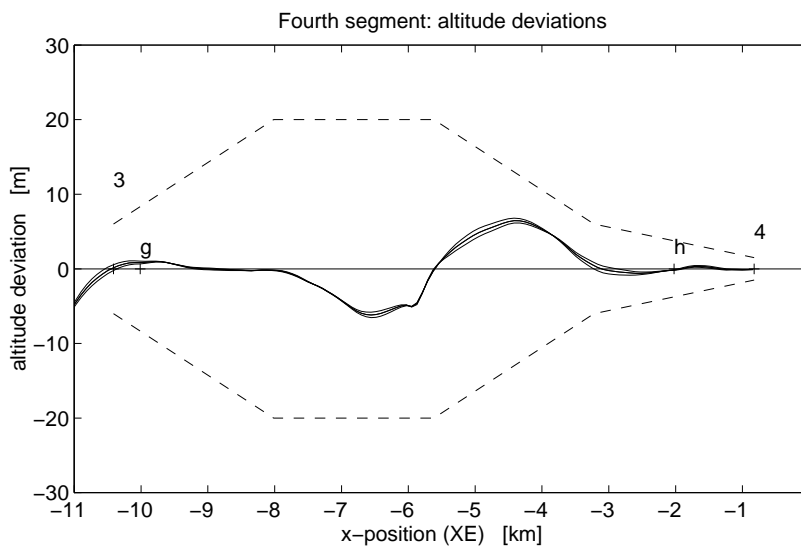


Fig.7.8 Segment IV: Vertical deviations during the final approach with bounds

### 7.1.6 Numerical results

Table 7.1 summarises the results as obtained by the controller along the landing approach. All the numerical values, except the power indicator, are normalised to maximal allowable bounds, such that a value of smaller than one is acceptable.

In general the results are good, except for the comfort criterion in Segment III, since the indices are less than 1. The problem with the comfort has already been explained, and it is basically due to a little high level of the vertical acceleration.

Among all these numeric results, it is important to emphasise the total robustness index as obtained: 0.1817. Since the main goal of this project is the design of robust controllers for the RCAM model, this number is a quite good result although it considers only variations of the CoG, and variations of the mass and velocity should have been taken into account. These analyses have been done in chapter 6.

	Segment I	Segment II	Segment III	Segment IV	Total
Performance	0.0764	0.4964	0.3285	0.1905	0.2730
Robustness	0.0309	0.0161	0.4926	0.1873	0.1817
Comfort	0.5432	0.7340	1.1808	0.4674	0.7314
Safety	0.0038	0.0382	0.0070	0.0345	0.0209
Power	0.0037	0.0027	0.0150	0.0309	0.0131

*Table 7.1 Numerical results of the evaluation procedure*

## 7.2 Results using the controller with proportional action on the output error

We present now the results obtained in the evaluation phase when the controller with proportional action on the output error is used.

We can see that there are small variations in segments I and II, as could be expected since both controller structures have the same behaviour against perturbations.

The main changes can be observed in the coordinated turn (segment II) and in the descent phase (segment III). Now the bounds never are surpassed. We can see in the numerical results given in Table 7.2, that in segment II the performance value has been reduced enormously but the other indices have been increased. Now the lateral acceleration surpass the maximum allowable value. Moreover, the safety and power entries have tripled their values with respect to table 7.1. However, the insensitivity has increased only a little. In segment III the main effect can be seen in performance, that has been reduced almost to the half, and in insensitivity that has also been reduced.

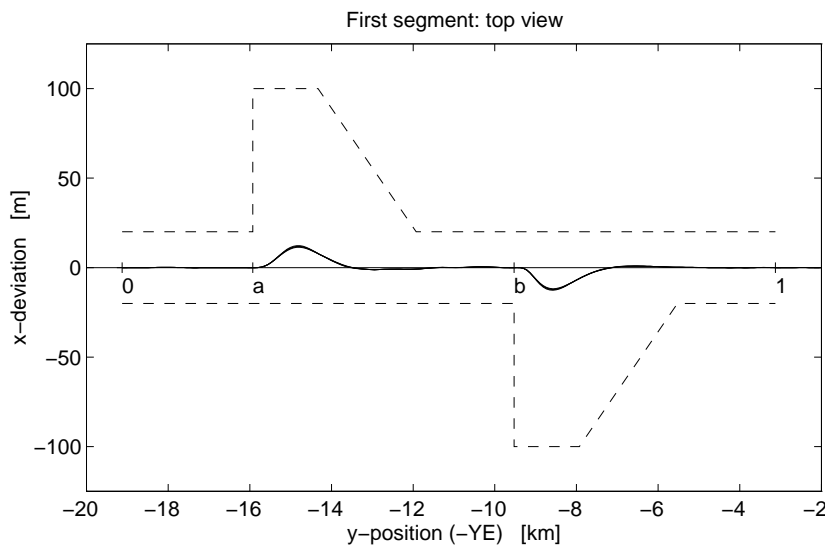


Fig.7.9 Segment I: The effect of engine failure with bounds

	Segment I	Segment II	Segment III	Segment IV	Total
Performance	0.0613	0.0818	0.1877	0.2051	0.1340
Robustness	0.0247	0.0204	0.3494	0.2642	0.1647
Comfort	0.5371	1.3663	1.1423	0.4623	0.8770
Safety	0.0039	0.0921	0.0087	0.0349	0.0349
Power	0.0037	0.0079	0.0150	0.0309	0.0144

Table 7.2 Numerical results of the evaluation procedure



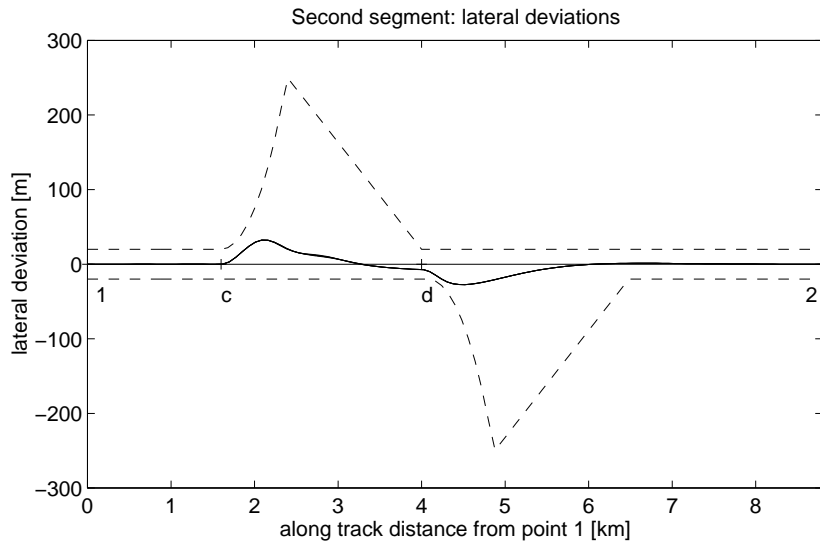


Fig.7.10 Segment II: Lateral deviations during the 90 degrees turn with bounds

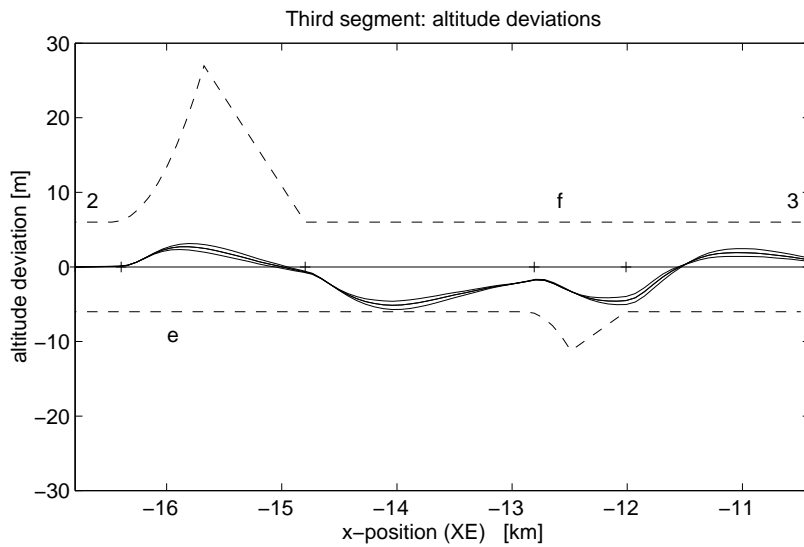


Fig.7.11 Segment III: Vertical deviations during the -6 and 3 degrees glidslope with bounds

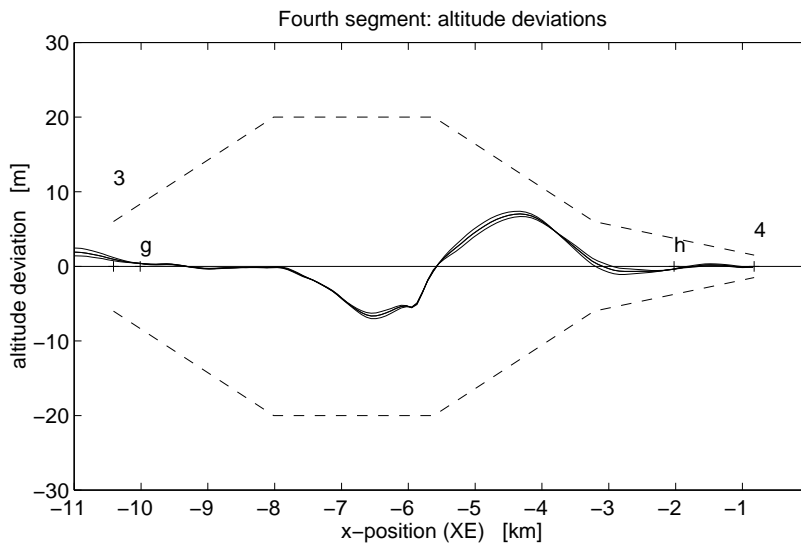


Fig.7.12 Segment IV: Vertical deviations during the final approach with bounds

## Conclusions

In this document the eigenstructure method has been applied to the RCAM benchmark problem.

The design was completed by making use of the classical approach of splitting up the controller into two parts, a longitudinal and a lateral controller, and in using the standard inner-outer loop control structure. In every inner loop the feedback outputs, command signals and integrated outputs have been chosen guided by the design specifications. For both inner loops a constant gain feedback matrix has been calculated using the eigenstructure technique. This method allows the designer to directly satisfy performance criteria given in terms of damping, settling time and decoupling, but not cope directly with system uncertainties. However, the eigenstructure has been chosen, in an iterative way, so that good stability margins have been obtained. In both outer loops a constant scalar gain has been used.

Moreover, two controller structures have been considered, without and with feedforward action. When using the former controller the following can be concluded:

- When analysing the controller with the non-linear model (chapter 6) all the design criteria are fulfilled but the maximal vertical acceleration is surpassed in certain conditions and the RMS of the heading angle error in closed loop is greater than in open loop.
- Good robustness results are obtained with respect to variations of the mass, centre of gravity and transport time delay. However, gain scheduling should be used with respect to velocity since bad results are obtained with speed variations, mainly at the engine failure case, as has been explained in chapter 6.
- The results obtained in the automatic evaluation procedure give good results in all of the design criteria except the comfort criteria. In our design this is due to the fact that the vertical acceleration cannot be diminished without violating other performance criteria. The bounds are surpassed in the lateral deviations during the 90 degrees turn and during the vertical deviations during the glidslope capture.

When using feedforward, worse robustness results in the inner loop are obtained. Moreover, overshoots to inner loop command step responses are obtained. However, the evaluation results show better behaviour since better performance results are obtained and the bounds never are surpassed.

The selection of a *good* eigenstructure follows an iterative process that can be time consuming. The process could be shorted if some optimisation method were used. Without any optimisation process the doubt of how good the controller is always remains.

## References

- [1] GARTEUR Action Group FM(AG08), *Communication Handbook*, Version 2, GARTEUR/TP-088-5, March, 1996.
- [2] GARTEUR Action Group FM(AG08), *Robust Flight Control Design Challenge Problem Formulation and Manual: Research Civil Aircraft Model (RCAM)*, Version 2, GARTEUR/TP-088-3, January, 1996.
- [3] Adams, R.J., Buffington, J.M., Sparks, A.G., Banda, S.S. *Robust Multivariable Flight Control* Springer-Verlag, 1994.
- [4] Andry, A.N., Shapiro, E.Y., Chung, J.C., 'Eigenstructure assignment for linear systems', *IEEE Trans. Aerosp. Electron. Syst.*, vol. AES-19, pp. 711-729, Sept. 1983.
- [5] Blight, J.D., Dailey, R.L. and Gangsaas, D., 'Practical control law design for aircraft using multivariable techniques', *Int. J. Contr.*, vol. 59, pp. 93-137, 1994.
- [6] Burken, J.J., 'Flight-Determined Multivariable Stability Analysis and Comparison of a Control System', *J. of Guidance, Control and Dynamics*, vol 16, n 6, pp. 1026-1031, 1993.
- [7] Burrows, S.P., Patton, R.J., Szymansky, E., 'Robust eigenstructure assignment with a control design package', *IEEE Control Systems Magazine*, vol. 9, pp. 29-32, 1989.
- [8] Dailey, R.L., 'Lecture Notes for the Workshop on  $H_{\infty}$  and  $\mu$  Methods for Robust Control', *IEEE Conference on Decision and Control*, Brighton, U.K., 1991.
- [9] Franklin, G.F., Powell, J.D., Emami Naeini, A., *Feedback control of dynamic systems* Addison-Wesley, 1994.
- [10] Kautsky, J., Nichols, N.K., Van Dooren, P., 'Robust pole assignment in linear state feedback', *Int. J. Contr.*, vol. 41, pp. 1129-1155, 1985.
- [11] Lehtomaki, N.A., Sandell, N.R. and Athans, M., 'Robustness Results in Linear-Quadratic Gaussian Based Multivariable Control Designs', *IEEE Trans. Automatic Control*, vol. AC-26, n 1, pp. 75-93, 1981.
- [12] Lin, C.F., *Advanced control design*, Prentice Hall, 1994.
- [13] 'Military Specifications - Flying Qualities of Piloted Vehicles', MIL-STD-1797A, March, 1987.
- [14] Moore, B.C., 'On the flexibility offered by state feedback in multivariable systems beyond closed-loop eigenvalue assignment', *IEEE Trans. Autom. Contr.*, vol AC-21, pp. 659-692, 1976.

- [15] Patton, R.J., Liu, G.P., Chen, J., 'Multiobjective controller design using eigenstructure assignment and the method of inequalities', *Journal of Guidance, Control and Dynamics*, vol. 17, pp. 862-864, 1994.
- [16] Piou, J.E., Sobel, K.M., Shapiro, E.Y., 'Robust Lyapunov constrained sampled data eigenstructure assignment using the delta operator with application to flight control design', *Proc. First IEEE Conference on Control Applications*, pp. 1000-1005, 1992.
- [17] Sobel, K.M., Shapiro, E.Y., Andry, A.N., 'Eigenstructure assignment', *Int. J. Contr.*, vol. 59, n 1, pp. 13-37, 1994.
- [18] Sobel, K.M., Yu, W., Lallman, F.J., 'Eigenstructure assignment with gain suppression using eigenvalue and eigenvectors derivatives', *Journal of Guidance, Control and Dynamics*, vol. 13, pp. 1008-1013, 1990.
- [19] Srinathkumar, S., 'Eigenvalue/eigenvector assignment using output feedback', *IEEE Trans. Autom. Contr.*, vol. AC-23, pp. 79-81, 1978.
- [20] White, B.A. *MATLAB toolboxes and applications for control*, Chapter 11: 'Eigenstructure assignment for aerospace applications.', Edited Chipperfield, A.J. and Fleming, P.J., Peter Peregrinus, 1993.

## A Software used

### A.1 Function EIGENAS

```
function [K,Kr]=eigenas(E,Ed,A,B,C,restrict)
%
%      K = eigenas(E,Ed,A,B,C,restrict)
%      [K,Kr] = eigenas(E,Ed,A,B,C,restrict)
%
% Calculate the output feedback matrix gain K using the
% method of Andry et al. (IEEE Trans. on Aerospace and
% Electronic Systems, 1983, vol. 19, pp. 711-729).
%
%      K      Gain without restrictions
%      Kr     Gain with restrictions (see parameter 'restrict')
%      A,B,C  Represent the usual system matrices
%      E      Vector of desired eigenvalues
%      Ev     Matrix with as much rows as states and where
%             every column is associated to the corresponding
%             eigenvalue, specifying the elements of the desired
%             eigenvector with:
%             1 component coupled with the eigenvalue
%             0 component uncoupled with the eigenvalue
%             -1 unspecified component
%      restrict: (optional) is a matrix indicating desirable fixed
%                zeros in the output feedback matrix Kr. Every
%                constraint has a row [i j] in 'restrict'
%                indicating Kr(i,j)=0.

% J.M. de la Cruz, J. Aranda and P. Ruiperez. Version 2-June-1996

if nargin <= 5, constr=[]; options=0;
elseif nargin == 6,
    constr=restrict; options=0;
else
    constr=restrict; options=opcion;
end
neigval=max(size(E));
nrows=size(Ed,1);
[nestad,ncontr]=size(B);
nmed=size(C,1);
V=[];
Z=[];
for ii=1:neigval,
    nasig=nnz(Ed(:,ii)+1);
    nonasig=nrows-nasig;
```

GARTEUR

```

nctna=0; nctas=0;
R=zeros(nrows,nrows);
for jj=1:nrows,
    if real(Ed(jj,ii))==1 | real(Ed(jj,ii))==0,
        nctas=nctas+1;
        R(nctas,jj)=1;
    else
        nctna=nctna+1;
        R(nasig+nctna,jj)=1;
    end
end
lid=R*Ed(:,ii);
lit=lid(1:nasig,1);
Li=inv(E(ii)*eye(nrows,nrows)-A)*B;
LiR=R*Li;
Lit=LiR(1:nasig,1:ncontr);
zi=pinv(Lit)*lit;
via=Li*zi;
V=[V,via];
Z=[Z,zi];
end

% Method of Andry et al.
[Q,Rr]=qr(B);
[d1,d2]=size(Rr);
RrI=[Rr(1:d2,:),zeros(d2,d1-d2);zeros(d1-d2,d2),eye(d1-d2)];
Q=Q*RrI;
Qi=inv(Q);
At=Qi*A*Q;
At1=At(1:d2,:);
Ct=C*Q;
Vt=Qi*V;
St=Vt(1:d2,:);
for ii=1:neigval,
    St(:,ii)=E(ii)*St(:,ii);
end
K=(St-At1*Vt)*inv(Ct*Vt);
K=real(K);

% Constraint Output Feedback
if constr==[],
    if nargout==2, Kr=K;end
    return
end
Omega=(Ct*Vt)';

```

```
Psi=(St-At1*Vt);
dim=size(constr);
Kr=zeros(ncontr,nmed);
for ii=1:ncontr,
    Omegat=[];
    nelim=0;
    for jj=1:nmed,
        elimina=0;
        for l=1:dim(1),
            if constr(l,2)==jj,
                if constr(l,1)==ii,
                    elimina=1;
                    nelim=nelim+1;
                end
            end
        end
        if elimina==0,
            Omegat=[Omegat,Omega(:,jj)];
        end
    end
    Kc=real((Omegat\Psi(ii,:))');
    if nelim==0,
        Kr(ii,:)=Kc';
    else
        nct=0;
        for jj=1:nmed,
            inserta=0;
            for l=1:dim(1),
                if constr(l,2)==jj,
                    if constr(l,1)==ii,
                        inserta=1;
                    end
                end
            end
            if inserta==0,
                nct=nct+1;
                Kr(ii,jj)=Kc(nct);
            else
                Kr(ii,jj)=0;
            end
        end
    end
end
end
```



## A.2 Function SSINTEG

```

function [An,Bn,Cn,Dn]=ssinteg(A,B,C,D,vec)
% SSINTEG Add new outputs which are integral of the original outputs
%
%           [An,Bn,Cn,Dn]=ssinteg(A,B,C,D,vec)
%
% Add a set of new outputs that are the result
% of integrate some of the existent outputs in the original system.
%
% A,B,C,D      Represent the usual system matrices
% vec          Vector with the indices of the outputs to be integrated
% An,Bn,Cn,Dn New system with (size(C,1)+length(vec)) outputs.

% J.M. de la Cruz, P. Ruiperez and J. Aranda. 3-June-1996

% Check input arguments:
mensaje=abcdchk(A,B,C,D);
if mensaje ~=[]
    error(mensaje)
end
medidas=size(C,1);
if sum(vec>medidas)~=0,
    error(['You are trying to integrate a non existing output.' ...
        'The system only has ', num2str(medidas),' outputs.'])
end
for i=1:length(vec)
    if sum(vec==i) > 1 ,
        error(['The ouput ', num2str(i),' can be integrated only once.']),
    end
end

% Body of the function
nn=length(vec);
[fA,cA]=size(A); [fC,cC]=size(C); [fD,cD]=size(D);
An=[A,                zeros(fA,nn);
    C(vec,:),         zeros(nn,nn)];
Bn=[B;
    D(vec,:)];
Cn=[C,                zeros(fC,nn);
    zeros(nn,cC),     eye(nn,nn)];
Dn=[D;
    zeros(nn,cD)];

```

### A.3 Function MXSSV

```
function [mxsgi,mxsgti,mxsgsti,mxsgo,mxsgto,mxsgsto]=mxssv(A,B,C,Kp,Ki,outpi)
% MXSSV      S, T, S+T input and output maxima singular values
%
% [mxsgi,mxsgti,mxsgsti,mxsgo,mxsgto,mxsgsto]=mxssv(A,B,C,Kp,Ki,outpi)
%
% mxssv      Computes the maxima singular values for the input and output
%             sensitivity functions S, T and S+T.
%
% A,B,C      Open loop system matrices
% Kp         Constant output feedback gain
% Ki         Constant integrated errors feedback gain
% outpi      vector with indices of the integrated outputs
%
% mxsgi      maximum singular value of S at the actuators input
% mxsgti     maximum singular value of T at the actuators input
% mxsgsti    maximum singular value of S+T at the actuators input
% mxsgo      maximum singular value of S at the sensors output
% mxsgto     maximum singular value of T at the sensors output
% mxsgsto    maximum singular value of S+T at the sensors output

% J.M. de la Cruz  10-IV-96
% UCM jmcruz@dia.ucm.es

p=size(C,1);
ni=size(outpi,2); % number of integrators
outpp=[];         % number of outputs
if ni==0,
    outpp=1:p;
else
    for i=1:p,
        isinit=0;
        for j=1:ni,
            if i==outpi(j), isinit=1; end
        end
        if isinit==0, outpp=[outpp,i]; end
    end
end
Cp=C(outpp,:); Ci=C(outpi,:);
Api=zeros(ni,ni); Bpi=eye(ni,ni); Cpi=Ki; Dpi=Api; % Integral controller
pi=pck(Api,Bpi,Cpi,Dpi);
lonrea=pck(A+B*Kp*C,B,Ci,zeros(size(Ci,1),size(B,2)));
double=[eye(ni,ni);eye(ni,ni)];

% Transfer function from the input error ei=u-y
```

GARTEUR

```

% to to the control input u
% (I+HG)ei=u

% maximum singular value of S (actuators)
errori=starp(mmult(double,double'),mmult(lonrea,pi),ni,ni);
[Alei,Blei,Clei,Dlei]=unpck(errori);
sgi=sigma(Alei,Blei,Clei,Dlei);
mxsgi=max(sgi');

% maximum singular value of T (actuators)
closedi=starp(mmult(lonrea,double'),mmult(double,pi),ni,ni);
[Alci,Blci,Clci,Dlci]=unpck(closedi);
sgti=sigma(Alci,Blci,Clci,Dlci);
mxsgti=max(sgti');

% maximum singular value of S+T (actuators)
sti=madd(errori,closedi);
[Ai,Bi,Ci,Di]=unpck(sti);
sgsti=sigma(Ai,Bi,Ci,Di);
mxsgsti=max(sgsti');

% Transfer function from the output error eo=-r+y
% to to the reference input r
% (I+GH)eo=-r

% maximum singular value of S (sensors)
resta=[-1*eye(ni,ni),eye(ni,ni)];
erroro=starp(mmult(double,resta),mmult(pi,lonrea),ni,ni);
[Aleo,Bleo,Cleo,Dleo]=unpck(erroro);
sgo=sigma(Aleo,Bleo,Cleo,Dleo);
mxsgo=max(sgo');

% maximum singular value of T (sensors)
closedo=starp(mmult(pi,resta),mmult(double,lonrea),ni,ni);
[Alco,Blco,Clco,Dlco]=unpck(closedo);
sgto=sigma(Alco,Blco,Clco,Dlco);
mxsgto=max(sgto');

% maximum singular value of S+T (sensors)
sto=madd(erroro,closedo);
[Ao,Bo,Co,Do]=unpck(sto);
sgsto=sigma(Ao,Bo,Co,Do);
mxsgsto=max(sgsto');

```

#### A.4 Function GFMAR

```
function [mg,mf]=gfmarm(xms,mxt,mxst)

% GFMAR Gain and phase margins
%
% [mg,mf]=gfmarm(xms,mxt,mxst)
%
% gfmarm      computes the gain and phase margins for S, T and S+T
%              using their maxima singular values
%
% xms: vector with the maxima singular values of S
% xmt: vector with the maxima singular values of T
% mxst: vector with the maxima singular values of S+T
%
% mg: a two columns matrix, the first with the downward
% gain margins and the second with the upward
% The rows corresponds to S, T and S+T
% mf: same structure than mg but for the phase

% J.M. de la Cruz 31-IV-96

km=1/max(xms);
mg(1,1)=20*log10(1/(1+km));
mg(1,2)=20*log10(1/(1-km));
mf(1,1)=-2*asin(km/2)*180/pi;
mf(1,2)=2*asin(km/2)*180/pi;

km=1/max(xmt);
mg(2,1)=20*log10(1-km);
mg(2,2)=20*log10(1+km);
mf(2,1)=-2*asin(km/2)*180/pi;
mf(2,2)=2*asin(km/2)*180/pi;

km=1/max(mxst);
mg(3,1)=20*log10((1-km)/(1+km));
mg(3,2)=20*log10((1+km)/(1-km));
mf(3,1)=-2*atan(km)*180/pi;
mf(3,2)=2*atan(km)*180/pi;
```

**A.5 Function TRTS**

```

function trs=trts(raices)
% TRTS Rise Time Settling Time
%
% trs=trts(raices)
%
% Computes the rise time and the settling time
% of the roots in vector raices
%
% 18/4/96

n=size(raices,1);
for i=1:n,
    if imag(raices(i,1))==0,
        tau=-1/raices(i,1);
        t10=tau*(-log(0.9));
        t90=tau*(-log(0.1));
        t9010=t90-t10;
        t99=tau*(-log(0.01));
    else
        [wn,psi]=damp(raices(i,1));
        t9010=(1-0.4167*psi+2.917*psi^2)/wn;
        t99=-log(0.01*sqrt(1-psi^2))/(psi*wn);
    end
    trs(i,1:3)=[raices(i,1),t9010,t99];
end
disp('Raiz      Rise time      Settling time')
```

## **B Designer's background and design environment**

The authors have wide experience in Inertial Navigation Systems, especially in the alignment process and in the integration of inertial sensors but, before beginning the project, we didn't have experience in flight mechanics neither in flight control. However we had a deep knowledge, practical and theoretical, on different control techniques (classical control, adaptive control, robust control, predictive control, etc.) and in system identification.

At the start of the project we only had theoretical knowledge about the Eigenstructure Assignment method.

For the design of the controller we have used Matlab with "Simulink", "Control Toolbox", "Robust Control Toolbox" and " $\mu$ -Analysis and Synthesis toolbox", combined with a set of functions we have developed for this project (see Appendix A).

We have spent the equivalent of 8.5 months/man: 7 months for the analysis and design, and 1.5 months for writing the report.